Variational h-adaptation for strongly coupled problems in thermo-mechanics

Rohit Pethe

UNIVERSITE BRETAGNE LOIRE

Centrale Nantes

Thèse de Doctorat

Rohit PETHE

Mémoire présenté en vue de l'obtention
du grade de Docteur de l'École Centrale de Nantes
sous le sceau de l'Université Bretagne Loire

École doctorale : Sciences Pour l'Ingénieur, Géosciences, Architecture (SPIGA)

Discipline : Génie mécanique
Unité de recherche : Institut de Recherche en Génie civil et Mécanique

Soutenue le 14 Décembre 2017

Variational h-adaptation for strongly coupled problems in thermo-mechanics

JURY

Président de jury :	**PONTHOT Jean-Philippe**, Professeur, University of Liège
Rapporteurs :	**MOSLER Jörn,** Professeur, TU Dortmund
	FOURMENT Lionel, Professeur, Mines Paris Tech
Examinateurs :	**DRAPIER Sylvain,** Professeur, Mines Saint-Étienne
	RASSINEUX Alain, Professeur, Université de technologie de Compiègne
	RACINEUX Guillaume, Professeur, Centrale Nantes
Directeur de thèse :	**STAINIER Laurent,** Professeur, Centrale Nantes
Co-encadrant de thèse :	**HEUZÉ Thomas,** Maitre de conférence, Centrale Nantes

École Centrale de Nantes
Université bretagne loire

École doctorale
Science Pour l'ingénieur, Géosciences, Architecture

Thèse de Doctorat

Spécialité : Mécanique des solides, des matériaux, des structures et des surfaces

Présentée et soutenue par:
ROHIT PETHE

Le – Novembre 2017
á l'École Centrale de Nantes

Variational h-adaptation for strongly coupled problems in thermo-mechanics.

JURY

Rapporteurs	JÖRN MOSLER	Technische universität dortmund
	LIONEL FOURMENT	Mines Paris Tech
Examinateurs	SYLVAIN DRAPIER	Mines Saint-Étienne
	JEAN-PHILIPPE PONTHOT	University of Liège
	ALAIN RASSINEUX	Université de Technologie de Compiègne
	GUILLAUME RACINEUX	École Centrale de Nantes
Directeur de thèse	LAURENT STAINIER	
Co-encadrant	THOMAS HEUZÉ	
Laboratoire	Institut de Recherche en Génie Civil et Mécanique	

Acknowledgements

It has been a privilege to be at Centrale Nantes, first as a masters student and now as a PhD candidate.

I am grateful to my director of thesis Prof. Laurent Stainier who guided me all along my research with a lot of enthusiasm, without which this work wouldn't have been possible. Apart from core research, I also learnt moral values because of his outlook towards life. I also thank my co-director of thesis Dr. Thomas Heuzé for his guidance and taking immense efforts to polish my manuscript and research articles. I am indeed very much happy and proud to have an opportunity to work under Prof. Laurent Stainier and Dr. Thomas Heuzé.

I would also like to thank various faculty members like Prof. Nicolas Möes, Prof. Anthony Nouy, Dr. Grégory Legrain, Mr. Alexis Salzmann whose courses helped me build strong foundation in computational mechanics. I thank my former colleague Dr. Prashant Rai for thought provoking discussions about life and motivations. I must thank my colleagues Adrien Renaud, Jorge De Anda Salazar, Tauno Tiirats, Abdullah Waseem, Benoit Le, Romain Hamonou, Simon Paroissien, Alina Krasnobrizha, Daria Serbichenko, Quentin Auoul-Guilmard and various others who directly or indirectly helped me in completing the thesis.

I would like to remember the company of friends like Akash Kumar, Gaganpreet Kaur, Amey Rangnekar, Pranav Pandit, and others who would make my weekends fun and re-energize me for the next week.

I am thankful to my sister Rajashree Pethe who would happily clear my doubts in C++. I should also thank my fiancée Avanti Shinde and her parents, for supporting me in difficult times and always believing in me. I sincerely

thank my friend Prathamesh Paigude from whom I learnt to be positive in any difficult situation. I also thank him for immense love and support towards me and my family.

Finally and most importantly I would like to thank my mother Manik Pethe, and my father Sanjay Pethe, for their blessings and active support all through my academic career and life so far, without whose sacrifices and initiatives, it would have been extremely hard to avail such a great opportunity of learning and experience.

Abstract

A mesh adaption approach for strongly coupled problems is proposed, based on a variational principle. The adaption technique relies on error indicated by an energy-like potential and is hence free from error estimates. According to the saddle point nature of this variational principle, a staggered solution approach appears more natural and leads to separate mesh adaption for mechanical and thermal fields. Using different meshes for different phenomena, precise solutions for various fields under consideration are obtained. Internal variables are considered constant over Voronoi cells, so no complex remapping procedures are necessary to transfer internal variables. Since the algorithm is based on a set of tolerance parameters, parametric analyses and a study of their respective influence on the mesh adaption is carried out. This detailed analysis is performed on uni-dimensional problems. The proposed method is shown to be cost effective than uniform meshing, some applications of the proposed approach to various 2D examples including shear bands and friction welding are presented.

Contents

List of Figures

Introduction générale

La concurrence sur le marché a obligé les entreprises à accélérer le processus de conception, de prototypage, de fabrication et de lancement de nouveaux produits sans compromettre leur qualité. Pour atteindre cet objectif, elles doivent repousser les limites technologiques. L'émergence d'équipements de prototypage rapide tels que les imprimantes 3D résulte de ces efforts. Toutefois, tous les produits ne peuvent pas être prototypés rapidement ni rentables. Une technologie qui peut permettre d'éliminer ou plutôt de réduire le besoin de prototype est donc nécessaire. La croissance des technologies de l'information et de l'informatique a augmenté le pouvoir de calcul comme jamais auparavant. En conséquence, un nouveau domaine de la science informatique a émergé en complément des sciences théoriques et expérimentales traditionnelles. La mécanique numérique est une science informatique qui traite des solutions approchées aux problèmes de mécanique en utilisant des techniques numériques. Ainsi, les simulations numériques permettent de réduire le besoin de prototypes, en fournissant des données virtuelles, simulées du comportement de tout ou partie d'un produit. Dans un monde idéal, une simulation numérique devrait produire des résultats très proches du monde réel. Dans le monde réel, chaque situation implique plusieurs phénomènes physiques. Par exemple, dans un moteur à combustion, l'énergie chimique du carburant est convertie en chaleur, qui est ensuite convertie en pression fluide qui, à son tour, produit le mouvement mécanique. Le processus implique l'effet de phénomènes chimiques, thermiques, fluides et structurels les uns sur les autres. Une méthode numérique qui incorpore ces intéractions sera capable de produire des résultats précis. Cependant pour des questions de coût de calcul, une simulation ne

peut out représenter, et est généralement produite en regard d'un objectif précis, et donne des résultats valides dans un domaine borné.

Une méthode numérique très populaire pour les problèmes structurels est la méthode des éléments finis. La méthode est basée sur une approche lagrangienne où un maillage représentant la géométrie suit les points matériels de la structure considérée. Pour les problèmes impliquant de grandes déformations, une distorsion de maille sévère est observée, pouvant conduire un jacobien négatif, et donc une solution non physique.

Par conséquent, une approche envisagée depuis dj fort longtemps est d'adapter la forme et la taille des mailles au cours de la transformation. Cela permet d'éviter le problème des distorsions sévères des mailles. De plus, en simulant des processus industriels fortement couplés comme le forgeage, l'usinage, le soudage par friction, etc., les effets dynamiques et transitoires font que les domaines d'intérêt changent rapidement. Dans le cadre de la méthode des éléments finis, cela signifie que les domaines d'intérêt changent de position au cours du temps. Par conséquent, une stratégie d'adaptation de maillage permet d'obtenir des solutions précises à chaque instant en affinant le maillage dans les domaines d'intérêt et en déraffinant le maillage dans d'autres domaines. Dans ce travail, nous présentons une stratégie d'adaptation de maillage basée sur un principe variationnel dédiés aux problèmes fortement couplés en thermo-mécanique.

Les stratégies d'adaptation sont basées sur des techniques et des critères d'adaptation. Les techniques d'adaptation traitent essentiellement des aspects géométriques de l'adaptation. Les critères d'adaptation reflètent la particularité du problème à l'étude. Les procédures d'adaptation de maillage globale créent un maillage complètement nouveau et utilisent des procédures de projection pour transférer des variables internes [50, 58]. Les méthodes basées sur le remaniement global du domaine d'intérêt nécessitent le transfert de variables internes entre les mailles, ce qui peut conduire à une diffusion artificielle de ce dernier. Rivara et al. [62, 61, 60] propose des mises à jour explicites pour les changements de maillage locaux. Grinspun et al. [26] ont propos la méthode CHARMS pour le raffinement de maillage de facon hiérarchique. Classiquement, les critères d'adaptation du maillage ont été

basés sur des estimations d'erreur ou l'asymétrie du maillage. L'estimation d'erreur de Z^2 couramment utilisée depuis Zienkiewicz et Zhu [74] utilise les contraintes dans un élément et est basée sur un processus de reconstruction de champ pour obtenir un champ de contrainte de référence. La différence dans l'élément entre les champs fournit une estimation d'erreur basée sur le dégradé. La majorité des critères d'adaptation des mailles proposés dans la littérature sont basés sur l'estimation d'erreurs. Dans ces méthodes, la stratégie consiste à adapter le maillage pour minimiser une erreur liée; ou par une application récursive des étapes de raffinement local [71, 2]. Mais ces méthodes ont certaines limites: ils fonctionnent bien avec des modèles constitutifs linéaires (par exemple l'élasticité), mais deviennent plus complexes lorsque des modèles constitutifs non linéaires sont utilisés. En outre, les champs admissibles doivent être reconstruits [37, 74]. De plus, les bornes d'erreur standard nécessitent une certaine régularité de la solution pour assoir leur validité [17]. Par conséquent, il peut être difficile et coûteux d'utiliser cette approche pour des problèmes complexes impliquant des modèles constitutifs non linéaires et / ou de grandes déformations. Une procédure d'adaptation de maillage alternative pour des problèmes purement mécaniques a été proposée par Mosler et al. [48, 49], basée sur une approche variationnelle de [51]. Cette technique utilise un indicateur d'erreur plutôt qu'un estimateur d'erreur. Dans une approche variationnelle, un potentiel d'énergie doit être minimisé (ou maximisé), dont la valeur scalaire indique un certain niveau de qualité de l'approximation effectuée. Aucune estimation d'erreur n'est utilisée à n'importe quel stade de l'algorithme. Cette approche permet l'adaptation de maillages en présence de grandes déformations et de comportements non linéaires.

Alors que l'adaptation des mailles à l'aide d'estimateurs d'erreur est bien établie pour les problèmes impliquant une seule physique, seules quelques tentatives ont été proposées en ce qui concerne les méthodes d'adaptation de maillage pour des problèmes fortement couplés. La plupart des méthodes disponibles dans la littérature adaptent le maillage pour un seul des champs considérés [5].

Dans le présent travail, nous présentons une stratégie d'adaptation de maillage pour des problèmes fortement couplés basés sur une approche variationnelle, et plus particulièrement des problèmes thermo-mécaniques. En effet, les principes variationnels sont basés sur la minimisation ou la maximisation d'une fonctionnelle, dont la valeur locale s'avère être un bon indicateur d'erreur numérique sur un patch d'éléments finis. Les objectifs du présent travail peuvent être énumérés comme suit:

1. *Proposer un algorithme de h−adaptation pour des problèmes fortement couplés en thermo-mécanique. Le défi dans les problèmes fortement couplés est que les deux phénomènes, mécaniques et thermiques peuvent être à des échelles spatio-temporelles très différentes. En outre, les emplacements spatiaux des domaines d'intérêt pour les deux champs peuvent être très différents. L'approche d'adaptation de maillage proposée repose sur une approche décalée [3] couplée avec des maillages différents pour différents champs. L'adaptation séquentielle de différents maillages permet de capturer les différentes échelles spatiales des différents champs.*

2. *L'approche proposée par Mosler et al. [48, 49] pour des problèmes uniphysique permet de s'affranchir d'estimateurs d'erreur, et donc de reconstructions coûteuse de champs. L'approche proposée a pour objet d'utiliser cet avantage et de l'étendre à des problèmes couplés. Par conséquent, le problème repose sur un indicateur d'erreur basé sur la valeur de la fonctionnelle variationnelle.*

3. *Éviter la diffusion numérique excessive causée par les procédures de projection complexes pour transférer des variables internes d'un maillage à l'autre. En effet, les méthodes basées sur le remaniement global du domaine d'intérêt provoquent une diffusion numérique significative, elles ne sont donc pas considérées dans ce travail. Plutôt, les techniques locales d'adaptation des mailles basées sur la bisection du bord sont préférées. Dans le présent travail, les techniques d'adaptation ne sont développées que pour les éléments triangulaires. En supposant une*

répartition constante des variables internes sur les cellules Voronoï, des procédures de projection complexes provoquant une diffusion numérique significative peuvent être évitées. Cet opérateur de transfert a été étudié en détail par Ortiz et Quigley [50].

4. *La méthode devrait être facilement adaptable pour différents problèmes. Différents cas test d'abord unidimensionnels puis bidimensionnels sont présentés aux chapitres 5 et 6, notamment des problèmes thermiques simples pour une illustration simple de la méthode, des problèmes fortement couplés associés à la thermo-élasticité, un problème de simulation du phénomène de bande de cisaillement et un cas représentatif de soudage par friction. Ces applications étendues démontrent l'adaptabilité de l'algorithme à différents problèmes.*

5. *L'algorithme proposé doir être efficient pour des problèmes suffisamment complexes, c'est-à-dire moins coteux à précision donnée qu'un raffinage uniforme, pour être utile dans des applications pratiques. Cette analyse des cots est effectuée sur différents cas test dans les chapitres 5 et 6 en profondeur et il est établi que l'algorithme est efficient par rapport à un raffinage uniforme.*

Chapter 1

Motivation and general context

1.1 Background

Innovation has been the key for successful product development for centuries. From the second part of 20^{th} century, competition in the market has forced companies to accelerate the process of designing, prototyping, manufacturing and launching of new products without compromising the product quality. Achieving this target requires to push technological boundaries. Emergence of rapid prototyping equipments such as 3D printers is an example of outcome of these efforts. However, neither every product can be rapid prototyped nor it is cost-effective. A technology that can either eliminate or reduce the need to prototype is thus needed. The growth in information technology and computer science has increased computational power like never before. As a result, a new field of computational science has emerged as a new leg of science, in addition to theoretical and experimental ones. Computational mechanics is a computational science that deals with finding approximate solutions to problems in mechanics by using numerical techniques. Thus, numerical simulations fulfill the need of technology that can reduce the need of prototypes. A numerical simulation is designed to produce results that are very close to the real world. In real world, every situation involves several physical phenomenon. For example in an internal combustion engine, the chemical energy of fuel is converted into heat, which is then converted to fluid pressure which in turn produces the mechanical movement. The process

involves effect of chemical, thermal, fluid and structural phenomena on each other. A numerical method that incorporates these interactions will be able to produce accurate results.

A very popular numerical method for structural problems is the finite element method. The method is based on a Lagrangian approach where a mesh is created that represents the geometry and the mesh follows material points. However, for problems involving large strains, severe mesh distortion may occur. For example, consider a simulation involving a high speed impact of metal bar as shown in figure 1.1. When simulated using a finite element approach with a mesh stuck on the body, a highly distorted mesh is obtained as shown in figure 1.2. This poses several numerical difficulties involving flat elements, Jacobian going to zero or negative etc.

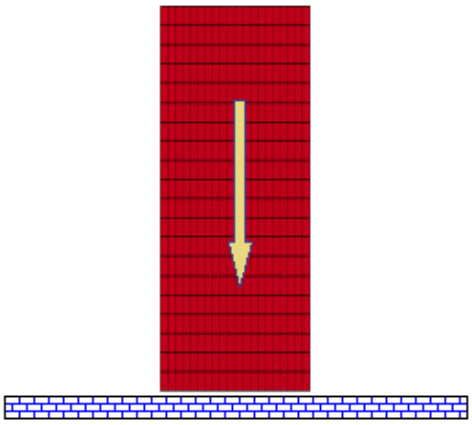

Figure 1.1: High speed impact of a metal bar [1].

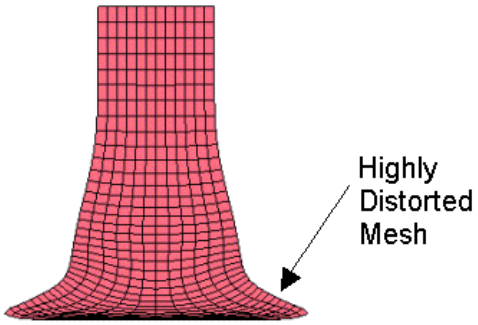

Figure 1.2: Finite element solution with fixed mesh produces highly distorted elements [1].

In order to overcome this difficulty, several authors have proposed different methods. First is an Eulerian method in which the mesh remains fixed in space. That is, material points flow through the mesh. This approach is suitable for problems in fluid mechanics such as flow problems. The channel flow problem depicted in figure 1.3 demonstrates this approach. In order to use this approach for structural problems, a very fine mesh would be needed to capture material response making the method computationally very expensive. In addition, transport of history variables causes loss in information

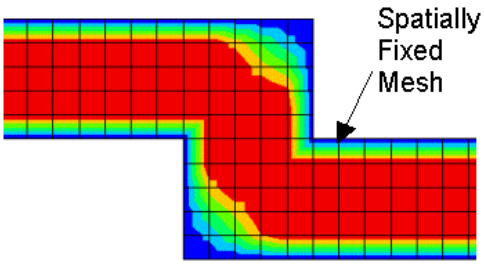

Figure 1.3: Channel flow simulation using Eulerian approach [1].

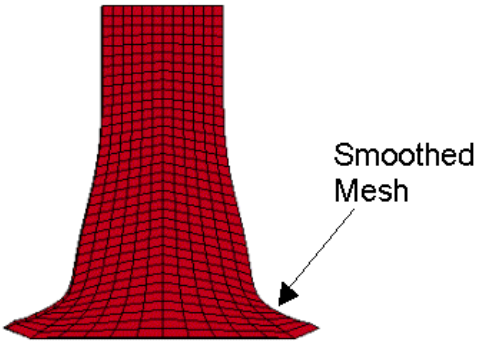

Figure 1.4: ALE simulation of metal bar impact problem [1].

and therefore accuracy. Second, are ALE (Arbitrary Lagrangian Eulerian) approaches in which the mesh inside the domain can move arbitrarily to optimize the shape of elements while the mesh on the boundaries and the interfaces of the domains can move along the materials to precisely track the boundaries and interfaces of a multi-material system. For metal bar impact problem, this is illustrated in figure 1.4. While it has the advantage that it allows smoothing of distorted mesh, the main difficulty is the path dependent behaviour of the plastic flow being modelled. Due to the path dependence, the relative motion between the mesh and the material must be accounted for in the material constitutive equations. In addition, the ALE method does not allow new (damaged) surfaces to be created and is limited to geometries where the material flow is relatively predictable [1]. Third, meshless methods are also proposed that (theoretically) do not depend on any mesh, but face difficulties in application of boundary conditions and robustness.

Therefore, one common idea is to consider mesh adaptation in the framework of finite element method. This allows to avoid the problem of severe mesh distortions. In addition, while simulating strongly coupled industrial process like forging, machining, friction welding, etc., dynamic and transient effects cause the domains of interest to change rapidly. In the framework of finite element method, this means that the domains of interest change their spatial location with time. Therefore, a mesh adaptation strategy also allows to obtain precise solutions at each time step by refining the mesh in

domains of interest and coarsening the mesh in other domains. In this work, we present a mesh adaptation strategy based on a variational principle for strongly coupled problems in thermo-mechanics.

The purpose of this chapter is to introduce the background of the problem, make a brief state of the art of mesh adaption, and define objectives and challenges. In order to put the work in context, a comprehensive literature review is presented which revisits the major work in mesh adaptation techniques, mesh adaptation criteria also the variational framework on which the proposed mesh adaptation technique is based. Then the objectives of the thesis along with the challenges are explained.

1.2 Literature review

1.2.1 Mesh adaptation

Numerical error in finite element approximation is related to the mesh size h, the degree of polynomial appearing in the element shape function p and regularity of the solution r as follows:

$$||e||_{\mathcal{H}^m} \leq ch^{\alpha}||u||_{\mathcal{H}^r} \tag{1.1}$$

where $\mathcal{H}^k$ is the space of functions possessing k square integrable derivatives, $||\cdot||_{\mathcal{H}^k}$ represents the Sobolev norm, c is a constant (element-dependent), u represents the exact solution, and the exponent α is given by:

$$\alpha = \min(p + 1 - m, r - m) \tag{1.2}$$

Mesh adaptation is a way to exploit this mathematical result in order to focus efforts in the domain of interest and release in other areas. Mesh adaptation processes can be divided into three broad categories. First is h-adaptation where the mesh size is optimized [21]. This means, element size is adapted using the same type of elements. Size is reduced where interpolation must be enriched to achieve better accuracy. On the other hand, size is increased where solution is sufficiently accurate. It may contain processes of element refinement and/or coarsening, thereby increasing and/or reducing the number

of degrees of freedom. Second, r-adaptation where the number of nodes are same but their location and connectivity is changed [39, 56]. The strategy simply involves redistribution of the nodes. This has advantage of preserving number of degrees of freedom thereby not increasing the computational cost. The data structure and the coding remains straightforward as it simply involves changes in node co-ordinates and connectivities. Third, p-adaptation where the order of interpolation polynomial within an element is changed [52]. The strategy involves using a fixed finite element mesh and adapting the interpolation order of the elements. In this strategy, the convergence to the exact solution is dictated by ch^{α} if the exact solution is smooth as seen from equation (1.1). A hybrid of h-adaptation and p-adaptation is also proposed in the literature, and called hp-adaptation [57]. In this strategy, along with mesh size, interpolation order is also adapted. The purpose of the present work is to introduce an approach based on h-adaptation, however, the extension of the strategy to p-adaptation is quite straightforward.

Mesh adaptation strategies depend on *adaptive techniques* and *adaptation criteria*. Adaptive techniques essentially deal with geometric aspects of adaptation. On the other hand, the adaptation criteria captures the peculiarities of the problem under consideration. The following subsections make a brief review of adaptation techniques for h-adaptation.

1.2.2 Adaptation techniques

Several mesh adaptation techniques have been proposed in the literature. Rivara et al. [62, 61, 60] propose explicit updates for local mesh changes. Molinari et al. [47] use local coarsening and refinement method based on mesh size for shear bands. Mesh adaptation for shear bands has also been studied in plane strain [7, 11]. Global mesh adaptation procedures create a completely new mesh and use remapping procedures to transfer internal variables [50, 58]. Using gradient based indicators, global remeshing technique has been applied to impact problems [22]. Global remeshing techniques also handle mesh distortions in machining problems [45]. Methods based on global remeshing of the domain of interest require to transfer internal variables between meshes,

which can lead to artificial diffusion of the latter unless specific methods are used [13]. Camacho et al. [15] propose remeshing methods using advancing front methods for ballistic penetration problems. In [19, 69], authors use mesh adaptation for shape optimization of structures. Grinspun et al. [26] proposed CHARMS method for hierarchical mesh refinement.

1.2.3 Adaptation criteria

Classically, the mesh adaptation criteria have been based on error-estimates or mesh skewness. The commonly used Z^2 error estimate proposed by Zienkiewicz and Zhu [74] uses stresses within an element and is based on a recovery process to obtain reference stress. The difference between element and reference stress provides gradient based error estimate. Curvature based error estimates have been proposed by Borouchaki et al. [12]. Error estimates based on constitutive relation error have also been studied [38, 18, 36]. In these methods, the finite element solution is described as a displacement-stress pair such that the displacements satisfy kinematic constraints like boundary conditions and initial conditions while the stresses satisfy the equilibrium conditions. The displacements and stresses do not satisfy the constitutive relations (stress-strain relations) which provides an error measure which they refer to as the constitutive relation error. Romero et al. [63] propose an error estimate based on time update. Gurtin [27] uses configurational forces for r-adaptation. Some authors also use gradients of physical quantities as mesh adaptation criteria [7, 11, 50]. Error estimates can also be based on variational principles [33, 34, 16, 58]. Many other error estimators are studied by various researchers [4, 35, 42, 24].

In the fluid mechanics community, the main emphasis is on the proper resolution of flow field. Therefore, in order to capture boundary layers, shock waves and high speed compressible flows, mesh adaptation techniques are necessary. Significant amount of work has been done for mesh adaptation for compressible flows [44, 54, 43, 29]. Most of these mesh adaptation criteria are based on error estimates from gradients of flow fields. In the calculation of lift

and drag of an airfoil in presence of shocks and viscous effects, error estimators based on bounds on functional outputs have been proposed [53, 70].

A majority of mesh adaptation criteria proposed in the literature are based on error-estimation. In these methods, the strategy is to adapt the mesh to minimize an error bound among all meshes of fixed size; or by recursive application of local refinement steps [71, 2]. But these methods have certain limitations. They work well with linear constitutive models (for example elasticity), but become more complex when non-linear constitutive models are used. Moreover, admissible fields need to be reconstructed [37, 74]. In addition, standard error bounds require a certain regularity of the solution for their validity [17]. Therefore, it can be difficult and costly to use this approach for complex problems involving non-linear constitutive models and/or large deformation.

An alternative mesh adaptation criterion for purely mechanical problems was proposed by Mosler et al. [48, 49], based on the variational approach of [51]. This technique uses an error indicator rather than an error estimator. In a variational approach, an energy like potential is to be minimized (or maximized), the scalar value of which indicates the level of approximation following the minimum (or maximum) criterion. No error estimates are used at any stage of the algorithm. It allows mesh adaptation in presence of large deformations and non-linear constitutive behavior. In addition, it was shown in [48] that variational h-adaptation could be combined with variational r-adaptation, at least for hyperelastic behavior. Indeed, r-adaptation would involve remapping in the presence of internal variables, and was not considered by these authors for dissipative behaviors. In [48, 49], the authors addressed isothermal, steady state mechanical problems.

1.2.4 Mesh adaptation for strongly coupled problems

While mesh adaptation using error estimation is well established for single field problems, only few attempts have been made towards mesh adaptation methods for strongly coupled problems. Most of the methods available in literature adapt the mesh for only one of the considered fields [5]. Solin et

al. [64] use multimesh adaptation approach for weakly coupled problems, but the method is limited to thermo-elasticity. Vokas et al. [72] consider a single mesh and h-refinement affects all fields simultaneously, therefore the method fails to capture different scales and spatial resolutions of different fields. Moreover, the mesh adaptation criteria relies on error estimators that work well with linear constitutive models, but are very complex in the case of non-linear constitutive models due to their need to reconstruct admissible fields. Therefore, it appears difficult and expensive to use this approach for strongly coupled problems with non-linear constitutive models and/or large deformation. Ramadan et al. [59] propose a bimesh method for strongly coupled thermo-mechanical problems with localized deformations. These authors propose a method in which a thermal mesh is uniformly fine; whereas, the mechanical mesh uses the thermal mesh in the deformation zone and coarsened version of thermal mesh in zone of insignificant deformation. This strategy was mainly proposed to speed up the calculations as the mechanical problem is quite expensive.

1.2.5 Variational framework

In the present work, we present a strategy of mesh adaptation for strongly coupled problems based on a variational approach. Indeed, variational principles are based on minimization or maximization of a functional, the local value of which turns out to be a good indicator of numerical error on a patch of finite elements. This idea has been proposed and exploited for purely structural problems by Mosler et al. [48, 49]. Its extension to strongly coupled problems requires an associated variational formulation. Thermo-elastic and thermo-visco-elastic problems have been extensively investigated in [10, 9, 6, 8, 30, 46]. But, formulations for coupled thermo-mechanical problems involving non-linear dissipative behaviour, such as thermo-elasto-visco-plasticity have been recently summarized by Stainier [66, 73], which itself is an extension of former work on variational visco-plastic constitutive updates proposed by Stainier and Ortiz [51].

1.3 Objectives and challenges

The major objective of the thesis is to propose an h-adaptation algorithm for strongly coupled problems in thermo-mechanics. The challenge in strongly coupled problems is that the two phenomena, mechanical and thermal can develop at very different spatial and temporal scales. Moreover, the spatial locations of domains of interest for the two fields can be very different. Therefore, it is very difficult to have a single adaptive mesh that can effectively capture both fields. The proposed mesh adaptation approach relies on a staggered approach [3] coupled with different meshes for different fields. Sequential adaptation of different meshes allows to capture different scales and spatial resolutions of different fields. The second chapter of the thesis gives an introduction to multi-physics and solution schemes in general setting. Then a specific problem of thermo-mechanics is taken into consideration where monolithic and staggered approaches are explained in detail.

The second objective is that the mesh adaptation criteria should be free from any error estimates because of the drawbacks mentioned in the previous section. In order to achieve this objective, the proposed approach extends the approach proposed by Mosler et al.[48, 49] for single field problems. Therefore, the problem relies on an error indicator based on the value of a variational functional. The proposed approach exploits this thermo-mechanical variational formulation of [66, 73]. The third chapter presents this variational framework for thermo-mechanical problems. These formulations allow to represent the thermo-mechanical problem as a saddle point problem. First, a continuum model is presented followed by a time discrete model. Some examples of constitutive models are also presented.

The third objective is to avoid the excessive numerical diffusion caused by the complex remapping procedures to transfer internal variables from one mesh to another. Because the methods based on global remeshing of the domain of interest cause significant numerical diffusion, they are not considered. Instead, local mesh adaptation techniques based on edge bisection are preferred. In the present work, adaptation techniques are only studied for triangular elements. Assuming a constant distribution of internal variables over Voronoï cells,

complex remapping procedures causing significant numerical diffusion can be avoided. This transfer operator was studied in detail by Ortiz and Quigley [50] and is presented in Chapter 4. The same holds true between the steps of the staggered scheme, avoiding significant numerical diffusion assuming a constant distribution of internal variables over elementary cells consisting of the intersection of Voronoï cells and triangular elements. Indeed, two mesh adaptation techniques are presented. First, a Single Edge Bisection (SEB) technique [48] is considered, allowing for anisotropic meshes. Second, Rivara's Longest Edge Propagation Path (LEPP) technique [62] is used which constrains the element aspect ratio. One could also extend this strategy for techniques like CHARMS [26] but this extension was not exploited here. The fourth chapter presents the proposed mesh adaptation algorithm. The considered adaptation techniques are presented in details followed by mesh adaptation criteria that depend on the variational framework presented in the third chapter.

Fourth, the proposed algorithm should be cost effective in case of sufficiently complex problems with respect to using a single uniform mesh for it to be useful in practical applications. An extensive cost analysis is performed on different test cases and it is established that the algorithm is indeed cost effective with respect to using single uniform mesh in case of sufficiently complex problems even using the most pessimistic cost estimate for the adaptive algorithm. Chapter 5 presents unidimensional test cases where analysis of the proposed algorithm is presented, demonstrating the cost effectiveness of the algorithm for complex problems. An extensive parametric analysis of the algorithm parameters is also presented in chapter 5.

The fifth objective is that the method should be easily adaptable for different problems. Different bidimensional test cases are presented in Chapter 6 including simple thermal problems, strongly coupled problems in thermoelasticity, a problem simulating shear band phenomenon and a representative case of friction welding. These wide applications demonstrate the adaptability of the algorithm to different problems.

1.4 Conclusion

In this chapter the mesh adaptation for strongly coupled problems was motivated. Following the literature review, the objectives and challenges of the thesis were stated. Strategies to achieve the proposed objectives were introduced and relevant bibliography was extracted.

Problèmes fortement couplés

Un problème qui implique de nombreux phénomènes physiques s'influençant les uns les autres est appelé un problème multiphysique couplé. Considérons par exemple une bande de cisaillement dans laquelle la dissipation d'énergie mécanique provoque une élévation de la température, laquelle amène le matériau à ramollir, ce qui conduit à des contraintes de cisaillement plus faibles. Pour résoudre ce problème, les ingénieurs doivent combiner des modèles physiques et des algorithmes, contenant tous les phénomènes physiques en présence pour rendre compte de l'effet observé. Pour beaucoup de problèmes de l'ingénieur, les effets physiques d'intérêt résultent de la combinaison de plusieurs physiques. Il est souvent rappelé que tous les problèmes devraient être supposés couplés avant (pour certains) pour infirmer cette proposition.

Un système sera considŕé fortement couplé, si les sous-systèmes 1 et 2 s'influencent mutuellement de façon significative, par exemple la thermo-mécanique, la thermo-viscoélasticité, l'aéroélasticité, etc. Un système est faiblement couplé si le sous-système 1 a une influence significative sur le sous-système 2, alors que le sous-système 2 a une influence modérée (ou petite) sur le sous-système 1, par exemple en aéro-acoustique. Dans ce cas, nous pouvons appliquer un schéma de résolution séquentiel o nous pouvons résoudre le premier sous-système 1 (sous-système 1 en entrée), puis nous résolvons le sous-système 2.

Il existe de nombreuses méthodes proposées dans la littérature afin de résoudre des problèmes couplés. Deux d'entre elles sont les plus couramment utilisées. Le premier est un schéma monolithique. Il consiste à résoudre simultanément les équations des différents champs simultanément (avec un algorithme implicite ou explicite). L'inconvénient est que le système devient

vite énorme, de sorte qu'il présente un cot de calcul élevé. Le second est le schéma étagé. L'objectif d'un schéma d'étagé est de diviser le problème couplé en un ensemble de sous-problèmes, donc le schéma étagé résout différents champs successivement. Les problèmes d'une préoccupation majeure pour nous sont des problèmes fortement couplés où les deux phénomènes physiques s'influencent mutuellement; En particulier, des problèmes thermomécaniques fortement couplés. Dans ce travail, nous nous occupons de l'utilisation de deux maillages différents pour les parties mécanique et thermique afin de pouvoir tenir compte des échelles spatiales propres à ces deux physiques, nous considérons donc uniquement l'approche étagée qui permet de séparer un problème couplé en sous-problèmes liés à chaque phénomène physique.

Chapter 2

Strongly coupled problems

2.1 Introduction

The purpose of this chapter is to introduce the problems of interest. First, an introduction to multiphysics is presented in general sense. This allows to introduce different solution schemes for strongly and weakly coupled problems. Then, specific thermo-mechanical problems are tackled starting from the presentation of balance equations. As an example of a constitutive model, thermo-elasticity is presented. Finally, finite element discretization for thermo-mechanical problems is recalled and solution schemes introduced in general setting are applied to thermo-elasticity problem.

2.2 Problems in multiphysics

A problem that involves many physical phenomena influencing each other is called a coupled multiphysics problem. Let's take for instance the example of a shear band in which mechanical dissipation causes temperature rise which leads the material to soften and then to increase shear strains. To deal with this issue, engineers must combine physical models and algorithms allowing to capture the occuring physical phenomena to simulate the observed effects. For many engineering problems, physical effects of interest result from combination of many physics. Essentially, every problem should be assumed to be coupled unless proven otherwise.

In coupled systems, subsystems interact through interfaces in its general sense, the interaction is called "one way" if there is no feedback between subsystems. The interaction is called "two-way" or "multiway" if there is feedback between sub-systems. We are interested in this latter case, where the response has to be obtained by solving simultaneously the coupled equations which model the system. In computational multi-physics, two types of coupling exist, named strong and weak couplings. Each of those two couplings is linked directly to the tightness of coupling between equations describing the system.

2.2.1 Strong coupling

A system is called strongly coupled, if both sub-system 1 and sub-system 2 have influences on each others, for example thermo-mechanics, thermo-visco-elasticity, aero-elasticity, etc. Consider for instance a system, where u_1 and u_2 are the two fields. We can write the coupled system $u_1(t)$ and $u_2(t)$ as:

$$\begin{aligned} \frac{du_1}{dt} &= \mathcal{L}_1(u_1, u_2) \\ \frac{du_2}{dt} &= \mathcal{L}_2(u_1, u_2) \end{aligned} \tag{2.1}$$

so that functions $\mathcal{L}_1$ and $\mathcal{L}_2$ are functions of both u_1 and u_2. In this case we can apply different kind of schemes to solve the problem :

- Concurrent solution scheme such as monolithic schemes, where we solve simultaneously all equations in one algorithm.
- Staggered schemes, where the coupled problem is split and each field is treated by a different strategy.
- Alternated schemes / Gauss-Seidel approaches for which a fixed point loop is added at each time step on the overall system. This approach should lead to same results as a monolithic scheme, when convergence is obtained.

2.2.2 Weak coupling

A system is weakly coupled if sub-system 1 has significant influence on sub-system 2, while subsystem 2 has moderate (or small) influence on subsystem 1, for example in aero-acoustics. In this case, we can apply a sequential solution scheme where we can solve sub-system 1 first (subsystem 1 as an input) and then solve sub-system 2.

$$\mathcal{L}_1(u_1, u_2) \approx \hat{\mathcal{L}_1}(u_1) \tag{2.2}$$

Therefore, equations (2.1) can be rewritten as:

$$\begin{aligned} \frac{du_1}{dt} &\approx \hat{\mathcal{L}_1}(u_1) \Rightarrow u_1(t) \\ \frac{du_2}{dt} &= \mathcal{L}_2(u_1(t), u_2) \end{aligned} \tag{2.3}$$

2.3 Solution schemes

2.3.1 Monolithic approach

Consider the interaction between two scalar fields u_1 and u_2 , where each field has only one state variable $u_1(t)$ and $u_2(t)$. The monolithic scheme consists of resolving simultaneously the fields equations $u(t)$ (in u_1 and u_2) in one step (whether implicit or explicit), where u(t) is defined as:

$$\{u(t)\} = \{u_1(t), u_2(t)\}^T \tag{2.4}$$

$$\{u(0)\} = \{u_0\} \tag{2.5}$$

$$\frac{d\{u\}}{dt} = \mathcal{L}(\{u\}) \tag{2.6}$$

Therefore, we obtain a complex system with a very large size, but have the benefit to be unconditional stable for implicit algorithms, meaning that we can go for larger time steps without affecting the stability of the system. On the other hand, explicit algorithms lead to conditional stability, which means

that the stability of the system is influenced by the size of time step, the time step shall be less than a critical time step $\Delta t < \Delta t_{crit}$. If we denote Δt_{crit1} the critical time step for the stability of the sub-system 1, and Δt_{crit2} the critical time step for the stability of the sub-system 2, $\min(\Delta t_{crit1}, \Delta t_{crit2})$ may be $<< \max(\Delta t_{crit1}, \Delta t_{crit2})$. Moreover, for a monolithic system, the critical time step for the whole system Δt_{crit} can be even smaller than the smallest critical time steps of each subsystem, that is $\Delta t_{crit} << \min(\Delta t_{crit1}, \Delta t_{crit2})$. The system obtained is very large, and the tangent matrix has the following form:

$$\begin{bmatrix} \frac{\partial \mathcal{L}_1}{\partial u_1} & \frac{\partial \mathcal{L}_1}{\partial u_2} \\ \frac{\partial \mathcal{L}_2}{\partial u_1} & \frac{\partial \mathcal{L}_2}{\partial u_2} \end{bmatrix} \tag{2.7}$$

The system obtained is generally non-symmetric due to the coupling terms of $\frac{\partial \mathcal{L}_1}{\partial u_2}$ and $\frac{\partial \mathcal{L}_2}{\partial u_1}$, and this leads to high computational cost generated by the inversion of the tangent matrix, especially when the coupling is strong, where the sub-diagonal matrices should be taken into account. In fact, when coupling is weak, these matrices can be neglected. Strong coupling may influence convergence, but not inversion time with direct solvers.

2.3.2 Staggered approach

The goal of a staggered scheme is to split the coupled problem into a set of sub-problems, therefore the staggered scheme (also called partitioned (without a fixed point)) solves different fields separately $\mathcal{L}(\{u\}) = \mathcal{L}_2(\{u\}) + \mathcal{L}_1(\{u\})$. The system becomes simpler due to the reduction of degrees of freedom of each sub-system. Some of the advantages is that we can use the best algorithm of resolution for each sub-system, the best discretization for each sub-system and may use the best time increments for each sub-system [25] (which is not so obvious in practice). One of the disadvantages is that a staggered scheme is not always stable [3]. In case of thermo-mechanical problems, staggered approach can be accomplished in two ways. First, the isothermal staggered scheme in which mechanical part is solved considering isothermal condition for thermal part. Second, the adiabatic staggered scheme in which mechanical part is solved considering adiabatic condition for the thermal part. These approached are examined in detail in the following section.

2.4 Introduction to thermo-mechanics

2.4.1 Balance equations

Let us begin by recalling the continuum balance equations. In the following, $\mathbf{u}$ is the displacement field, T is the external temperature, Θ is the internal temperature and $\mathbf{F}$ is the deformation gradient tensor: $\mathbf{grad}(\mathbf{u})$.

Principle of mass conservation states that mass can neither be created nor be destroyed. Therefore, mass of a material point dm always remains the same.

$$dm = \rho_0 dV_0 = \rho dV \tag{2.8}$$

where ρ_0 is the initial material density, dV_0 is the initial volume, ρ is the material density and dV is the volume of the material point after deformation. Equation (2.8) can be rewritten in terms of the deformation gradient tensor $\mathbf{F}$ as follows:

$$\rho \det[\mathbf{F}] = \rho_0 \tag{2.9}$$

where, $\det[\mathbf{F}]$ represents the change in volume of the material point.

Principle of conservation of linear momentum is obtained from Newton's second law of motion which states that sum of the forces acting on a body is equal to the rate of change of momentum of the body, which yeilds in local form:

$$\rho\dot{\mathbf{v}} = \rho\mathbf{b} + \mathbf{div}\{\boldsymbol{\sigma}\} \tag{2.10}$$

where $\mathbf{v}$ is the velocity of the particle, $\mathbf{b}$ are the applied body forces and $\boldsymbol{\sigma}$ is the Cauchy stress tensor, the divergence of which gives internal forces.

Conservation of angular momentum imposes that Cauchy stress tensor $\boldsymbol{\sigma}$ should be symmetric. That is,

$$\boldsymbol{\sigma} = \boldsymbol{\sigma}^T \tag{2.11}$$

or equivalently,

$$\mathbf{P}\mathbf{F}^T = \mathbf{F}\mathbf{P}^T \tag{2.12}$$

where, $\mathbf{P}$ is the first Piola-Kirchchoff stress tensor.

The first law of thermodynamics states that energy can be transformed, but cannot be created nor destroyed. It is usually formulated as a balance of internal energy by stating that the change in the internal energy of a system is equal to the amount of heat supplied to the system, minus the amount of work performed by the system on its surroundings, in other words it is a transformation from heat energy to mechanical energy and vice-versa. It can be written as:

$$\rho \dot{U} = \boldsymbol{P} : \dot{\mathbf{F}} + \rho_0 r - \mathrm{div}_0\{\mathbf{q}\} \tag{2.13}$$

where U is the internal energy density (per unit volume), $\mathbf{q}$ is the heat flux, and div_0 is divergence with respect to reference co-ordinates.

The second law of thermodynamics is rather an evolution principle than a balance law. It is an expression of the tendency that over time, differences in temperature, pressure, and chemical potential equilibrate in an isolated physical system. From the state of thermodynamic equilibrium, the law deduced the principle of the increase of entropy and explains the phenomenon of irreversibility in nature. The first law of thermodynamics provides the basic definition of thermodynamic energy (or internal energy), associated with all thermodynamic systems, and states the rule of conservation of energy in nature. However, the concept of energy in the first law does not account for the observation that natural processes have a preferred direction of progress. For example, spontaneously, heat always flows to regions of lower temperature, never to regions of higher temperature without external work being performed on the system. The first law is completely symmetrical with respect to the initial and final states of an evolving system. The key concept for the explanation of this phenomenon through the second law of thermodynamics is the definition of a new physical property, the entropy S, defined as :

$$S = \int_\Omega \rho \eta d\Omega \tag{2.14}$$

where η is the specific entropy. The second law of thermodynamics can be represented as follows:

$$\dot{S} - \int_\Omega \frac{\rho r}{T} d\Omega - \int_{\partial\Omega} \frac{\mathbf{q} \cdot \mathbf{n}}{T} dS \geq 0 \tag{2.15}$$

which can be rewritten as:

$$\int_{\Omega} \left\{ \rho\dot{\eta} - \frac{\rho r}{T} + \text{div}\left(\frac{\mathbf{q}}{T}\right) \right\} d\Omega \geq 0 \tag{2.16}$$

As the domain Ω is arbitrary, one can obtain Clausius-Duhem inequality from equation (2.16) and (2.13) as follows:

$$\dot{\Gamma}T = \rho T\dot{\eta} + \boldsymbol{\sigma} : \mathbf{D} - \rho\dot{U} - \frac{1}{T}\mathbf{q} \cdot \mathbf{grad}\{T\} \geq 0 \tag{2.17}$$

where $\dot{\Gamma}T$ represents the dissipated power.

2.4.2 Thermo-elasticity example

As an example of a strongly coupled thermo-mechanical problem, let us consider thermo-elasticity. In this case, the stress tensor $\boldsymbol{\sigma}$ is related to both, the elastic strain $\boldsymbol{\epsilon}$ and temperature rise $\theta = T - T_{ref}$ as follows:

$$\boldsymbol{\sigma} = \mathbf{E} : (\boldsymbol{\epsilon} - \boldsymbol{\alpha}\theta) \tag{2.18}$$

where $\mathbf{E}$ is the elasticity tensor, T_{ref} a reference temperature, and $\boldsymbol{\alpha}$ is the coefficient of thermal expansion tensor. Rise in temperature causes the material to expand without inducing any stress. Therefore, strain responsible for stress in the body is the difference between the total strain and strain caused due to the thermal expansion of the material. This very phenomenon is explained by the equation (2.18). Now, one can write the linear momentum conservation equation (2.10) for thermo-elasticity as follows:

$$\rho\dot{\mathbf{v}} = \mathbf{div}\left\{\mathbf{E} : (\boldsymbol{\epsilon} - \boldsymbol{\alpha}\theta)\right\} + \rho\mathbf{b} \tag{2.19}$$

Equation (2.19) represents the effect of thermal part on the mechanical part for thermo-elasticity. On the other hand, expansion of material causes its temperature to decrease and contraction causes its temperature to rise. One can write the thermal problem as follows in order to incorporate this effect:

$$\tilde{c}\,\dot{\theta} = \text{div}\{\tilde{\mathbf{K}} \cdot \mathbf{grad}(\theta)\} - \boldsymbol{\alpha} : \mathbf{E} : \dot{\boldsymbol{\epsilon}} + \frac{r}{T_{ref}} \tag{2.20}$$

where r is the external heat source, c is the heat capacity and $\tilde{c} = \frac{c}{T_{ref}}$, similarly, $\mathbf{K}$ is the thermal conductivity tensor and $\tilde{\mathbf{K}} = \frac{\mathbf{K}}{T_{ref}}$. Equations

(2.19) and (2.20) represent the strong form of coupled thermo-mechanical problem.[1] One can obtain the weak form easily by multiplying the equations with test functions and integrating over the domain. For time integration, one can consider Newmark scheme:

$$\begin{aligned}\mathbf{a}_{n+1} &= \frac{\mathbf{u}_{n+1}-\mathbf{u}_n}{\beta\Delta t^2} - \frac{\mathbf{v}_n}{\beta\Delta t} - \frac{0.5-\beta}{\beta}\mathbf{a}_n \\ \mathbf{v}_{n+1} &= \mathbf{v}_n + (1-\gamma)\Delta t\mathbf{a}_n + \gamma\Delta t\mathbf{a}_{n+1}\end{aligned} \tag{2.21}$$

here subscripts represent time step considered, $\mathbf{a} = \dot{\mathbf{v}} = \ddot{\mathbf{u}}$ the acceleration, β and γ are the algorithm parameters. For good stability, integration parameters are chosen as $\beta = \frac{1}{4}$ and $\gamma = \frac{1}{2}$. For finite element space discretization, we consider finite element interpolation:

$$\begin{aligned}\mathbf{u} &= \sum_{i=1}^{Nnodes} N_i(\mathbf{x})\mathbf{u}_i \\ \theta &= \sum_{i=1}^{Nnodes} N_i(\mathbf{x})\theta_i\end{aligned} \tag{2.22}$$

where $N_i(\mathbf{x})$ are the nodal shape functions, $\mathbf{u}_i$ are nodal displacements and θ_i are nodal temperatures. Mass matrix can be given from finite element interpolation as a function of shape function matrix $[N^e]$ as follows:

$$[M^e] = \sum_{i=1}^{nElements} \int_{\Omega^e} \rho[N^e]^T[N^e]d\Omega \tag{2.23}$$

The stiffness matrix is given as derivative of shape function matrix with respect to spatial coordinates $[D^e]$:

$$[E] = \sum_{i=1}^{nElements} \int_{\Omega^e} [D^e]^T[E][D^e]d\Omega \tag{2.24}$$

[1] A more formal derivation of these equations will be provided in chapter 3.

In case of thermo-elasticity problem we have the coupling matrix given as follows:

$$[B] = \sum_{i=1}^{nElements} - \int_{\Omega^e} [D^e]^T [\alpha E][N^e] d\Omega \tag{2.25}$$

Capacity matrix is similar to mass matrix and it is given by:

$$[\tilde{C}] = \sum_{i=1}^{nElements} \int_{\Omega^e} \frac{c}{T_{ref}} [N^e]^T [N^e] d\Omega \tag{2.26}$$

Conductivity matrix is similar to stiffness matrix and is given by:

$$[\tilde{K}] = \sum_{i=1}^{nElements} \int_{\Omega^e} \frac{1}{T_{ref}} [D^e]^T [K][D^e] d\Omega \tag{2.27}$$

Using the matrices defined above, the mechanical part of the finite element problem can be written as follows:

$$\frac{1}{\beta \Delta t^2}[M]\{u_{n+1}\} + [E]\{u_{n+1}\} + [B]\{\theta_{n+1}\} = \frac{1}{\beta \Delta t^2}[M]\{u_n\} + \frac{1}{\beta \Delta t}[M]\{\{v_n\} + (0.5 - \beta)\Delta t\{a_n\}\} + \{b\} + \{t\} \tag{2.28}$$

Whereas, the thermal problem is given as:

$$[B]^T\{u_{n+1}\} - [\tilde{C}]\{\theta_{n+1}\} - \Delta t[\tilde{K}]\{\theta_{n+1}\} = -[\tilde{C}]\{\theta_n\} + [B]^T\{u_n\} - \left\{\frac{r}{T_{ref}}\right\} + \frac{\Delta t}{T_{ref}}\{q_n\} \tag{2.29}$$

2.4.2.1 Monolithic approach

In the monolithic approach, we solve both the mechanical and thermal problems simultaneously. The problem can be stated as follows:

$$\begin{bmatrix} \frac{1}{\beta \Delta t^2}[M] + [E] & [B] \\ [B]^T & -[\tilde{C}] - \Delta t[\tilde{K}] \end{bmatrix} \begin{Bmatrix} \{u_{n+1}\} \\ \{\theta_{n+1}\} \end{Bmatrix} = \begin{Bmatrix} \{F_u\} \\ \{F_\theta\} \end{Bmatrix} \tag{2.30}$$

Where, $\{F_u\}$ and $\{F_\theta\}$ can be given as follows:

$$\{F_u\} = \frac{[M]}{\beta\Delta t^2}\{u_n\} + \frac{[M]}{\beta\Delta t}\{\{v_n\} + (0.5-\beta)\Delta t\{a_n\}\} + \{b\} + \{t\}$$
$$\{F_\theta\} = -[\tilde{C}]\{\theta_n\} + [B]^T\{u_n\} - \frac{\{r\}}{T_{ref}} + \frac{\Delta t}{T_{ref}}\{q_n\} \tag{2.31}$$

Velocity and acceleration can be given as represented by equation 2.21. As explained earlier, this approach is unconditionally stable. However, if one uses monolithic approach, the problem size is very big, therefore more computational power is needed. Another disadvantage is that one can not use two different meshes for mechanical and thermal part while using monolithic approach. This is mainly because of the inability to construct a single coupling matrix $[B]$ on two different meshes.

2.4.2.2 Staggered approach with isothermal split

In a staggered approach, thermal and mechanical problems are split and then are solved one by one. The simplest staggered technique is to consider isothermal split in which first the mechanical problem is solved assuming no variation in temperature and then the thermal problem is solved at fixed geometry:

$$\left[\frac{1}{\beta\Delta t^2}[M] + [E]\right]\{u_{n+1}\} = \{F_u\} - [B]\{\theta_n\} \tag{2.32}$$

$$\left[-[\tilde{C}] - \Delta t[\tilde{K}]\right]\{\theta_{n+1}\} = \{F_\theta\} - [B]^T\{u_{n+1}\} \tag{2.33}$$

The advantage of using isothermal split is that it is very simple to implement, one can use different meshes for mechanical and thermal part. This allows us to divide one big problem into two smaller problems. The main limitation of using isothermal split is that the algorithm is not unconditionally stable as shown by Simo et al.[3].

2.4.2.3 Staggered approach with adiabatic split

In order to have a stable algorithm, one can use an adiabatic split in which, while solving the mechanical part, adiabatic thermal conditions are assumed. It is represented as follows:

$$\begin{bmatrix} \frac{1}{\beta\Delta t^2}[M]+[E] & [B] \\ [B]^T & -[\tilde{C}]] \end{bmatrix} \begin{Bmatrix} \{u_{n+1}\} \\ \{\theta_{ad}\} \end{Bmatrix} = \begin{Bmatrix} \{F_u\} \\ \{F_\theta\} \end{Bmatrix} \tag{2.34}$$

$$\left[-[\tilde{C}]-\Delta t[\tilde{K}]\right]\{\theta_{n+1}\} = \{F_\theta\} - [B]^T\{u_{n+1}\} \tag{2.35}$$

Note that in the mechanical step, one does not need to calculate θ_{ad} since it is not needed in the calculations. This split makes the algorithm stable when used with a constant time step [3].

When using a staggered scheme with different meshes for mechanical and thermal part, first thermal fields need to be interpolated on mechanical mesh and then mechanical problem is solved. In this step, the coupling matrix $[B]$ is constructed only on the mechanical mesh. Then, the calculated displacement field $\{u_{n+1}\}$ is interpolated on the thermal mesh and then the thermal problem is solved. Here, the coupling matrix $[B]$ is constructed only on the thermal mesh. Note that we only perform interpolations from one mesh to the other, no extrapolations are performed.

2.5 Conclusion

This chapter introduced problems in multiphysics and relevant solution schemes in general. Weak coupling and strong coupling in multiphysics was presented. The problems of prime concern for us are strongly coupled problems where both physical phenomena influence each other.

Particularly, we focus on thermo-mechanical problems which were presented in the final section, with example of thermo-elasticity, monolithic and staggered approaches were presented. In this work, we are concerned with using two different meshes for mechanical and thermal parts in order to have separate mesh adaptation, therefore we only consider the staggered approach which allows separation of a coupled problem in subproblems related to each physical phenomena.

The proposed mesh adaptation is based on variational principle which is introduced in the following chapter.

Formulation variationnelle en thermo-mécanique couplée

L'algorithme d'adaptation de maillage proposé utilise un principe variationnel. Pour les problèmes simples impliquant un phénomène physique unique, le principe de l'énergie potentielle minimale constitue ce principe variationnel, l'énergie potentielle étant la fonctionnelle. Cependant, dans les problèmes complexes impliquant des variables internes et des problèmes thermomécaniques couplés, la fonctionnelle associée au principe variationnel n'est pas toujours évidente à identifier et nécessite une construction spécifique. Yang et al. [73] ont proposé une fonctionnelle basée sur une thermique à deux champs. Ces formulations variationnelles ont récemment été résumées par Stainier [66].

Il a été montré dans [73] qu'en utilisant deux idées clées, le problème aux valeurs limites et initiales thermomécanique peut être resymétrisé. Tout d'abord, une formulation thermique à deux champs permettant de séparer la température interne Θ et la température extérieure inconnue T dans l'équation d'énergie est introduite. L'égalité entre ces deux températures est imposée comme une liaison interne et relâchée dans l'équation de Gibbs. Deuxièmement, afin de trouver une forme variationnelle du problème général en taux, un facteur d'intégration permettant de restaurer la symétrie requise du système d'équations est identifié. Dans le travail de Yang et al. [73], les auteurs ont considéré un facteur d'intégration obtenu en effectuant un rééchelonnement temporel des processus en taux irréversibles.

En utilisant la fonctionnelle proposée, le problème thermo-mécanique apparaît comme un problème de type point selle. La fonctionnelle est convexe par rapport au champ de vitesse et concave par rapport au champ de température.

Puisque cette fonctionnelle est une quantité scalaire, et donc additive, elle est égale à la somme de toutes ses valeurs locales dans les éléments. Dans ce travail, cette caractéristique est exploitée pour l'adaptation de maillage. La valeur de la fonctionnelle est utilisée comme indicateur d'erreur.

Chapter 3

Variational formulation in coupled thermo mechanics

3.1 Introduction

The proposed mesh adaption algorithm is based on a variational principle. In case of simple problems involving single physical phenomenon, principle of minimum potential energy makes this variational functional evident. For example, steady state thermal problem can be described by the following potential:

$$\phi(T) = \frac{1}{2}\int_{\Omega} \boldsymbol{\nabla}(T) \cdot \mathbf{K} \cdot \boldsymbol{\nabla}(T) d\Omega - \int_{\Omega} rT d\Omega \tag{3.1}$$

where T is the temperature field, $\mathbf{K}$ is the conductivity tensor and r is the external heat source density. Taking the first variation of the above equation and equating to zero, one can easily recover weak form of a steady state thermal equation:

$$\int_{\Omega} \mathbf{K} \cdot \boldsymbol{\nabla}(T) \cdot \boldsymbol{\nabla}(\delta T) d\Omega = \int_{\Omega} r \cdot \delta T d\Omega \tag{3.2}$$

However, in complex problems involving internal variables and coupled thermo-mechanical processes, the variational functional is not evident and requires a specific construction.

Yang et al.[73] proposed a variational functional that uses a two-fields thermal construction. It allows to represent the thermo-mechanical problem as a saddle point optimization problem. In many cases, the functional

is convex in displacement and concave in temperature. These variational formulations were recently summarized by Stainier [66]. This chapter revisits these variational principles for thermo-elasticity, thermo-visco-elasticity and thermo-plasticity.

The structure of the chapter is as follows: the next section introduces continuum framework in which after introducing some concepts like free energy, a local problem at Gauss points is developed. It is followed by a variational boundary value problem in the continuum framework. In the third section, time discrete framework is presented, in which time is considered to have discrete increments. In this context, one needs to approximate the time integral of the function over the time step. The variational functional is incremental in this case and this allows to treat inertia terms in dynamics which is also introduced. The fourth section gives some examples of constitutive models in purely thermal transient problems, linear thermo-elasticity, plasticity and thermo-elasto-visco-plasticity. The last section details the algorithm for solving a strongly coupled thermo-mechanical problem using the presented variational principle.

3.2 Continuum modelling framework

3.2.1 Free energy and dissipation potential

The Helmholtz free energy density potential is defined from internal energy:

$$W = U - T\rho_0\eta \tag{3.3}$$

where η is the specific entropy and $\rho_0\eta$ is the nominal entropy density. The free energy can be represented in terms of state variables, deformation gradient tensor $\mathbf{F}$, temperature T and internal variables $\mathbf{Z}$.

$$W = W\left(\mathbf{F}, T, \mathbf{Z}\right) \tag{3.4}$$

On similar lines, a convex dissipation pseudo-potential ψ for generalized standard materials [28] is defined as:

$$\psi = \psi(\dot{\mathbf{F}}, \dot{\mathbf{Z}}; \mathbf{F}, T, \mathbf{Z}) \tag{3.5}$$

Forces conjugate to state variables are additively decomposed in equilibrium part derived from free energy (3.4), and dissipative part derived from dissipation pseudo-potential (3.5). The first Piola-Kirchchoff stress tensor is conjugate to deformation gradient tensor:

$$\mathbf{P} = \mathbf{P}^e + \mathbf{P}^d \tag{3.6}$$

where $\mathbf{P}^e$ and $\mathbf{P}^d$ are the equilibrium and dissipative part of $\mathbf{P}$ respectively given by:

$$\mathbf{P}^e = \frac{\partial W}{\partial \mathbf{F}}(\mathbf{F}, T, \mathbf{Z}) \tag{3.7}$$

$$\mathbf{P}^d = \frac{\partial \psi}{\partial \dot{\mathbf{F}}}(\dot{\mathbf{F}}, \dot{\mathbf{Z}}; \mathbf{F}, T, \mathbf{Z}) \tag{3.8}$$

similarly,

$$\mathbf{Y} = \mathbf{Y}^e + \mathbf{Y}^d \tag{3.9}$$

where $\mathbf{Y}$ is the force conjugate to internal variables $\mathbf{Z}$. Since they are associated to internal processes, these forces should not produce any work. i.e.:

$$\mathbf{Y} \cdot \dot{\mathbf{Z}} = \left(\mathbf{Y}^e + \mathbf{Y}^d\right) \dot{\mathbf{Z}} = 0, \forall \mathbf{Z} \tag{3.10}$$

Therefore, evolution laws for internal variables $\mathbf{Z}$ are obtained:

$$\frac{\partial W}{\partial \mathbf{Z}}(\mathbf{F}, T, \mathbf{Z}) + \frac{\partial \psi}{\partial \dot{\mathbf{Z}}}(\dot{\mathbf{F}}, \dot{\mathbf{Z}}; \mathbf{F}, T, \mathbf{Z}) = 0 \tag{3.11}$$

In this work, it is assumed that the local thermal equilibrium is always verified such that entropy η is given by:

$$\rho_0 \eta = -\frac{\partial W}{\partial T}(\mathbf{F}, T, \mathbf{Z}) \tag{3.12}$$

However for the purpose of writing a variational formulation, it is convenient to define an equilibrium temperature Θ, that is the temperature that satisfies local thermal equilibrium in terms of internal energy density:

$$\Theta = \frac{1}{\rho_0} \frac{\partial U}{\partial \eta}(\mathbf{F}, \eta, \mathbf{Z}) \tag{3.13}$$

which is *a priori* independent of the external temperature T.

3.2.2 Local evolution problem

The variational formulation of thermo-mechanical boundary value problems consist of a functional admitting a saddle point involving internal variables $\mathbf{Z}$ and external fields, i.e. displacement $\mathbf{u}$ and temperature T. Since, the optimality of the functional with respect to internal variables involves local quantities defined at the scale of material point, while its optimality with respect to external fields involve quantities defined on the whole domain Ω, both can be described separately. In this subsection, evolution of internal variables is considered, in the next subsection, evolution of external fields will be considered.

Let's consider a material point, the set of constitutive equations for a nonlinear dissipative model can admit a variational principle by defining the following functional:

$$D(\dot{\mathbf{F}}, \dot{\eta}, \dot{\mathbf{Z}}, T; \mathbf{F}, \eta, \mathbf{Z}) = \frac{d}{dt}[U(\mathbf{F}, \eta, \mathbf{Z})] - \rho_0 \dot{\eta} T + \psi \left(\dot{\mathbf{F}}, \dot{\mathbf{Z}}; \mathbf{F}, \Theta(\mathbf{F}, \eta, \mathbf{Z}), \mathbf{Z}\right) \tag{3.14}$$

In the above equation, Θ is the equilibrium or internal temperature defined by equation (3.13). Using equation (3.3), one can rewrite the above equation in terms of free energy W as follows:

$$D(\dot{\mathbf{F}}, \dot{\eta}, \dot{\mathbf{Z}}, T; \mathbf{F}, \eta, \mathbf{Z}) = \frac{d}{dt}[W(\mathbf{F}, T, \mathbf{Z})] + \rho_0 \eta \dot{T} + \psi \left(\dot{\mathbf{F}}, \dot{\mathbf{Z}}; \mathbf{F}, \Theta(\mathbf{F}, \eta, \mathbf{Z}), \mathbf{Z}\right) \tag{3.15}$$

Notice that the functional D can be interpreted as the sum of the reversible power per unit volume received by the system $\dot{w}_\tau$:

$$\dot{w}_\tau = \frac{d}{dt}[U(\mathbf{F}, \eta, \mathbf{Z})] - \rho_0 \dot{\eta} T = \frac{d}{dt}[W(\mathbf{F}, T, \mathbf{Z})] + \rho_0 \eta \dot{T} \tag{3.16}$$

and the dissipation potential representing the power per unit volume that can be dissipated. Therefore, the functional D is the sum of the two homogeneous terms representing power per unit volume, one is associated to reversible processes, other is associated to irreversible processes.

The general rate problem does not have an obvious variational structure. Weak formulation obtained by multiplying balance equations of energy and linear momentum by admissible variation of fields does not derive from a

potential. It was shown in [73] that by using two key ideas, the thermo-mechanical initial boundary value problem can be made symmetric. First, a thermal two-fields formulation that allows to separate internal temperature Θ and unknown external temperature T in the energy equation is introduced. Equality between these two temperatures is enforced as an internal constraint and relaxed within the Gibbs' equation. Second, in order to find a variational form of the general rate problem, an integration factor that allows to recover the requisite symmetry of the system of equations needs to be identified. In the work of Yang et al.[73], the authors considered an integrating factor obtained by performing a time rescaling of irreversible rate processes. So, the pseudo dissipation potential ψ is written:

$$\psi = \psi(f(T,\Theta)\dot{\mathbf{F}}, f(T,\Theta)\dot{\mathbf{Z}}; \mathbf{F}, T, \mathbf{Z}) \tag{3.17}$$

so that the time is rescaled by the factor $f(T,\Theta)$. When external and internal temperatures match, there should be no time scaling. Therefore:

$$f(T,T) = 1 \tag{3.18}$$

As shown in [73], a symmetric weak form is obtained by using:

$$f(T,\Theta) = \frac{T}{\Theta} \tag{3.19}$$

Now, using this form of the dissipation potential in equation (3.17) and using the above definition of $f(T,\Theta)$, D can be rewritten as:

$$D(\dot{\mathbf{F}}, \dot{\eta}, \dot{\mathbf{Z}}, T; \mathbf{F}, \eta, \mathbf{Z}) = \frac{d}{dt}[U(\mathbf{F}, \eta, \mathbf{Z})] - \rho_0 \dot{\eta} T + \psi\left(\frac{T}{\Theta}\dot{\mathbf{F}}, \frac{T}{\Theta}\dot{\mathbf{Z}}; \mathbf{F}, \Theta, \mathbf{Z}\right) \tag{3.20}$$

The local thermal equilibrium imposes that $\Theta = T$, which corresponds to the stationarity of D with respect to $\dot{\eta}$:

$$\underset{\dot{\eta}}{\text{stat}} D(\dot{\mathbf{F}}, \dot{\eta}, \dot{\mathbf{Z}}, T; \mathbf{F}, \eta, \mathbf{Z}) \Leftrightarrow \frac{\partial U}{\partial \eta} - \rho_0 T = 0 \Leftrightarrow T = \Theta(\mathbf{F}, T, \mathbf{Z}) \tag{3.21}$$

Stationarity of D with respect to $\dot{\mathbf{Z}}$ gives evolution laws, so that:

$$\dot{\mathbf{Z}} = \arg\inf_{\dot{\mathbf{Z}}} D(\dot{\mathbf{F}}, \dot{\eta}, \dot{\mathbf{Z}}, T; \mathbf{F}, \eta, \mathbf{Z}) \tag{3.22}$$

The effective value of D, that is the minimum value of D over $\dot{\mathbf{Z}}$ is represented by D_{eff}:

$$D_{\text{eff}}(\dot{\mathbf{F}}, \dot{\eta}, T; \mathbf{F}, \eta, \mathbf{Z}) = \inf_{\dot{\mathbf{Z}}} D(\dot{\mathbf{F}}, \dot{\eta}, \dot{\mathbf{Z}}, T; \mathbf{F}, \eta, \mathbf{Z}) \tag{3.23}$$

We recover the Piola-Kirchchoff stress tensor $\mathbf{P}$ by variation of D_{eff} with respect to $\dot{\mathbf{F}}$:

$$\frac{\partial D_{\text{eff}}}{\partial \dot{\mathbf{F}}} = \mathbf{P}^e + \mathbf{P}^d \tag{3.24}$$

where the dissipative part of $\mathbf{P}$ is given by scaled dissipation potential:

$$\mathbf{P}^d = \frac{T}{\Theta} \frac{\partial \psi}{\partial \dot{\mathbf{F}}} \tag{3.25}$$

whereas the variation with respect to external temperature T leads to:

$$\frac{\partial D_{\text{eff}}}{\partial T} = -\rho_0 \dot{\eta} + \frac{\mathcal{D}_{int}}{T} \tag{3.26}$$

where $\mathcal{D}_{int}$ is the energy dissipation caused by dissipative forces viz. $\mathbf{P}^d$ and $\mathbf{Y}^d$.

3.2.3 Variational formulation of the initial boundary value problem

The initial boundary value problem consists of the transient heat transfer problem plus a quasi-static mechanical one, and involves determining displacement field $\mathbf{u}$, temperature field T and internal variables $\mathbf{Z}$. For this, one needs to solve for momentum balance (2.10) without inertial terms, energy balance (2.13) and constitutive equation summarized by the potential D (3.20). We shall assume that the boundary $\partial\Omega$ of the domain Ω admits the decomposition:

$$\begin{aligned} \partial\Omega &= \partial\Omega_u \cup \partial\Omega_t \ ; \ \partial\Omega_u \cap \partial\Omega_t = \emptyset \\ \partial\Omega &= \partial\Omega_T \cup \partial\Omega_q \ ; \ \partial\Omega_T \cap \partial\Omega_q = \emptyset \end{aligned} \tag{3.27}$$

on which given boundary conditions $\mathbf{u} = \bar{\mathbf{u}}$ on $\partial_u\Omega$, $\boldsymbol{\sigma}\cdot\mathbf{n} = \bar{\mathbf{t}}$ on $\partial_t\Omega$, $T = \bar{T}$ on $\partial_T\Omega$ and $\mathbf{q}\cdot\mathbf{n} = \bar{q}$ on $\partial_q\Omega$, where $\bar{\mathbf{u}}$, $\bar{\mathbf{t}}$, $\bar{T}$ and $\bar{q}$ are the imposed displacement, applied traction, imposed temperature and applied head flux respectively.

As shown by Yang et al. [73], the variational functional for this boundary value problem is given by:

$$\begin{aligned}\Phi(\dot{\mathbf{u}},\dot{\eta},T) = \int_\Omega \left[D_{\text{eff}}(\dot{\mathbf{F}},\dot{\eta},T) - \chi\left(-\frac{\mathbf{grad}T}{T};\mathbf{F},\Theta(\mathbf{F},\eta,\mathbf{Z}),\mathbf{Z}\right)\right] d\Omega \\ + \int_\Omega \left[\rho r\frac{T}{\Theta} - \rho\mathbf{b}\cdot\dot{\mathbf{u}}\right] d\Omega - \int_{\partial_t\Omega}\bar{\mathbf{t}}\cdot\dot{\mathbf{u}}dS - \int_{\partial_q\Omega}\bar{q}\frac{T}{\Theta}dS \end{aligned} \tag{3.28}$$

Heat conduction potential (Biot) χ is given as follows:

$$\chi = \frac{\Theta}{2}\frac{\mathbf{grad}(T)}{T}\cdot\mathbf{K}\cdot\frac{\mathbf{grad}(T)}{T} \tag{3.29}$$

where $\mathbf{K}$ is the thermal conductivity tensor. Stationarity of Φ with respect to $\dot{\mathbf{u}}$ yields the balance equations of linear momentum (2.10) in its weak form:

$$< D_{\dot{\mathbf{u}}}\Phi, \delta\mathbf{u} >= -\int_\Omega \delta\mathbf{u}\cdot\{\boldsymbol{\nabla}_0\mathbf{P} + \rho\mathbf{b}\}\, d\Omega - \int_{\partial_t\Omega}\delta\mathbf{u}\cdot(\bar{\mathbf{t}} - \mathbf{P}\cdot\mathbf{n}) = 0 \tag{3.30}$$

and with respect to T yields the energy conservation equation (2.13) in its weak form:

$$\begin{aligned}< D_T\Phi, \delta T >= \int_\Omega \delta T\left\{-\rho_0\dot{\eta} + \frac{\mathcal{D}_{int}}{T}\right\} d\Omega + \int_\Omega \Theta\boldsymbol{\nabla}\left(\frac{\delta T}{T}\right)\cdot\mathbf{K}\cdot\frac{\boldsymbol{\nabla}(T)}{T}d\Omega \\ + \int_\Omega \frac{\rho r\delta T}{\Theta}d\Omega - \int_{\partial_q\Omega}\frac{\bar{q}\delta T}{\Theta} = 0\end{aligned} \tag{3.31}$$

Note that the factor $\frac{T}{\Theta}$ is obtained as unity through optimality with respect to $\dot{\eta}$.

3.3 Time discrete modelling framework

3.3.1 Local constitutive problem

Consider the discrete time increment $\Delta t = t - t_0$. It is assumed that the local material state at time t_0 i.e. $\{\mathbf{F}_0, \eta_0, \mathbf{Z}_0\}$ is completely known. In order to

compute internal variables $\mathbf{Z}$ given $\mathbf{F}$ and η at time t, we need to approximate the integral of the functional D in equation (3.20) over the time increment Δt:

$$\mathscr{I}(\mathbf{F}, T, \mathbf{Z}; \mathbf{F}_0, T_0, \mathbf{Z}_0) \approx \int_{t_0}^{t} D(\dot{\mathbf{F}}, \dot{\eta}, \dot{\mathbf{Z}}, T(\tau); \mathbf{F}(\tau), \eta(\tau), \mathbf{Z}(\tau)) d\tau \tag{3.32}$$

Using the identity $\dot{U} - \rho_0 \dot{\eta} T = \dot{W} + \rho_0 \eta \dot{T}$, one can approximate the above integral as:

$$\mathscr{I} = W(\mathbf{F}, T, \mathbf{Z}) - W_0 + \rho_0 \eta_0 \Delta T + \Delta t \left\langle \psi \left(\frac{T}{T_0} \frac{\Delta \mathbf{F}}{\Delta t}, \frac{T}{T_0} \frac{\Delta \mathbf{Z}}{\Delta t}; \mathbf{F}(\tau), T(\tau), \mathbf{Z}(\tau) \right) \right\rangle \tag{3.33}$$

In the above equation, $\Delta(\cdot) = (\cdot) - (\cdot)_0$, $W_0 = W(\mathbf{F}_0, T_0, \mathbf{Z}_0)$ and factors $\frac{T}{\Theta}$ have been replaced by $\frac{T}{T_0}$ (Note that T_0 denotes here temperature at the beginning of timestep, not necessarily at $t = 0$). The last term on right hand side between brackets denotes a consistent average value of the dissipation function over the time increment Δt. An expression for this term that satisfies all the consistency conditions was proposed in [65]:

$$\left\langle \psi \left(\frac{T}{T_0} \frac{\Delta \mathbf{F}}{\Delta t}, \frac{T}{T_0} \frac{\Delta \mathbf{Z}}{\Delta t}; \mathbf{F}(\tau), T(\tau), \mathbf{Z}(\tau) \right) \right\rangle = \frac{T}{T_0} \psi \left(\frac{T}{T_0} \frac{\Delta \mathbf{F}}{\Delta t}, \frac{T}{T_0} \frac{\Delta \mathbf{Z}}{\Delta t}; \mathbf{F}_\alpha, T_0, \mathbf{Z}_\alpha \right) + \frac{\Delta T}{T} \psi \left(\frac{T}{T_0} \frac{\Delta \mathbf{F}}{\Delta t}, \frac{T}{T_0} \frac{\Delta \mathbf{Z}}{\Delta t}; \mathbf{F}_\alpha, T_\alpha, \mathbf{Z}_\alpha \right) \tag{3.34}$$

with algorithmic parameter $\alpha \in [0, 1]$. A detailed study of influence of parameter α on precision and convergence properties of variational update in case of elasto-visco-plasticity can be found in [14].

Now, the variational update for internal variables $\mathbf{Z}$, takes following minimization form:

$$\mathcal{W}(\mathbf{F}, T; \mathbf{F}_0, T_0, \mathbf{Z}_0) = \inf_{\mathbf{Z}} \mathscr{I}(\mathbf{F}, T, \mathbf{Z}; \mathbf{F}_0, T_0, \mathbf{Z}_0) \tag{3.35}$$

That is:

$$\frac{\partial W}{\partial \mathbf{Z}} + \frac{T}{T_0} \frac{\partial}{\partial \dot{\mathbf{Z}}} \left\langle \psi \left(\frac{T}{T_0} \frac{\Delta \mathbf{F}}{\Delta t}, \frac{T}{T_0} \frac{\Delta \mathbf{Z}}{\Delta t} \right) \right\rangle = 0 \tag{3.36}$$

and

$$\lim_{\Delta t \to 0} \frac{\partial}{\partial \dot{\mathbf{Z}}} \left\langle \psi \left(\frac{T}{T_0} \frac{\Delta \mathbf{F}}{\Delta t}, \frac{T}{T_0} \frac{\Delta \mathbf{Z}}{\Delta t} \right) \right\rangle = \frac{\partial \psi}{\partial \dot{\mathbf{Z}}} \left(\dot{\mathbf{F}}, \dot{\mathbf{Z}} \right) \tag{3.37}$$

Hence, provided external fields $\{\mathbf{F}, T\}$, the internal variables $\mathbf{Z}$ can be computed at each integration point at each discrete time step.

3.3.2 Incremental boundary value problem

Now consider discrete time increment for the variational boundary value problem in order to compute external fields $\{\mathbf{u}, T\}$ at each time step. Here, one needs to approximate the integral of the functional Φ (3.28) over time increment Δt:

$$\begin{aligned} I(\mathbf{u}, T) = &\int_\Omega \left[\mathcal{W}(\mathbf{F}, T; \mathbf{F}_0, T_0, \mathbf{Z}_0) - \Delta t \left\langle \chi \left(-\frac{\mathbf{grad} T}{T}; \mathbf{F}(\tau), T(\tau), \mathbf{Z}(\tau) \right) \right\rangle \right] d\Omega \\ &+ \int_\Omega \left[\Delta t \ \rho \ r \log \frac{T}{T_0} - \rho \mathbf{b} \cdot \Delta \mathbf{u} \right] d\Omega - \int_{\partial_t \Omega} \bar{\mathbf{t}} \cdot \Delta \mathbf{u} dS - \int_{\partial_q \Omega} \Delta t \ \bar{q} \ \log \frac{T}{T_0} \ dS \end{aligned} \tag{3.38}$$

here, the average conduction dissipation potential $\langle \chi \rangle$ can be treated in a similar fashion as that of the dissipation potential $\langle \psi \rangle$ in the previous subsection. Thus, external fields $\{\mathbf{u}, T\}$ can be computed as optimizers of the above functional $I(\mathbf{u}, T)$ (3.38).

$$\{\mathbf{u}, T\} = \arg \operatorname*{stat}_{\mathbf{u}, T} I(\mathbf{u}, T) \tag{3.39}$$

Except for the cases of material instabilities like buckling, the incremental potential $\mathcal{W}(\mathbf{F}, T)$ is normally a convex function of $\mathbf{F}$ and concave function of T. Therefore, solution fields can be characterized as a saddle point of the incremental functional:

$$\{\mathbf{u}, T\} = \arg \inf_{\mathbf{u}} \sup_{T} I(\mathbf{u}, T) \tag{3.40}$$

By repeating this optimization problem at each time step, taking results of the previous time step as initial conditions $\{\mathbf{u}_0, T_0, \mathbf{Z}_0\}$ for the current time

step, the evolution of thermo-mechanical systems can be computed. Note that this problem yields a unique solution even in large strain framework because of the convexity of the functional with respect to displacement field and concavity with respect to the temperature field. However, this doesn't hold true for instabilities like buckling.

3.3.3 Dynamics

The introduction of inertia terms in the variational formulation is only possible in the discrete time setting and in order to incorporate inertia terms in the functional I (3.38), a specific time discretization (here Newmark) needs to be embedded within the formulation. One can overcome this difficulty, by extending approach proposed in [58] in isothermal context. However, functional I in equation (3.38) accounts for transient thermal effects and rate dependent behaviour. The modified functional I in order to take into account inertia terms is given as [66]:

$$I(\mathbf{u},T) = \int_\Omega \left[\frac{\rho}{2\beta\Delta t^2}\Delta\mathbf{u}\cdot\Delta\mathbf{u} + \mathcal{W}(\mathbf{F},T) - \Delta t \left\langle \chi\left(-\frac{\mathbf{grad}T}{T};\mathbf{F}(\tau),T(\tau),\mathbf{Z}(\tau)\right)\right\rangle \right] d\Omega$$
$$+ \int_\Omega \left[\Delta t\ \rho\ r \log\frac{T}{T_0} - \rho\mathbf{b}^*\cdot\Delta\mathbf{u}\right] d\Omega - \int_{\partial_t\Omega} \bar{\mathbf{t}}\cdot\Delta\mathbf{u} dS - \int_{\partial_q\Omega} \Delta t\ \bar{q}\ \log\frac{T}{T_0}\ dS \tag{3.41}$$

In the above equation, $\mathbf{b}^* = \mathbf{b} - \frac{1}{\beta\Delta t}(\dot{u}_0 + (\frac{1}{2}-\beta)\Delta t\ddot{u}_0)$. Thus, the incremental boundary value problem takes the variational form:

$$\{\mathbf{u},T\} = \arg\ \inf_{\mathbf{u}}\ \sup_{T}\ I(\mathbf{u},T) \tag{3.42}$$

Combined with following update rule for accelerations and velocities:

$$\ddot{\mathbf{u}} = \frac{\frac{1}{2}-\beta}{\beta}\ddot{\mathbf{u}}_0 + \frac{1}{\beta\Delta t}\dot{\mathbf{u}}_0 + \frac{\Delta\mathbf{u}}{\beta\Delta t^2} \tag{3.43}$$

$$\dot{\mathbf{u}} = \dot{\mathbf{u}}_0 + (1-\gamma)\Delta t\ddot{\mathbf{u}}_0 + \gamma\Delta t\ddot{\mathbf{u}} \tag{3.44}$$

the stationary condition with respect to $\mathbf{u}$ yields a discrete conservation of momentum equation corresponding to classical Newmark integration scheme of dynamics.

The classical Newmark scheme is typically used with parameters $\beta = \frac{1}{4}$ and $\gamma = \frac{1}{2}$ in implicit dynamics so that unconditional stability in linear elasto-dynamics is ensured.

3.4 Examples of constitutive models

3.4.1 Purely thermal transient problem

In case of purely thermal problem, the incremental potential (3.38) takes the following form:

$$I(T) = \int_\Omega \left\{ \frac{C}{2\Delta t}(T_{n+1} - T_n)^2 + \frac{1}{2}\mathbf{grad}(T_{n+1}) \cdot \mathbf{K} \cdot \mathbf{grad}(T_{n+1}) - r(T_{n+1} - T_n) \right\} d\Omega \tag{3.45}$$

It is easy to see that the discrete weak form is obtained by taking the first variation of the functional above:

$$< DI, T^* >= \int_\Omega \left\{ \frac{C}{\Delta t}(T_{n+1} - T_n)T^* + \mathbf{grad}(T^*) \cdot \mathbf{K} \cdot \mathbf{grad}(T_{n+1}) - rT^* \right\} d\Omega = 0 \tag{3.46}$$

3.4.2 Linear thermo-elasticity

For linear thermo-elasticity, the Helmholtz free energy takes the form:

$$W(\boldsymbol{\epsilon}, T) = \frac{1}{2}\boldsymbol{\epsilon} : \mathbf{E} : \boldsymbol{\epsilon} - \boldsymbol{\epsilon} : \mathbf{E} : \boldsymbol{\alpha}(T - T_r) - \frac{1}{2}\rho_0 C \frac{(T - T_r)^2}{T_r} \tag{3.47}$$

where, $\mathbf{E}$ is the elasticity tensor, $\boldsymbol{\alpha}$ is thermal dilatation tensor, C is the specific heat capacity and T_r is the reference temperature. Denoting the temperature increment as $\theta = T - T_r$, the constitutive law reads:

$$\boldsymbol{\sigma} = \frac{\partial(W)}{\partial \boldsymbol{\epsilon}} + 0 = \mathbf{E} : (\boldsymbol{\epsilon} - \boldsymbol{\alpha}\theta) \tag{3.48}$$

$$\rho_0 \eta = -\frac{\partial W}{\partial T} = \rho_0 C \frac{\Theta}{T_r} \tag{3.49}$$

The incremental variational functional (3.41) takes the following form:

$$I(\mathbf{u}_{n+1},\theta_{n+1}) = \int_\Omega \left[\frac{\rho}{2\beta}\left(\frac{\Delta\mathbf{u}}{\Delta t}\right)^2 + W(\boldsymbol{\epsilon}_{n+1},\theta_{n+1}) - W(\boldsymbol{\epsilon}_n,\theta_n) + \eta_n\Delta\theta \right.$$
$$\left. - \frac{\rho}{\beta}\left(\mathbf{v}_n + \left(\frac{1}{2}-\beta\right)\Delta t\ \mathbf{a}_n\right)\frac{\Delta\mathbf{u}}{\Delta t} - \Delta t\ \chi(\theta_{n+1}) + \Delta t\frac{r}{T_r}\Delta\theta - b\Delta\mathbf{u}\right] d\Omega$$
$$- \int_{\partial_t\Omega} \mathbf{t}\cdot\Delta\mathbf{u} dS - \int_{\partial_q\Omega} \bar{q}\frac{\Delta\theta}{T_r} dS \quad (3.50)$$

Taking first variation of the above functional with respect to displacement field i.e. $< D_{\mathbf{u}_{n+1}} I, \mathbf{u}^* >$, one can obtain the mechanical discrete equations (2.28). Similarly the first variation with respect to the temperature field i.e. $< D_{\theta_{n+1}} I, \theta^* >$, gives the thermal discrete equations (2.29).

3.4.3 Thermo-elasto-visco-plasticity

In case of thermo-elasto-visco-plasticity in small strains and displacements, the strain $\boldsymbol{\epsilon}$ is split into elastic and plastic part $\boldsymbol{\epsilon} = \boldsymbol{\epsilon}^e + \boldsymbol{\epsilon}^p$. The plastic part $\boldsymbol{\epsilon}^p$ of the strain tensor is treated as an internal variable. Note that in case of finite strains, a multiplicative split between elastic and plastic deformation tensors is considered $\mathbf{F} = \mathbf{F}^e\mathbf{F}^p$. However, for the sake of simplicity of presentation, only the small strain case is described in this subsection. The free energy in this case is defined as:

$$W(\boldsymbol{\epsilon},\boldsymbol{\epsilon}^p,T) = W^e(\boldsymbol{\epsilon}-\boldsymbol{\epsilon}^p,T) + W^p(\boldsymbol{\epsilon}^p,T) + W^t(T) \quad (3.51)$$

where W^e is the elastically stored energy (recoverable), W^p is the plastically stored energy (not directly recoverable) and W^t the thermally stored energy (heat capacity). Then the reversible stress $\boldsymbol{\sigma}^{rev}$ is given by:

$$\boldsymbol{\sigma}^{rev} = \frac{\partial W}{\partial \boldsymbol{\epsilon}} = \frac{\partial W^e}{\partial \boldsymbol{\epsilon}} = \mathbf{E} : ((\boldsymbol{\epsilon}-\boldsymbol{\epsilon}^p) - \boldsymbol{\alpha}\theta) \quad (3.52)$$

Denoting the back stress by $\boldsymbol{\sigma}^c \equiv \frac{\partial W^p}{\partial \boldsymbol{\epsilon}^p}$, the mechanical dissipation D^*_{mech} can be given by:

$$D^*_{mech} = -\frac{\partial W}{\partial \boldsymbol{\epsilon}^p} : \dot{\boldsymbol{\epsilon}}^p = \left(\frac{\partial W^e}{\partial \boldsymbol{\epsilon}^e} - \frac{\partial W^p}{\partial \boldsymbol{\epsilon}^p}\right) : \dot{\boldsymbol{\epsilon}}^p = (\boldsymbol{\sigma}-\boldsymbol{\sigma}^c) : \dot{\boldsymbol{\epsilon}}^p \quad (3.53)$$

A plastic flow rule corresponding to von Mises-type plasticity reads:

$$\dot{\boldsymbol{\epsilon}^p} = \dot{\overline{\epsilon}^p}\mathbf{M} \tag{3.54}$$

where $\dot{\overline{\epsilon}^p}$ is the magnitude of equivalent plastic strain rate, and $\mathbf{M}$ its direction. The dissipation potential $\psi(\dot{\overline{\epsilon}^p}; \overline{\epsilon}^p, T)$ takes the general form:

$$\psi(\dot{\overline{\epsilon}^p}; \overline{\epsilon}^p, T) = \begin{cases} \varkappa(\dot{\overline{\epsilon}^p}; \overline{\epsilon}^p, T) & \text{if } \dot{\overline{\epsilon}^p} \geq 0 \\ +\infty & \text{otherwise} \end{cases} \tag{3.55}$$

where $\varkappa$ is a convex function of its argument, and such that $\varkappa(0; \overline{\epsilon}^p, T) = 0$ and $\partial_{\dot{\overline{\epsilon}^p}} \varkappa(0; \overline{\epsilon}^p, T) = \sigma_Y(\overline{\epsilon}^p, T) \geq 0$. As an example, ψ can be considered as:

$$\psi = \sigma_Y |\dot{\overline{\epsilon}^p}| \tag{3.56}$$

3.5 Staggered algorithms

As seen in this chapter, one can transform a coupled thermo-mechanical problem into an optimization problem using a variational formulation. It can indeed be used to solve the problem using a staggered approach. First, a mechanical problem is solved in which functional $I(\mathbf{u}, T)$ in equation (3.41) is minimized with respect to displacement field $\mathbf{u}$. During this step, a local optimization problem (3.35) is solved at each Gauss point and internal variables $\mathbf{Z}$ are updated. One can use either isothermal setting or adiabatic setting during this step. Once a solution for displacement field is obtained, thermal problem can be solved. Now the functional $I(\mathbf{u}, T)$ is maximized with respect to temperature field T. Again, a local optimization problem (3.35) is solved at each Gauss point during the computation and internal variables $\mathbf{Z}$ are updated.

The above algorithm needs to use smaller time steps because the effect of thermal problem on the mechanical field is lagged by a time step. Indeed, one can imagine using thermal problem prior to mechanical one, in this case effect of mechanical problem on thermal field is lagged by a time step. In case of weak coupling, the independent physical phenomenon can be solved first so that there is no lag. In order to be able to use larger time steps, one

Algorithm 1 A general algorithm for staggered resolution of thermo-mechanical problem using a variational approach.

1: **for** n= start time to n= end time (Time loop) **do**
2: Mechanical Problem
3: **while** Convergence is obtained, iterate k **do**
4: find $\mathbf{u}_n^k$ by minimizing functional $I(\mathbf{u}_n^k, T_{n-1})$
5: during the computation update $\mathbf{Z}_n^k$ at each Gauss point by minimizing functional $\mathscr{I}(\mathbf{F}_n^k, T_{n-1}, \mathbf{Z}_n^k)$
6: **end while**
7: Thermal Problem
8: **while** Convergence is obtained, iterate k **do**
9: find T_n^k by maximizing functional $I(\mathbf{u}_n^k, T_n)$
10: during the computation update $\mathbf{Z}_n^k$ at each Gauss point by minimizing functional $\mathscr{I}(\mathbf{F}_n^k, T_n, \mathbf{Z}_n^k)$
11: **end while**
12: **end for**

can imagine an alternated version of time integration in which mechanical and thermal steps are iterated within a time step until convergence. This is a way to deal with lagged effect of one field on another. In our work we do not consider this alternated scheme.

The algorithm to solve thermo-mechanical problems for general dissipative solids using variational approach explained can be summarized as shown in algorithm 1.

Isothermal and adiabatic staggered schemes differ in the 4th and 5th step of the algorithm in algorithm 1. In these, an isothermal and adiabatic thermal conditions are respectively assumed locally (i.e. at each material point).

3.6 Conclusion

This chapter presented the variational formulations for coupled thermo-mechanical problems. It is seen that using the functional proposed, one can represent a thermo-mechanical problem as a saddle point problem. The functional is often convex in displacement and concave in temperature. Therefore the optimization for mechanical part is minimization and for the thermal part is maximization. In some problems that involve material instabilities,

such as buckling the convexity (or concavity) of functionals is not guaranteed. However, in this work, we are only concerned with cases when the convexity (or concavity) of the functionals is guaranteed. An important characteristic of the variational functional is that it is additive. That is, the global value of the energy like potential is a sum over all its local values over all elements. In this work, we intend to exploit this characteristic of the functional for mesh adaptation. The value of the functional is used as an indicator of error. This algorithm is explained in detail in the next chapter.

Algorithme d'adaptation de maillage

Comme expliqué précédemment, les stratégies d'adaptation de maillage dépendent des techniques d'adaptation qui affectent les aspects géométriques du maillage et des critères d'adaptation qui captent le phénomène physique sous-jacent.

Deux techniques d'adaptation basées sur la bisection de bord sont utilisées dans le présent travail. Tout d'abord, la technique de bisection à bord unique (SEB). Dans ce cas, un seul bord à diviser est identifié et divisé en deux pour que les triangles adjacents soient divisés en deux triangles chacun. Il n'y a aucune contrainte sur le rapport d'aspect de l'élément dans cette technique. Cela conduit à la génération de mailles anisotropes. Deuxièmement, la technique du chemin de propagation de bord le plus long de Rivara (LEPP). Dans cette technique, les bords plus longs sont divisés en deux fois par rapport aux plus courts. Cela donne une limite supérieure sur le rapport d'aspect de l'élément.

Le processus d'adaptation consiste à diviser la géométrie en plusieurs patchs. Sur chaque patch, la décision de l'affiner (ou pas) est prise en résolvant un problème thermomécanique sur sa version raffinée, puis en utilisant des critères basés sur la croissance (ou la décroissance) de la fonctionnelle énergétique calculée sur ce patch. Ce processus est poursuivi de façon récursive jusqu'à ce qu'une tolérance soit satisfaite, et pour chaque patch. L'ensemble des patchs (raffinés ou non) recouvrant le domaine de calcul constitue dès lors le nouveau maillage sur lequel le problème global est résolu à nouveau. Ce processus est itéré jusqu'à convergence. La convergence

est définie par un critère basé encore sur un incrément de la fonctionnelle énergétique.

Chapter 4

Mesh adaptation Algorithm

4.1 Introduction

As explained in the first chapter, mesh adaption strategies depend on adaptive techniques and adaption criteria. Adaptive techniques essentially deal with geometric aspects of adaption. The objective of the thesis is to propose a mesh adaption algorithm that avoids complex remapping procedures to transfer internal variable data from one mesh to other. For r-adaption [56], where the number of nodes are the same but their location and connectivity is changed, remapping procedures can incur a lot of numerical diffusion. Hence, the proposed approach is essentially for h-adaption [21] techniques based on edge bisection. The basic idea can easily be extended for p-adaption [52].

The proposed algorithm exploits the additive property of the variational functional. Variational functional is additive, that is all the local values of the potential sum up to give the global value. Therefore, improvement in the local value of the potential leads to the improvement in the global value of the energy like potential. This allows to decompose the domain of computation in a number of different patches and apply local refinement techniques to these patches to improve the local values of energy-like potential. In this way, domains of interest can be identified and can be refined by using local refinement techniques.

In next section, mesh adaptation techniques are presented. All the techniques are presented in 2D. The third section details the mesh adaptation

criteria including refinement and coarsening strategies. The technique for mesh coarsening is also presented. Management of internal variables is a very important aspect of mesh adaptation and is dealt with in the fourth section.

4.2 Local adaptation techniques

Two adaption techniques based on edge bisection are used in the present work. First, the single edge bisection (SEB) technique and second, Rivara's Longest Edge Propagation Path (LEPP) technique [62, 61].

4.2.1 Single Edge Bisection technique (SEB)

In this technique, a single edge to be bisected is identified. The patch then consists of the ring of elements around this edge. If the edge is on the boundary, the patch will consist of a single element, otherwise, the patch will contain two elements. The refined version of the patch contains the bisected edge. For $P1$ elements, one patch introduces only one new node as shown in figures 4.1 and 4.2. For $P2$ elements, if the target edge is on the boundary, three new nodes are added as shown in figure 4.4, otherwise four new nodes are added as shown in figure 4.3.

The advantage of this technique is that it is a very simple technique and no constraints are imposed on the geometrical properties of the mesh. Therefore, only mesh adaption criteria drives the mesh adaption and coarsening. The drawback is that there is no bound on the element aspect ratio, therefore meshes obtained tend to be anisotropic. Hence, this technique allows to obtain differing degrees of spatial resolution in different directions suitable for the problem under investigation at the cost of elongated elements.

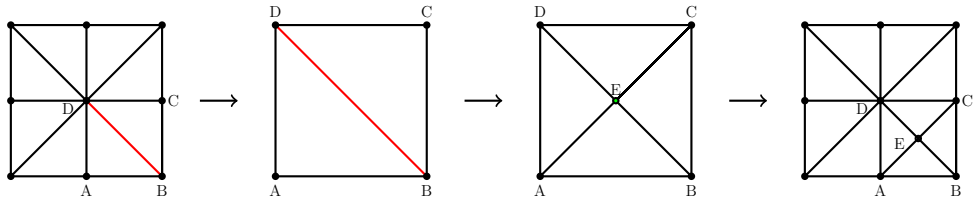

Figure 4.1: The edge identified is BD. Therefore, the patch contains two elements adjacent to edge BD. The refined version of patch contains the new node E.

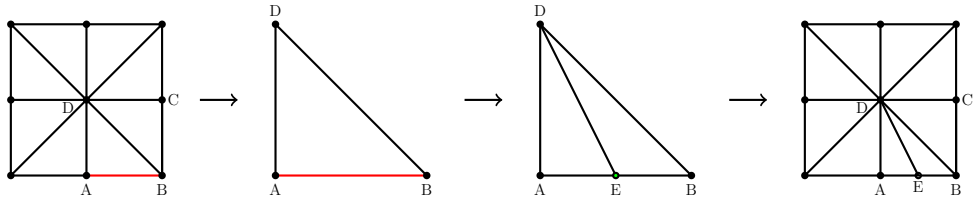

Figure 4.2: The edge identified is AB, which is on the boundary. Therefore, the patch contains a single element DAB. The refined version of the patch contains the new node E.

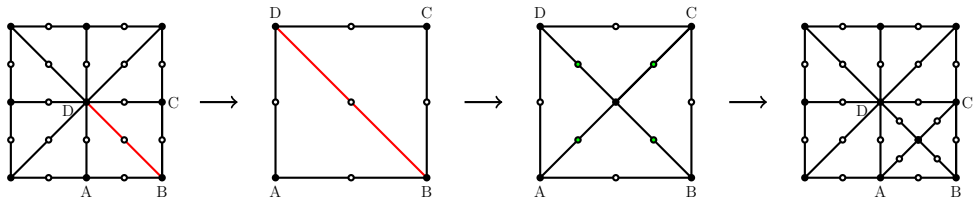

Figure 4.3: The edge identified is BD. Therefore, the patch contains two elements adjacent to edge BD. The refined version of patch contains four new nodes shown in green.

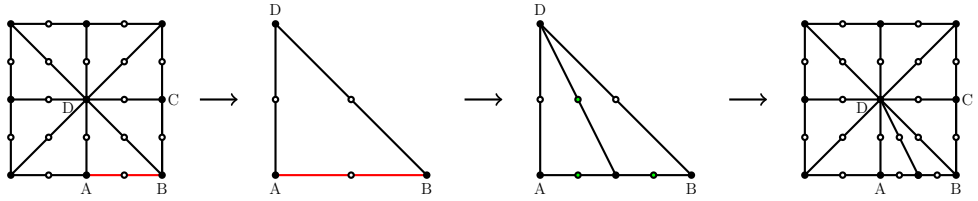

Figure 4.4: The edge identified is AB which is on the boundary. Therefore, the patch contains the single element DAB. The refined version of patch contains three new nodes shown in green.

Algorithm 2 Rivara's original algorithm for Backward LEPP refinement of a triangle t.

```
1: Backward-Longest-Edge-Bisection (T,𝒯)
2: while T remains without being bisected do
3:    Find the LEPP(T)
4:    if T*, the last triangle of the LEPP(T), is a terminal boundary triangle
      then
5:       Bisect T*
6:    else
7:       Bisect the (last) pair of terminal triangles of LEPP(T).
8:    end if
9: end while
```

4.2.2 A Backward Longest Edge Propagation Path (LEPP) Algorithm

This algorithm was proposed by Rivara in 1997 [61]. In this algorithm, a simple edge bisection technique is performed several times. Provided that the initial mesh is isotropic, the algorithm guarantees an upper bound on the element aspect ratio. The triangulations obtained with the LEPP-Delaunay algorithm have a smallest angle greater than 30° [61].

For any triangle T_0 of any conforming triangulation $\mathscr{T}$, the LEPP of T_0 will be the ordered list of all triangles T_0,T_1,...T_{n-1},T_n, such that T_i is the neighbour triangle of T_{i-1} by the longest side of T_{i-1}, for $i = 1, 2, ..., n$ where n is the number of triangles in the LEPP [61]. For any triangle T of any conforming triangulation of any bounded 2-D geometry Ω, the following properties hold: (a) for any T, the LEPP(T) is always finite; (b) the triangles T_0,T_1,...T_{n-1},T_n have strictly increasing longest side (if $n > 1$); (c) For the triangle T_n of the LEPP of any triangle T_0, it holds that either (i) T_n has its longest edge along the boundary, and this is greater than the longest edge of T_{n-1}, or (ii) T_n and T_{n-1} share the same common longest edge [61].

The original algorithm proposed by RIVARA is based on triangle bisection. It is given in [61] as shown in algorithm 2.

For example, consider figure 4.5. The target triangle is T_0. The longest edge of triangle T_0 is CD. Edge CD is shared by triangles T_0 and T_1. Longest

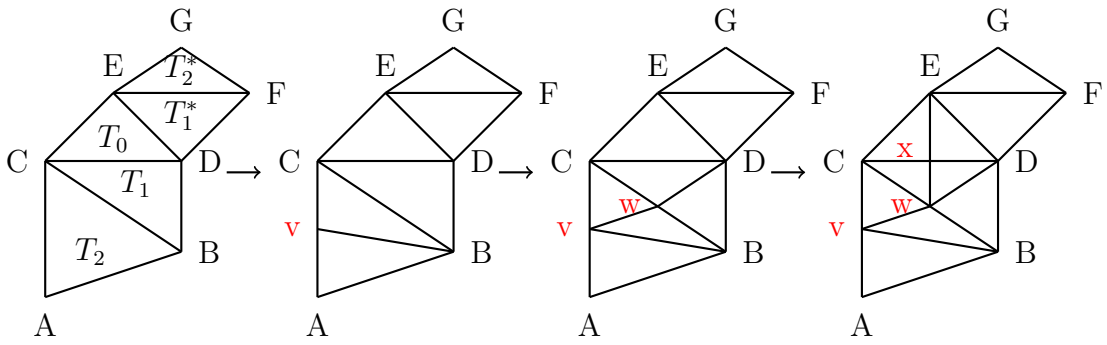

Figure 4.5: Original algorithm of Rivara [61] based on target triangle. Target triangle is t_0.

edge of T_1 is CB. Edge CB is shared by triangles T_1 and T_2. Longest edge of T_2 is CA, which is on the boundary. Therefore LEPP of triangle T_0 is {CED,BCD,ACB}. The terminal triangle is ACB. Therefore, in the first step, its longest edge i.e. CA it is bisected. Now the updated LEPP for triangle T_0 is {CED,BCD,BvC}. The pair of terminal triangles in this case is {BCD,BvC}. They share longest edge CB which is bisected in the second step. The updated LEPP now contains only terminal triangles {CED,CwD}. They share longest edge CD which is bisected in the third step. This way, in order to refine triangle T_0, we needed to introduce three new nodes v,w and x. As shown in [61], the size of the patch always remains finite as it always terminated either at the boundary or at the longest edge shared by two triangles.

The proposed mesh adaption strategy in this work is based on an edge bisection technique in which a single edge to be bisected is to be identified as opposed to identifying a triangle to be bisected. Therefore, the LEPP algorithm needs to be modified to focus on an edge to be bisected. The modified LEPP algorithm proposes to use LEPP for both triangles connected to the edge under consideration until it is bisected. The modified LEPP algorithm is given as shown in algorithm 3.

For example, consider figure 4.6. Here, target edge is ED. Adjacent triangles of edge ED are CED and DEF. Edge ED is the longest edge of neither of triangles. Therefore, backward LEPP of both triangles is performed.

Algorithm 3 Proposed backward LEPP refinement of an edge e.

Identify edge e to be bisected.
while e is not bisected **do**
  Find adjacent triangles T_1 and T_2 of edge e
  if e is the longest side of one of the triangles. **then**
    T = Other triangle
    Perform Backward LEPP for T as shown in figure 4.5.
  else if e is the longest edge of both triangles T_1 and T_2 **then**
    Perform simple edge bisection
  else
    Perform backward LEPP of T_1 as shown in figure 4.5.
    Perform backward LEPP of T_2 as shown in figure 4.5.
  end if
end while

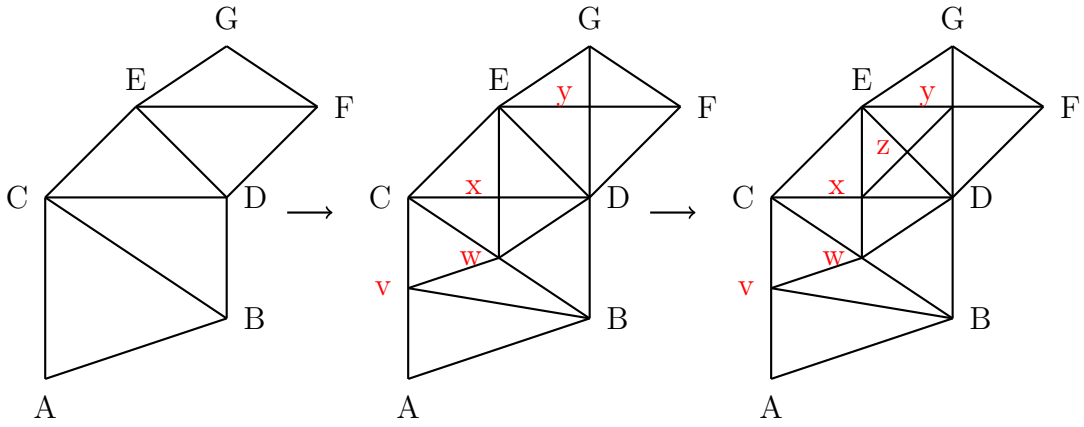

Figure 4.6: The proposed algorithm based on target edge. Target edge is ED.

The backward LEPP of CED introduces 3 nodes v,w,x as seen previously in figure 4.5. Longest edge of triangle DEF is EF which is shared with triangle EFG. For triangle EFG also, the longest edge is EF. Therefore, EF is bisected and node y is introduced. Now, adjacent triangles of edge ED are ExD and EyD. ED is the longest edge of both the triangles. Therefore, simple edge bisection of ED is performed and node z is introduced. The corresponding patch would therefore contain polygon ABDFGEC with five new nodes.

4.3 Adaption criteria

4.3.1 Refinement

As seen in the previous chapter, the incremental variational problem is an optimization problem of the form:

$$\inf_{\mathbf{u}\in\mathcal{V}} \quad \sup_{\theta\in\mathcal{W}} \quad I(\mathbf{u},\theta) \tag{4.1}$$

where $I(\mathbf{u},\theta)$ is a semi-discrete functional (only time has been discretized), so $\mathcal{V}$ and $\mathcal{W}$ are spaces of continuous and regular functions defined in the problem domain Ω respecting Dirichlet boundary conditions. A staggered solution scheme for the coupled problem [3] is preferred which allows to use different meshes for mechanical and thermal parts.

In finite element analysis, the solutions lie in subspaces $\mathcal{V}_h$ and $\mathcal{W}_h$ of $\mathcal{V}$ and $\mathcal{W}$ respectively, which are finite element interpolations on triangulations $\mathscr{T}_u$ and $\mathscr{T}_T$ of the domain Ω. In the present context of mesh adaption, $\mathcal{V}_h$ and $\mathcal{W}_h$ are the nets of linear spaces generated by edge bisection and parameterized by a directed index set A[1]. Hence, $\mathcal{V}_{h1} \leq \mathcal{V}_{h2}$ if triangulation $\mathscr{T}_{h2}$ corresponding to $\mathcal{V}_{h2}$ can be reached from $\mathscr{T}_{h1}$ corresponding to $\mathcal{V}_{h1}$ by successive edge bisections. The initial triangulation and solution space corresponding to the initial mesh are $\mathscr{T}_0$ and $\mathcal{V}_0$ respectively, therefore, the corresponding element $0 \in A$ precedes all the other elements.

The variational functional being convex in displacement and concave in temperature, provides a comparison criterion to judge the quality of meshes. Thus, triangulation $\mathscr{T}_{u_1}$ with displacement field $\mathbf{u_1}$ is better than triangulation $\mathscr{T}_{u_2}$ with displacement field $\mathbf{u_2}$ if and only if $I(\mathbf{u_1},\theta) < I(\mathbf{u_2},\theta)$. Similarly, triangulation $\mathscr{T}_{T_1}$ with temperature field θ_1 is better than triangulation $\mathscr{T}_{T_2}$ with temperature field θ_2 if and only if $I(\mathbf{u},\theta_1) > I(\mathbf{u},\theta_2)$. This allows to formulate the problem of variational mesh adaption as an optimization problem:

$$\inf_{\mathbf{u}\in\mathcal{V}_h} \quad \sup_{\theta\in\mathcal{W}_h} \left\{ I_h(\mathbf{u},\theta) + \mu_g^u N_u - \mu_g^T N_T \right\} \tag{4.2}$$

[1]A directed set is a nonempty set A together with a binary relation $\leq$ with properties of reflexivity($a \leq a$, $\forall a \in A$), transitivity(if $a \leq b$ and $b \leq c$, then $a \leq c$), and directedness(for any pair $a, b \in A$, there exists a $c \in A$ such that $a \leq c$ and $b \leq c$).

where, N_u and N_T are the number of nodes in the triangulations of the mechanical and thermal meshes respectively. Indeed, parameters μ_g^u and μ_g^T are needed to define a criterion to stop the mesh adaption process because additional degrees of freedom will never worsen the variational potential. When a node is added into a mechanical mesh, the value of the potential I_h decreases because of the additional degree of freedom. At the same time, N_u increases by one. The net effect of addition of one node is offset by an amount μ_g^u due to the second term in equation (4.2). *Hence, mesh refinement is admissible only if additional node in mechanical mesh reduces the potential I_h by a value greater than μ_g^u.* So, these parameters are penalization parameters linked to the cost of refinement of the mesh. Similarly, when a node is added to the thermal mesh, the value of the potential I_h increases due to the additional degree of freedom and N_T increases by one. The net effect of additional node in thermal mesh in equation (4.2), is offset by an amount μ_g^T due to the third term. For the thermal part, the mesh refinement is admissible only if the additional node in the thermal mesh increases the potential I_h by a value greater than μ_g^T. Therefore, parameters μ_g^u and μ_g^T are the energy costs of adding a new node in mechanical and thermal meshes respectively which should be strictly positive. If the improvement in the value of energy potential is more than that of the cost of a node, refinement is admissible.

Assuming the mechanical problem is solved prior to the thermal problem in *an isothermal staggered approach*, the mesh adaption problem (4.2) can be represented separately for mechanical and thermal meshes at time step n as:

$$\begin{aligned} \inf_{\mathbf{u}\in\mathcal{V}_h} \left\{ I_h(\mathbf{u}_n, \theta_{n-1}) + \mu_g^u N_u \right\} &\equiv \inf_{\mathbf{u}\in\{\mathcal{V}_h\}} \mathcal{I}_u(\mathbf{u}_n, \theta_{n-1}, N_u) \\ \sup_{\theta\in\mathcal{W}_h} \left\{ I_h(\mathbf{u}_n, \theta_n) - \mu_g^T N_T \right\} &\equiv \sup_{\theta\in\{\mathcal{W}_h\}} \mathcal{I}_T(\mathbf{u}_n, \theta_n, N_T) \end{aligned} \tag{4.3}$$

here $\{\mathcal{V}_h\}$ and $\{\mathcal{W}_h\}$ denote a set of enriched spaces that contain all the possible combinations of edge splitting in the base mesh of mechanical and thermal part respectively. However, it is sometimes convenient to solve the

thermal problem prior to the mechanical problem, especially in the case of weak coupling with one-way effect of thermal part on the mechanical part. In such scenario, the mesh adaption problem can be stated as follows:

$$\begin{aligned} \sup_{\theta \in \mathcal{W}_h} \left\{ I_h(\mathbf{u}_{n-1}, \theta_n) - \mu_g^T N_T \right\} &\equiv \sup_{\theta \in \{\mathcal{W}_h\}} \mathcal{I}_T(\mathbf{u}_{n-1}, \theta_n, N_T) \\ \inf_{\mathbf{u} \in \mathcal{V}_h} \left\{ I_h(\mathbf{u}_n, \theta_n) + \mu_g^u N_u \right\} &\equiv \inf_{\mathbf{u} \in \{\mathcal{V}_h\}} \mathcal{I}_u(\mathbf{u}_n, \theta_n, N_u) \end{aligned} \tag{4.4}$$

Here, fields with subscript $n-1$ are calculated at previous time step, hence considered given in the above equations. In problem (4.3), the first equation adapts the mechanical mesh and the displacement solution $\mathbf{u}_n$ at time n is obtained. The second equation considers $\mathbf{u}_n$ as given and adapts thermal mesh and the thermal solution θ_n at time n is obtained. Problems (4.3) and (4.4) are of combinatorial complexity, that is, for each value of number of nodes, several meshes with different values of incremental variational functional are possible, also infinite choices for number of nodes are possible. This combinatorial complexity makes these problems very hard to solve in general. Hence, a greedy approach is used for iterative procedure taking advantage of the additive property of the variational potential, $I_h(\mathbf{u}, \theta) = \sum_i^{nElem} I_i(\mathbf{u}_i, \theta_i)$. The geometry is divided into number of patches and refinable elements are collected from each patch. This is done by locally refining each patch and checking the following condition for the mechanical part:

$$I_i(\mathbf{u}_1, \theta) - \inf_{\mathbf{u}_2 \in \mathcal{V}_h} I_i(\mathbf{u}_2, \theta) > \mu_r^u \Delta N_u \tag{4.5}$$

where I_i represents the local variational potential for the i^{th} patch, $\mathbf{u}_1$ is the local displacement field calculated on the original patch, $\mathbf{u}_2$ is the local displacement field calculated for the refined patch, θ is the local thermal field interpolated from a different thermal mesh, μ_r^u is the cost of adding a new node in the local patch of the mechanical mesh and ΔN_u are the number of new nodes introduced in the refined patch. Similarly, the following condition

is verified for the thermal part:

$$\sup_{\theta_2 \in \mathcal{W}_h} I_i(\mathbf{u}, \theta_2) - I_i(\mathbf{u}, \theta_1) > \mu_r^T \Delta N_T \tag{4.6}$$

where θ_1 is the local temperature field calculated on the original patch, θ_2 is the local temperature field calculated on the refined patch, $\mathbf{u}$ is the local displacement field interpolated from a different mechanical mesh, μ_r^T is the cost of adding a new node in the local patch of thermal mesh and ΔN_T are the number of new nodes introduced in the refined patch. If the improvement due to the additional node in the value of the local energy like potential is more than the energy cost of adding a node in that local patch, the refined version of patch is retained, otherwise, the original patch is retained. Checking conditions (4.5) and (4.6) involves solving a local problem on the refined patch with fixed Dirichlet boundary conditions on the boundary of the patch (which are available from the previous global solution).

4.3.2 Coarsening

For transient problems, domains of interest evolve over time and according to the loading. Therefore, mesh coarsening is also important to adapt the sole domain of interest. The process of mesh coarsening is similar to that of mesh refinement. Just by identifying a previously refined edge for potential coarsening allows to go back to the original mesh irrespective of the method of refinement used. For example, consider the refinement obtained by LEPP strategy in figure 4.7. One can easily go back to the original mesh by two step coarsening procedure as shown in figure 4.7. Therefore, for coarsening the following condition is checked for mechanical problem on each patch:

$$\inf_{\mathbf{u}_2 \in \mathcal{V}_h} I_i(\mathbf{u}_2, \theta) - I_i(\mathbf{u}_1, \theta) < \mu_d^u \tag{4.7}$$

where, $\mathbf{u}_2$ is the local displacement field on the coarsened patch, $\mathbf{u}_1$ is the original displacement field and μ_d^u is the cost of a node in the local patch of mechanical mesh. Note that only one node is removed from patch, therefore the resulting increase in potential should be less than energy cost of a single

node. Similarly for a thermal problem, the following condition is checked on each patch:

$$I_i(\mathbf{u}, \theta_1) - \sup_{\theta_2 \in \mathcal{W}_h} I_i(\mathbf{u}, \theta_2) < \mu_d^T \tag{4.8}$$

here θ_1 is the local temperature field on original patch, θ_2 is the local temperature field on coarsened patch and μ_d^T is the cost of a node in the local patch of thermal mesh. Here, decrease in energy caused by coarsening should be less than energy cost of a single node. In other words, if saving in the energy cost of a node is more than the effect on solution field due to a node removal, the patch can be coarsened. Whereas if the deterioration in the solution due to node removal is significant with respect to the energy cost of a node, the patch is not coarsened in order to obtain precise solution.

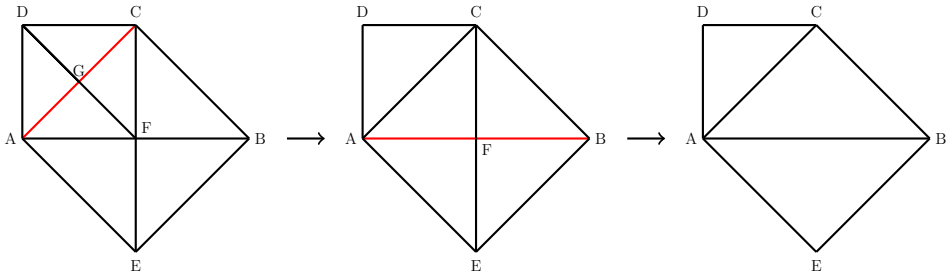

Figure 4.7: The LEPP algorithm gives the single step refinement of several edges. They are coarsened one by one. Here edge AGC is coarsened to AC first, then edge AFB is coarsened to AB.

In case of single field adaptation, first, the global problem is solved and the value of initial functional I_{G1} is obtained. Then the geometry is divided into number of different patches and each patch is checked for potential coarsening. If the domains of interest remain in vicinity between two time steps and refinement is considered prior to coarsening, the refinement builds children elements with refined elements at the previous time step as parents. This does not allow effective coarsening. Therefore, in order to have effective refinement and coarsening, it is necessary to carry out the coarsening process prior to that of refinement. After coarsening, the geometry is again divided into patches for potential refinement. For each patch, the condition for refinement is checked and necessary changes in the global mesh are made. Therefore,

at the end, one obtains a new adapted mesh. Again, a global solution is computed on this mesh and new value of functional I_{G2} is obtained. This procedure is repeated until convergence.

For practical considerations, it is more convenient to consider relative improvements of functionals with respect to their previous values as opposed to absolute improvements. This allows to define an elegant convergence criterion. Therefore, an algorithm is considered to be converged when relative improvement in the value of energy like potential is insignificant. Any further refinement of the mesh will add significant computational cost without considerable improvement in the accuracy. One can define convergence parameter Tol_0 to represent the threshold relative improvement in the global value of energy like potential. Similar arguments can be applied at the local level and a parameter Tol_r representing the threshold relative improvement in the local value of energy like potential upon refinement can be introduced. In case of coarsening, again relative deterioration of the solution upon coarsening is considered and parameter Tol_d is introduced to represent the threshold relative deterioration in the value of energy like potential. In the work that follows, relative improvement parameters Tol_0, Tol_r and Tol_d are used as opposed to their absolute improvement counterparts μ_g, μ_r and μ_d respectively. Note that allowing different values for parameters Tol_r^u, Tol_r^T, Tol_d^u, Tol_d^T, Tol_0^u and Tol_0^T, a better control over the adaption procedure can be obtained.

The algorithm for a single field adaptation $\inf \mathcal{I}_u(\mathbf{u}_n, \theta_{n-1}, N_u)$ or $\sup \mathcal{I}_T(\mathbf{u}_n, \theta_n, N_T)$ in equations (4.3) and (4.4) is described in algorithm 4.

Note that in the case of transient problems, at the beginning of each time step, the mesh is coarsened to save computation cost as shown in the algorithm above. The procedure for mesh adaption for coupled problems is shown in algorithm 5.

4.4 Equivalence with error norms

The variational functional I in equation (3.38) is equivalent to $\mathcal{H}_1$ norm. We demonstrate this here for transient purely thermal problem for simplicity.

Algorithm 4 Single field mesh adaptation.

if Maximization (thermal problem in case of coupled adaption) problem **then**
  $\lambda = 1$
else
  $\lambda = -1$
end if
We begin with an arbitrary coarse mesh and solve our problem on that mesh. Get energy like potential I_{G_1}.
$i = 0$
while $\frac{\lambda(I_{G_2} - I_{G_1})}{I_{G_1}} \leq Tol_0$ **do**
  $I_{G_1} = I_{G_2}$
  if $i = 0$ **then**
    Division of our full geometry Ω into different patches Ω_i for coarsening purpose.
    for Ω_i = First Patch **to** Ω_i = Last Patch **do**
      Locally coarsen the mesh on the patch.
      Calculate the values of fields on deleted nodes by interpolation.
      Calculate local values of energy like potentials with interpolated values I_{L_2} and calculated values I_{L_1}.
      if $\frac{\lambda(I_{L_1} - I_{L_2})}{I_{L_1}} < Tol_d$ **then**
        Coarsen the patch in the global mesh.
      end if
    end for
  end if
  Division of our full geometry Ω into different patches Ω_i for refinement purpose.
  for Ω_i = First Patch **to** Ω_i = Last Patch **do**
    Refine the current patch locally and solve a local problem on this small patch with the temperature field on the boundary of the patch imposed (given by the complete solution we calculated in earlier iteration).
    Calculate the local energy like potential I_{L_2}.
    if $\frac{\lambda(I_{L_2} - I_{L_1})}{I_{L_1}} > Tol_r$ **then**
      Refine the patch in global mesh.
    end if
  end for
  Solve the problem again on the new mesh thus obtained and calculate ϕ_{G_2}.
  $i = i + 1$
end while

Algorithm 5 Mesh adaptation for coupled problems.

1: **for** t = initial time **to** t = final time **do**
2: Adapt the mechanical mesh by solving $\inf \mathfrak{I}_u(\mathbf{u}_n, \theta_{n-1}, N_u)$ by using the algorithm described in box 4. Adiabatic or isothermal conditions can be considered in this step.
3: Adapt the thermal mesh by solving $\sup \mathfrak{I}_T(\mathbf{u}_n, \theta_n, N_T)$ by using the algorithm described in box 4.
4: **end for**

One can rewrite equation (3.45) by ommitting the source term and diving by a reference temperature T_{ref} for transient purely thermal problem as:

$$I(T_{n+1}) = \int_0^L \left\{ -\frac{C}{T_{ref}} \frac{T_{n+1}^2}{2} + \frac{C T_{n+1} T_n}{T_{ref}} - \frac{C T_n^2}{2 T_{ref}} - \Delta t \frac{K}{2 T_{ref}} \boldsymbol{\nabla} T \cdot \boldsymbol{\nabla} T \right\} dx \tag{4.9}$$

One can substitute $\theta = \frac{T}{T_{ref}}$, $x = \frac{x \Delta t k}{c}$ and $J = -\frac{I(\theta)}{c T_{ref}}$ to obtain:

$$J = -\frac{I(\theta)}{c T_{ref}} = \int_0^L \left\{ \frac{1}{2} (\theta - \theta_n)^2 + \frac{1}{2} \boldsymbol{\nabla} \theta \cdot \boldsymbol{\nabla} \theta \right\} dx \tag{4.10}$$

One can write the bilinear form as:

$$a(u, v) = \int_\Omega \{ uv + \boldsymbol{\nabla} u \cdot \boldsymbol{\nabla} v \} \, d\Omega \tag{4.11}$$

It is easy to see that $a(u, u)$ is the $\mathcal{H}_1$ norm of u. Now, θ_n is the temperature field at previous time step which is an input for the current time step. so, the linear form can be written as:

$$l(u) = \int_\Omega u \theta_n d\Omega \tag{4.12}$$

Using these forms, $J(\theta)$ can be rewritten as:

$$J(\theta) = \frac{1}{2} a(\theta, \theta) - l(\theta) + c_1 \tag{4.13}$$

where the constant c_1 can be given as:

$$c_1 = \int_0^L \frac{1}{2} \theta_n^2 dx \tag{4.14}$$

One can obtain weak form by minimizing functional $J(\theta)$. The exact problem can be written in the weak form assuming homogeneous dirichlet boundary conditions as follows: Find $\theta \in \mathcal{V}$ such that for all $\delta\theta \in \mathcal{V}$:

$$a(\theta, \delta\theta) - l(\delta\theta) = 0 \tag{4.15}$$

where, $\mathcal{V}$ is the space of continuous real valued functions in the problem domain Ω.[2]

Let θ_h be the finite element solution and θ be the exact solution. The error in potential J due to finite element discretization is:

$$J(\theta) - J(\theta_h) = \frac{1}{2}\left(a(\theta, \theta) - a(\theta_h, \theta_h)\right) + \left(l(\theta_h) - l(\theta)\right) \tag{4.16}$$

Rearranging the terms, one can obtain:

$$l(\theta_h) = \frac{1}{2}a(\theta_h, \theta_h) - \frac{1}{2}a(\theta, \theta) + l(\theta) + J(\theta) - J(\theta_h) \tag{4.17}$$

Now, $\mathcal{H}_1$ norm of error is the bilinear form from equation (4.11):

$$||\theta - \theta_h||_{\mathcal{H}_1} = a(\theta - \theta_n, \theta - \theta_n) \tag{4.18}$$

One can expand $a(\theta - \theta_n, \theta - \theta_n)$ to obtain:

$$||\theta - \theta_h||_{\mathcal{H}_1} = a(\theta, \theta) + a(\theta_h, \theta_h) - 2a(\theta, \theta_h) \tag{4.19}$$

Now, $\theta_h \in \mathcal{V}$, so one can use equation (4.15) to obtain:

$$\frac{1}{2}||\theta - \theta_h||_{\mathcal{H}_1} = \frac{1}{2}a(\theta, \theta) + \frac{1}{2}a(\theta_h, \theta_h) - l(\theta_h) \tag{4.20}$$

Substituting $l(\theta_h)$ from equation (4.17):

$$\frac{1}{2}||\theta - \theta_h||_{\mathcal{H}_1} = a(\theta, \theta) - l(\theta) + J(\theta_h) - J(\theta) \tag{4.21}$$

Again, $\theta \in \mathcal{V}$, therefore again equation (4.15) can be used to obtain:

$$\frac{1}{2}||\theta - \theta_h||_{\mathcal{H}_1} = J(\theta_h) - J(\theta) \tag{4.22}$$

[2]Assumption of homogeneous boundary conditions makes variation space and trial solution space same. Indeed, this assumption can be relaxed and one can still obtain the demonstrated results by mathematical manipulations.

Therefore, the difference in variational potential is directly related to the $\mathcal{H}_1$ norm of the interpolation error.

The algorithm explained in the preceding section exploits the additive property of the energy like potential I which is equivalent to J. The global value of I is sum of its local values over all elements. Therefore, improvement in local value of I at a patch corresponds to improvement in global value of I and thus results in reduction of error. Therefore, on each patch, one would like to converge to the best possible discretization that minimizes I at a computational cost determined by Tol_r. Doing this on all patches reduces the error norm on global level and the level of improvement at global level is determined by Tol_0 parameter. Indeed, parameters Tol_0,Tol_r and Tol_d are not independant. But in order to study the sole effect of one parameter, other paramters are set to a constant value and the paramer under study is varied in the parametric analysis of the algorithm.

4.5 Management of fields and internal variables

4.5.1 Management of internal variables during adaption procedure

Mesh adaption problems often involve complex remapping procedures for transferring the internal variable set from an initial mesh to an adapted mesh. Remapping of internal variables causes significant numerical diffusion. In the present work, the internal variables are assumed to be piece-wise constant over the domains of an element (piece of Voronoï cells defined by integration points). The piece of the Voronoï cell around a Gauss point, intersected with the current element, represents the domain of influence of that Gauss point. *Therefore, at any given point in an element, the values of internal variables are assumed to be equal to that of the closest integration point within that element as shown in figure 4.8.*

Upon edge bisection, when a new integration point is created, the process of remapping involves simple inheritance of internal variables at the new

integration point from the closest integration point in the parent element. In this way, children elements remain consistent with the history of deformation of their parent elements and satisfy the internal constraints. Upon coarsening, again the old integration point inherits internal variables from the closest integration point within the refined elements. Again, parent elements remain consistent with the average history of deformation of their children elements and satisfy the internal constraints. This process is demonstrated in figure 4.8. This variational transfer operator is dealt with in detail by Ortiz and Quigley [50].

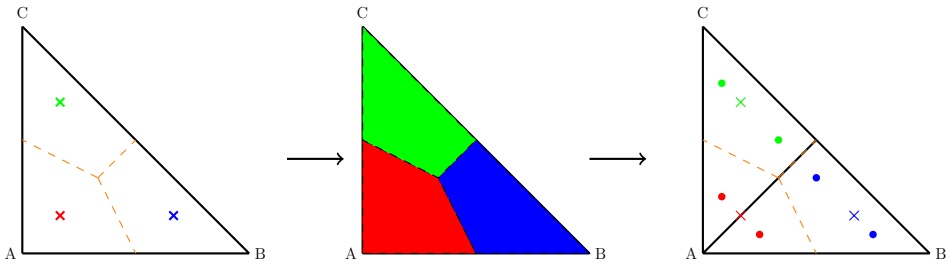

Figure 4.8: The diagram on the left shows a triangular parent element with three integration points shown in different colours. The pieces of Voronoï cells intersected with triangle corresponding to each Gauss point are shown in the figure in the middle with respective colours. These Voronoï cells represent the domain of influence of each Gauss point. The diagram on the right shows the bisected triangle. Two new triangles are formed as a result of bisection. The children Gauss points inherit data from parent Gauss points shown in same colors in the figure above.

4.5.2 Interpolation of fields from one mesh to other

The problem of interest consists in using two different meshes for mechanical and thermal problem. In order to deal with the coupling effects, information transfer from one mesh to another is necessary. In case of nodal fields, this transfer consists of simple interpolation of fields to the Gauss points of the other mesh. Therefore, given an integration point, a search is made to find the element in the other mesh in which the integration point lies. Using the nodal values, a finite element interpolation is performed. In case of variables defined at integration points, the process consists of finding the

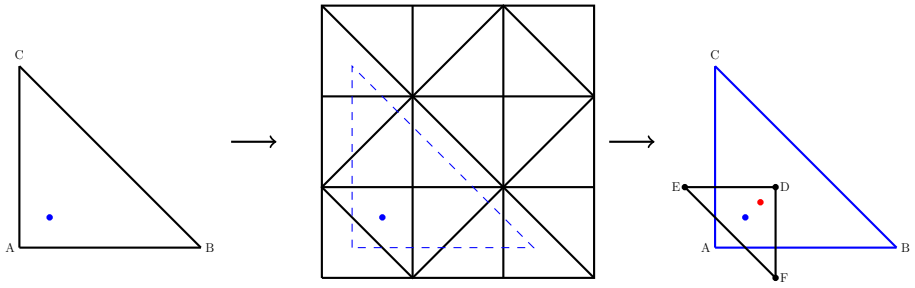

Figure 4.9: Figure on the left shows an element ABC and one of its Gauss points on which fields from the other mesh are to be interpolated. The figure in the middle shows the other mesh and the element ABC in dotted blue. The element in which Gauss point of element ABC lies is identified as element DEF as shown in the figure on the right. Therefore, the external fields can be interpolated from nodal values at nodes D, E and F. Variables at integration points are inherited from the closest integration point in element DEF which is shown in red.

closest integration point in the other mesh and the values are inherited. Using spatial coordinates, a linear search can allow to obtain the element in other mesh in which the current integration point lies. This process is represented in figure 4.9.

4.6 Conclusion

This chapter presented the algorithm for mesh adaption for strongly coupled problems in thermo-mechanics. Two refinement techniques based on edge bisection are presented viz. SEB and LEPP. Using only edge bisection technique allows the effective management of internal variables avoiding significant numerical diffusion as explained in the previous section. The mesh adaptation criteria is based on the variational functional which was introduced in Chapter 2. The problem of mesh optimization was also represented as an optimization problem using the variational functional. Algorithms for refinement and coarsening of the mesh were presented.

It is necessary to critically analyze the algorithm and confirm the adaptability of the algorithm to complex problems, moreover, cost effectiveness of the algorithm over using uniform mesh needs to be established. This is

the topic of the following chapters that present analysis of the presented algorithm with help of different test cases.

Cas test unidimensionnels

L'algorithme d'adaptation de maillage proposé dans le chapitre précédent est appliqué aux problèmes 1D de ce chapitre. La simplicité des problèmes 1D les rend adaptés à l'analyse de l'algorithme. Pour des éléments P1, le raffinement consiste simplement à introduire un noeud au milieu d'un élément, pour en définir deux. Pour un déraffinement, un noeud peut être supprimé pour fusionner deux éléments.

Tout d'abord, un problème purement thermique stationnaire admettant une solution analytique est considéré. Dans ce problème, un gradient de température important permet d'observer une adaptation très visible du maillage. L'existence d'une solution analytique permet une analyse d'erreur exacte et une meilleure efficience de l'algorithme proposé para rapport à un raffinement uniforme du maillage est montrée numériquement. Une analyse de sensibilité aux paramètres algorithmiques est réalisée. Le paramètre Tol_r contrôle la précision de la solution. Le paramètre Tol_r ajuste un compromis entre la précision et le cot de calcul. Le paramètre Tol_d dépend du paramètre Tol_r et doit être choisi égal ou inférieur au paramètre Tol_r. D'autre part, le paramètre Tol_0 contrôle la convergence globale de l'algorithme.

Deuxièmement, un problème de thermo-élasticité fortement couplé est analysé. Ce problème a été analysé dans [3] qui a permis d'obtenir une solution de référence. Encore une fois, l'efficience de l'algorithme est analysée. Troisièmement, un cas test basé sur le viscomètre de Couette avec un matériau thermo-élastoplastique avec couplage faible est présenté.

Chapter 5

Unidimensional test cases

5.1 Introduction

The algorithm for mesh adaptation proposed in the previous chapter is applied to 1D problems in this chapter. Simplicity of 1D problems makes them suitable for algorithm analysis. In this case, the refinement simply consists of introducing a node in the middle of an element. For coarsening, a node can be deleted to merge two adjacent edges. In 1D problems, one is not constrained by the initial mesh provided and mesh can be coarsened even beyond the initial mesh.

In the second section, a steady state thermal test case is studied. Existence of an analytical solution allows a detailed parametric analysis. Insights obtained from parametric analysis allow to check the algorithm for potential improvement and extension. One such strategy is also checked and a parametric analysis of this version is also performed. In the third section, a strongly coupled problem in thermo-elasticity is examined. Cost effectiveness analysis for both fields is presented. In the fourth section, an intermediate test case with weak coupling studied. This is an axisymmetric test case with an analytical solution. 2D problems will be treated in the next chapter.

5.2 Steady state

5.2.1 Analytical solution

Consider a 1D steady state purely thermal problem with an external heat source given by:

$$r = x^q \tag{5.1}$$

where x is the spatial coordinate, q is a constant and r is the external heat source. Recalling the unidimensional steady state heat equation:

$$k\frac{d^2T}{dx^2} + r = 0 \quad \forall x \in]0, L[\tag{5.2}$$

where k is the conductivity. Consider zero temperature imposed at both ends:

$$\begin{aligned} T(x = 0) &= 0 \\ T(x = L) &= 0 \end{aligned} \tag{5.3}$$

One can analytically integrate equation (5.2) and use value of r from equation (5.1):

$$k\frac{dT}{dx} + \frac{x^{q+1}}{q+1} = c_1 \quad \forall x \in]0, L[\tag{5.4}$$

where c_1 is an integration constant. Integrating the above equation again with respect to x, one can obtain the form for temperature field T:

$$kT + \frac{x^{q+2}}{(q+1)(q+2)} = c_1 x + c_2 \quad \forall x \in]0, L[\tag{5.5}$$

One can obtain values of the two integration constants c_1 and c_2 by using the two prescribed boundary conditions (5.3). Therefore, the analytical solution of the problem for bar of length L reads:

$$T = \frac{1}{k}\left[\frac{L^{q+1}x}{(q+1)(q+2)} - \frac{x^{q+2}}{(q+1)(q+2)}\right] \tag{5.6}$$

The energy potential is given by

$$\begin{aligned}\Phi(T) = \frac{k}{2} L^{2q+3} \left[\frac{1}{(q+1)^2(2q+3)} - \frac{1}{(q+1)^2(q+2)^2} \right] \\ - L^{2q+3} \left[\frac{1}{(q+1)(q+2)^2} - \frac{1}{(q+1)(q+2)(2q+3)} \right]\end{aligned} \tag{5.7}$$

This analytical solution is plotted in figure 5.1 with $q = 51$. Indeed, a high value of q leads to a sharp temperature gradient which is interesting for testing our mesh adaption algorithm.

5.2.2 Numerical solution

The algorithm is started with a coarse initial mesh of 4 elements, shown in figure 5.2. Figure 5.3 shows the solution on an intermediate mesh; one can observe mesh refinement being initialized in the region of sharp gradient. The solution on the final mesh can be represented as shown in figure 5.4. From figure 5.4, one can observe that on the right hand side, where a sharp temperature gradient occurs, a greater number of elements have been introduced to precisely capture the solution. However, in the remaining part of the domain, the algorithm puts fewer elements which is sufficient to represent the solution. In particular, nodes present in the initial mesh on the left side of the domain have been removed.

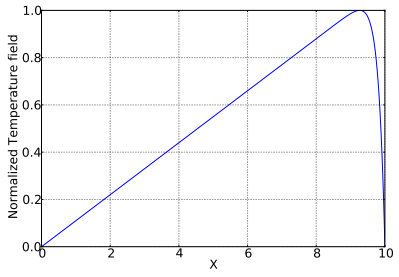

Figure 5.1: Analytical solution.

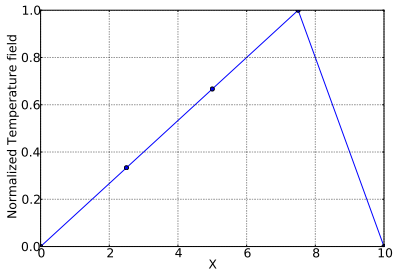

Figure 5.2: Numerical solution on the initial mesh.

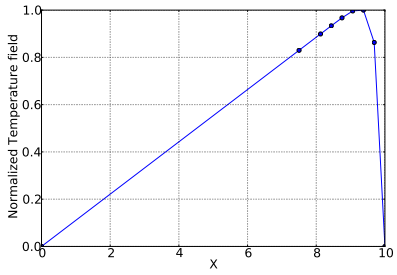

Figure 5.3: Numerical solution on an intermediate mesh.

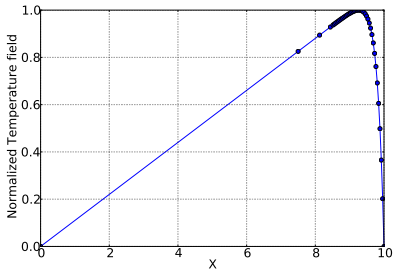

Figure 5.4: Numerical solution on the final mesh.

5.2.3 Cost analysis

In order to assess the usefulness of this algorithm, the error of the computed solution with respect to the analytical one can be plotted as a function of the number of nodes of the mesh. Three cases are considered. In the first case, plot is made for the uniform refinement of the mesh. This will be used as a reference. In the second case, we plot the error at each refinement iteration in the adaptive mesh algorithm with respect to the number of nodes of the mesh. However, since the mesh adaption is done in several iterations, a consistent comparison between a uniform refinement and the variational one should account for the path of refinement followed during mesh adaption. One way to accomplish this is to account for a cumulated number of nodes associated to all the calculations performed during the mesh adaption process. Therefore, in the third case, the error at each refinement iteration in the variational adaptive mesh algorithm is plotted with respect to the cumulative number of nodes. Indeed, this analysis gives a very pessimistic idea of the cost with respect to uniform mesh because essentially, it is assumed that algorithm complexity of the computation is $\mathcal{O}(n)$ which is never possible. The best one can do is an algorithm with cost $\mathcal{O}(n \log n)$, but this case is also very rare. If the matrix is full, algorithm complexity is cubical i.e.$\mathcal{O}(n^3)$ and in this case, there is significant amount of cost saving when solving two problems with n degrees of freedom than solving a single problem of $2n$ degrees of freedom.

Figure 5.5 shows this plot for L_2 norm of error in temperature field and figure 5.6 shows the plot for energy norm of error in the energy like potential

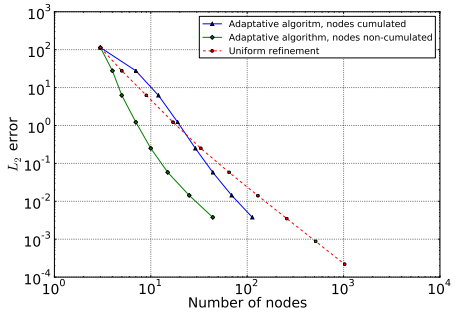

Figure 5.5: L_2 norm error in temperature field with respect to number of nodes.

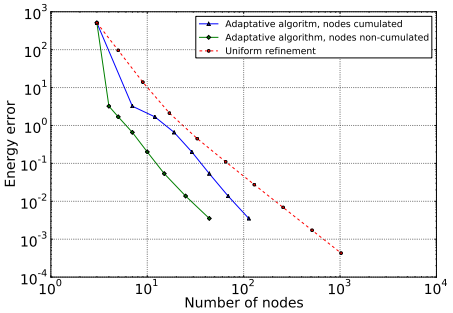

Figure 5.6: Energy norm error in energy like potential with respect to number of nodes.

Φ which is given in equation (5.8).

$$||\text{error}||_\Phi = \frac{\Phi(T_h) - \Phi(T_{exact})}{\Phi(T_{exact})} \tag{5.8}$$

From figures 5.5 and 5.6, the curve of adaptive meshing algorithm is below the curve of uniform mesh refinement. Considering cumulated number of nodes, the curve of adaptive meshing crosses from above the uniform mesh one, showing there is a number of nodes beyond which the adaptive remeshing technique is more performant and more cost effective than a uniform mesh technique.

5.2.4 Parametric analysis

Three tolerance parameters have been introduced in the algorithm which influence its performance.

Effect of Tol_0: Figures 5.7 and 5.8 show the influence of the tolerance parameter Tol_0, while fixing Tol_r and Tol_d to a particular value.

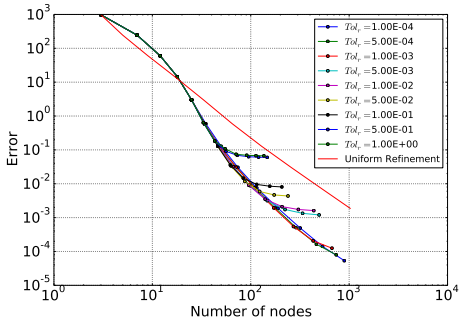

Figure 5.9: Effect of Tol_r when Tol_0 is 10^{-2} and Tol_d is 10^{-4}.

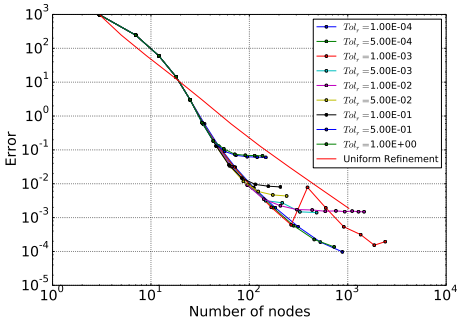

Figure 5.10: Effect of Tol_r when Tol_0 and Tol_d are fixed to 10^{-2}.

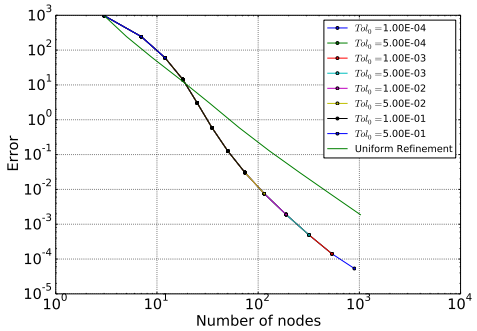

Figure 5.7: Effect of Tol_0 when Tol_r and Tol_d are fixed to 10^{-4}.

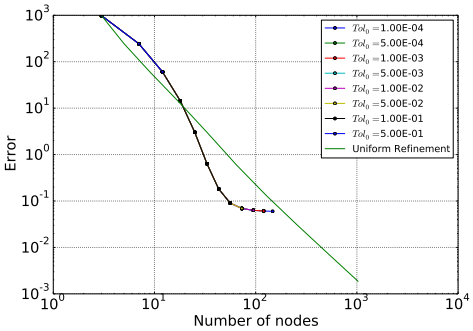

Figure 5.8: Effect of Tol_0 when Tol_r and Tol_d are fixed to 0.5.

The parameter Tol_0 allows to decide when to stop the algorithm. It doesn't have any effect on the path followed. Therefore, one can observe that as it decreases, the number of iterations followed increases. Therefore, the parameter Tol_0 should be selected such that the algorithm stops when a solution of a required precision (with respect to the current Tol_r) has been obtained. For example as shown in figure 5.8, since the Tol_r and Tol_d parameters are set at 0.5, a value of Tol_0 ranging between 10^{-3} and 10^{-2} is enough.

Effect of Tol_r: Figures 5.9 and 5.10 show the influence of the tolerance parameter Tol_r, while fixing Tol_0 and Tol_d to a particular value. The parameter Tol_r drives the precision of the converged solution. As shown in

figure 5.9, when the Tol_r ranges between 5×10^{-3} and 10^{-2} the error in converged solution is of the order of 10^{-3}. In the graphs, one can observe that the algorithm carries out few more iterations even after convergence; this is because in order to study the sole effect of Tol_r, we have set the value of Tol_0 to a constant value. Whereas, in normal circumstances we change it according to the value of Tol_r so that the algorithm stops immediately after reaching convergence.

Effect of Tol_d: The results are shown in the figures 5.11 and 5.12. Convergence and stability of the algorithm depends on parameter Tol_d. Tol_d should be less than or equal to Tol_r otherwise, the algorithm will keep on refining and derefining the same patch entering in unending loop. For example, in figure 5.12, Tol_r is fixed to 10^2. All the curves which correspond to values of Tol_d less than or equal to 10^2 are converged to the solution, whereas all the other curves diverge. This effect can also be observed in one of the curves of figure 5.10.

5.2.5 Improved algorithm

In problems involving sharp gradients of the main field, many iterations of this iterative adaption process may be performed before convergence occurs, particularly if the initial mesh is coarse. Hence, it could be interesting to accelerate the refinement procedure by dividing an element in more than two elements. An application of this idea is shown in figures 5.13 and 5.14. The refinement procedure is shown in algorithm 6.

Algorithm 6 Improved in the proposed algorithm.

1: **if** $\frac{I_{L_2} - I_{L_1}}{I_{L_1}} > Tol_u$ **then**
2: Subdivide 1 element in 4 elements, where $Tol_u > Tol_r$.
3: **else if** $Tol_u > \frac{I_{L_2} - I_{L_1}}{I_{L_1}} > Tol_r$ **then**
4: Subdivide 1 element in 2 elements.
5: **else if** $\frac{I_{L_2} - I_{L_1}}{I_{L_1}} < Tol_d$ **then**
6: Consider derefinement.
7: **end if**

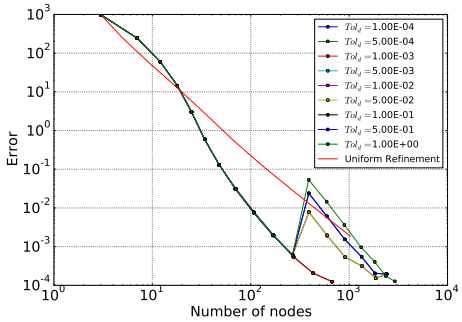

Figure 5.11: Effect of Tol_d when Tol_0 is 10^{-2} and Tol_r is 10^{-3}.

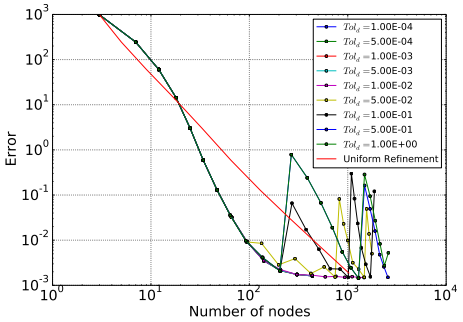

Figure 5.12: Effect of Tol_d when Tol_0 is 10^{-2} and Tol_r is 10^{-2}.

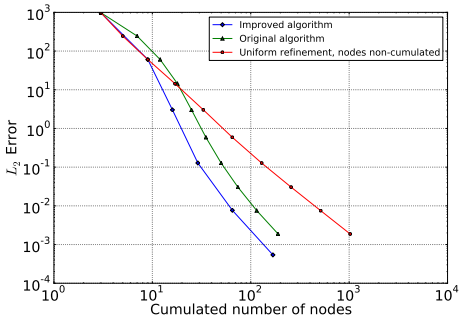

Figure 5.13: Comparison of L_2 error in Temperature analysis between original and improved algorithm.

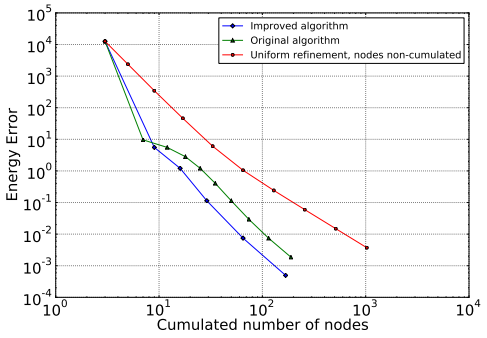

Figure 5.14: Comparison of energy error analysis between original and improved algorithm.

Parametric Analysis: Figures 5.15 and 5.16 show the results of a parametric analysis carried out for the parameter Tol_u while keeping Tol_r constant at 10^{-4}. All algorithms give equivalent results after convergence and at the beginning. However, there is a big difference in the path followed to reach the converged state.

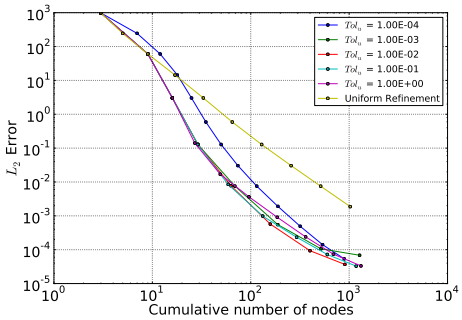

Figure 5.15: Parametric analysis of Tol_u represented in terms of L2 error in Temperature.

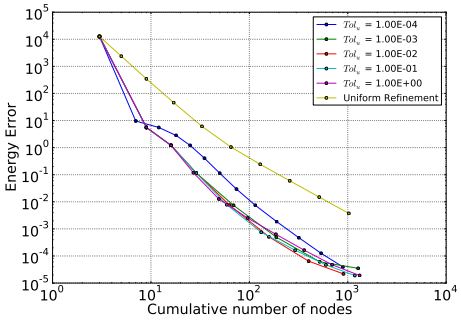

Figure 5.16: Parametric analysis of Tol_u represented in terms of energy error.

5.3 Thermo-elasticity

Consider a bar with homogeneous Dirichlet thermal and mechanical boundary conditions at its two ends:

$$T(0,t) = T(L,t) = 0; \qquad u(0,t) = u(L,t) = 0 \qquad \forall t \tag{5.9}$$

along with sinusoidal initial velocity:

$$u(x,0) = 0; \qquad v(x,0) = sin\left(\frac{\pi x}{L}\right); \qquad T(x,0) = 0 \qquad \forall x \in]0, L[\tag{5.10}$$

This test case has been introduced in [3]. With these conditions, the bar is expected to vibrate, though damped through thermal dissipation.

5.3.1 Numerical solution fields

An adiabatic staggered scheme is used for the solution and the algorithm of mesh adaption as explained in Chapter 3. The time step is set at 1 second in this test case. The problem is solved on a very fine mesh (4097 nodes) to obtain a reference solution, which has also been compared with the results obtained in [3] to ensure correctness.

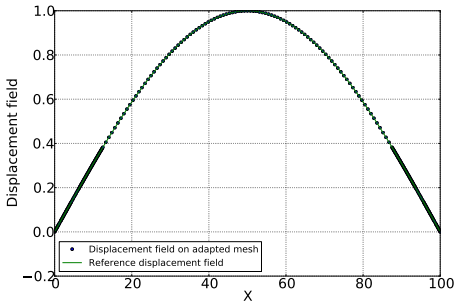

Figure 5.17: Displacement field at time = 1 second.

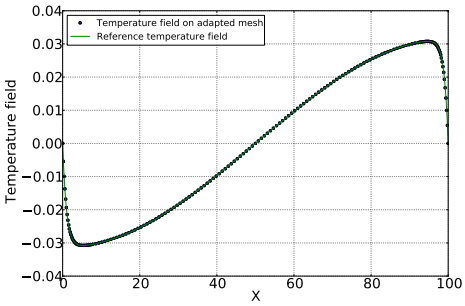

Figure 5.18: Temperature field at time = 1 second.

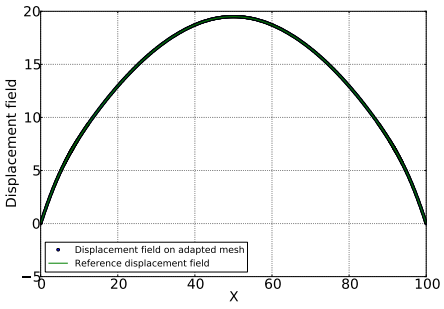

Figure 5.19: Displacement field at time = 50 seconds.

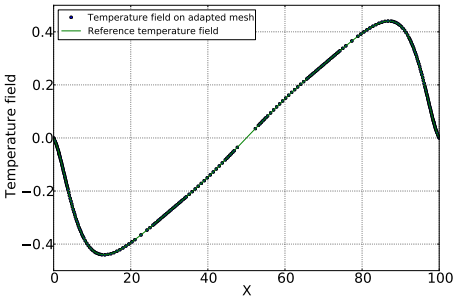

Figure 5.20: Temperature field at time = 50 seconds.

Figures 5.17, 5.18, 5.19, 5.20, 5.21 and 5.22 show the displacement and temperature fields at times 1, 50 and 301 seconds respectively. In some parts of the bar, the algorithm has put more nodes even where the solution field does not vary much. First, our criterion for mesh refinement is not directly related to smoothness of the solution profile but to the value of the energy like potential (which also takes into account the variation of the solution field with respect to time). Second, the mesh is not adapted at each time step in order to achieve better cost effectiveness. Therefore, some more nodes observed in the figures are needed to capture the solution at different time

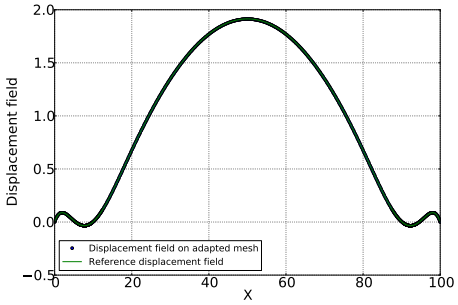

Figure 5.21: Displacement field at time = 301 seconds.

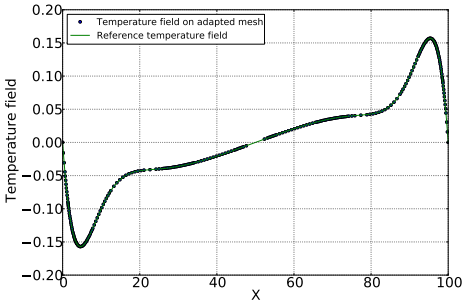

Figure 5.22: Temperature field at time = 301 seconds.

steps for which the same mesh is used. This maintains the accuracy of the solution field and also the cost-effectiveness of the algorithm.

However, it is evident from figures that a very good solution field is captured at all the time steps.

5.3.2 Cost analysis

A cost analysis is performed on both meshes, that is the thermal mesh and the mechanical mesh. L_2 errors of the displacement field and the temperature field are computed on mechanical and thermal meshes respectively.

The results are shown in figures 5.23, 5.24, 5.25, 5.26, 5.27, and 5.28. Here, in order to obtain the results on a uniform mesh, a full solution at all time steps is computed successively by uniformly refining a fixed mesh. It is evident that the introduced mesh adaption algorithm is almost always more cost-effective with respect to a simple uniform mesh for both thermal and mechanical meshes.

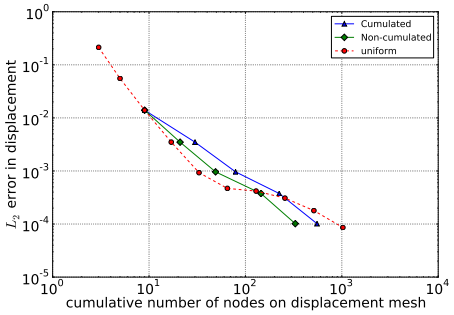

Figure 5.23: Cost analysis of mechanical mesh at time=1 second.

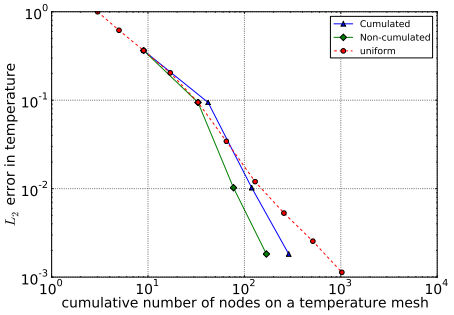

Figure 5.24: Cost analysis of thermal mesh at time=1 second.

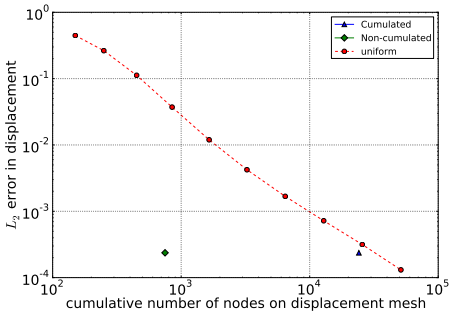

Figure 5.25: Cost analysis of mechanical mesh at time=50 seconds.

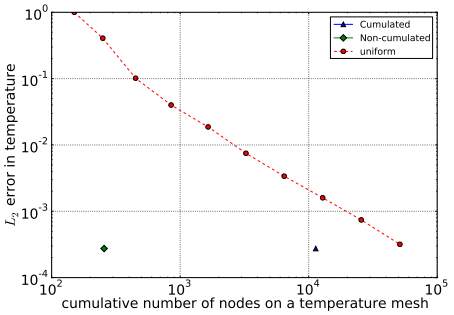

Figure 5.26: Cost analysis of thermal mesh at time=50 seconds.

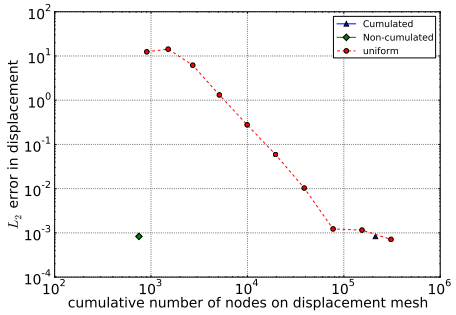

Figure 5.27: Cost analysis of mechanical mesh at time=301 seconds.

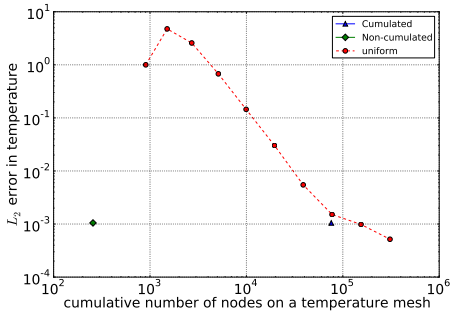

Figure 5.28: Cost analysis of thermal mesh at time=301 seconds.

Recall that having cost-effectiveness and a good accuracy of the solution at the first time step of calculation is very important, since the following adapted meshes depend on the previous ones. For example, at time steps 50 and 301, any mesh adaption is not carried out because the mesh used at the previous time step is good enough to represent the solution.

In this test case, the solution fields do not vary sharply with respect to time and space. Therefore, the algorithm performs mesh adaption at very few time steps, from time 1 to 301 seconds, mechanical mesh is adapted at only 4 time steps whereas, the thermal mesh is adapted only at 3 time steps.

5.4 Thermo-elasto-plasticity

5.4.1 Numerical solution fields

Heuzé et al. [31] have extended the well-known viscometer test case to thermo-elastic-plastic solid behaviors in small and large strains. In this test case, the mechanical part only acts on the thermal part so that the mechanical problem is solved independently of the thermal problem. The mechanical problem is first solved followed by the thermal one taking into account the effect of the mechanical solution. The geometry of the problem is shown in figure 5.29. The gap between the two cylinders is discretized by a radial 1D mesh. Zero displacement is prescribed on the inner cylinder while a driven

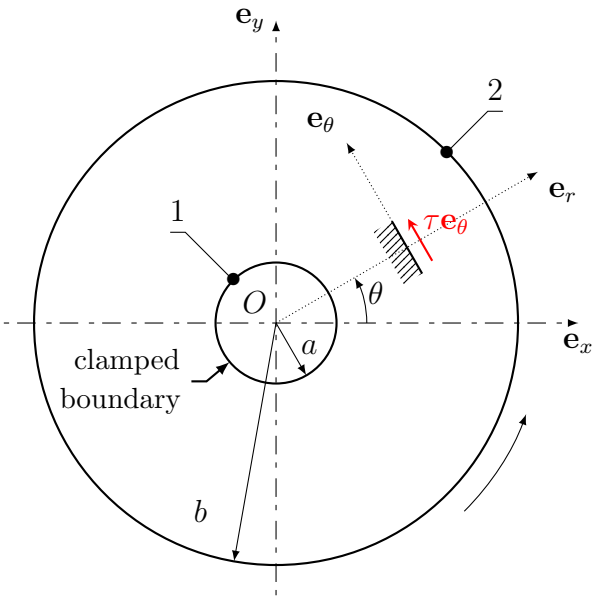

Figure 5.29: Geometry of the test case [31].

rotation is prescribed on the outer cylinder. Temperature of external and internal cylinders are fixed to zero. Therefore, the boundary conditions in the problem can be stated as:

$$\begin{aligned} u_\theta(r=a) &= 0 \\ u_\theta(r=b) &= u_\theta(b) \\ T(r=a) &= 0 \\ T(r=b) &= 0 \end{aligned} \tag{5.11}$$

where a and b denote the inner and outer radii respectively, and $u_\theta(b)$ the curved arc length swept since the finite strain framework is assumed. However the following differences arise between the test case given in [31] and the test case dealt here. A hyperelastic-plastic constitutive law is considered, whereas, in the article a hypo-elastic-plastic constitutive law was used. The analytical solution developed in [31] relies on certain assumptions, that is: dilatation effects are neglected, thermal and mechanical parameters are fixed independently of the temperature and additional terms linked to the objective derivative are neglected. The solution developed in small strains is extended

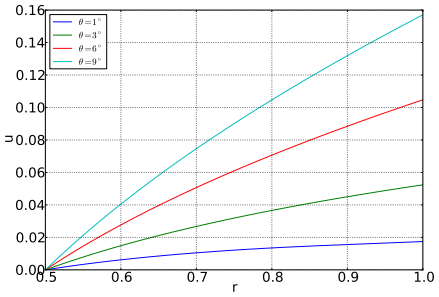

Figure 5.30: Reference solution in displacement [31].

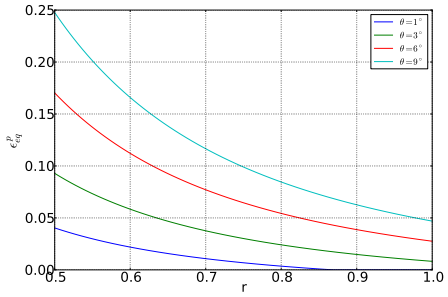

Figure 5.31: Reference equivalent plastic strain [31].

to the large strains in a straightforward manner, but its validity remains bounded from above when rotations and hence the objective derivative become important. We solve the problem on a very fine mesh (5000 elements) with the numerical data of [31] and use that solution as a reference solution.

The reference solutions in displacement and equivalent plastic strains are plotted in figures 5.30 and 5.31 respectively. According to [31], the thermal solution is valid once the viscometer is completely elastic-plastic. As seen in figure 5.31, at rotation of $\theta = 3°$ of the outer cylinder, the viscometer is completely elastic-plastic. Therefore, a coupled mechanical problem is solved starting at a rotation of outer cylinder of 3 degrees, provided the initial temperature being given by the analytical solution at that rotation, and a rotation evolution of the outer cylinder prescribed so that the plastic crown radius varies exponentially in time (eq.(35) of [31]), consistently with eq.(24) of [31]. The reference solution in temperature is shown in figure 5.32. As seen from figure 5.30, the displacement field does not vary much but the thermal field presents the interest of a strong temperature gradient close to the inner cylinder. Therefore, it will not be very interesting to use adaptive meshing technique on the displacement mesh. Therefore, we solve our problem by adapting only the thermal mesh and keeping the mechanical mesh constant.

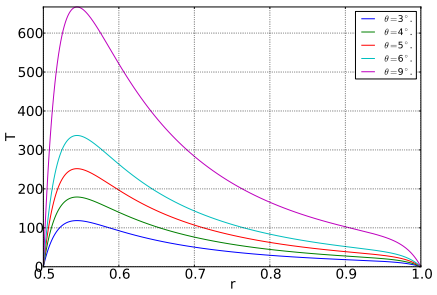

Figure 5.32: Reference solution in temperature.

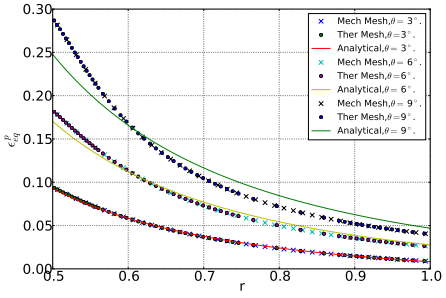

Figure 5.33: Equivalent plastic strain analytical[31] and numerical.

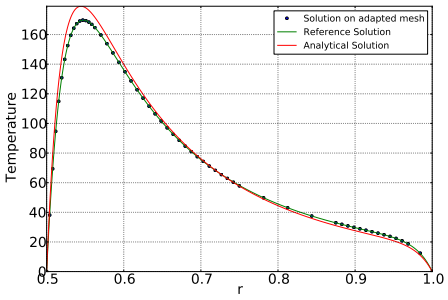

Figure 5.34: Solution on adapted mesh at rotation $\theta = 4°$ of outer cylinder.

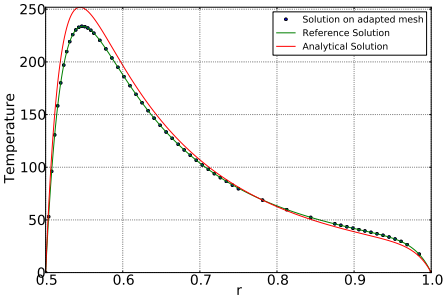

Figure 5.35: Solution on adapted mesh at rotation $\theta = 5°$ of outer cylinder.

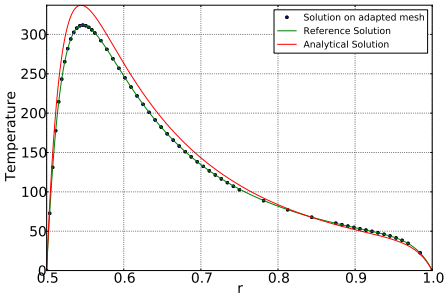

Figure 5.36: Solution on adapted mesh at rotation $\theta = 6°$ of outer cylinder.

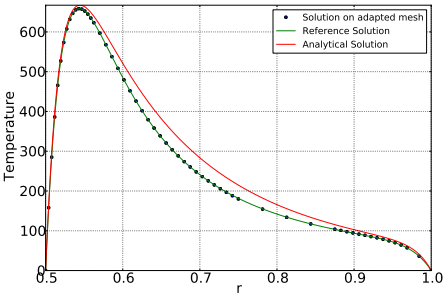

Figure 5.37: Solution on adapted mesh at rotation $\theta = 9°$ of outer cylinder.

Figures 5.34, 5.35, 5.36 and 5.37 show solutions on adapted mesh at rotations $\theta = 4°, 5°, 6°, 9°$ of the outer cylinder respectively. Figure 5.33 shows analytical and numerical plastic strain distribution. One can observe that the numerical solution is very close to the analytical solution. The small differences between the numerical solution and the analytical one can be attributed to the different formulations of the mechanical constitutive models in large strains adopted in these two solutions. However, it is harmless for the mesh adaption purpose we are interested in here.

5.4.2 Analysis

As seen from figure, 5.32, the important domains in the solutions field (domains with high gradients of temperature) do not evolve much with time. Therefore, our algorithm adapts mesh only at the first time step and then it decides to use the same mesh for following time steps.

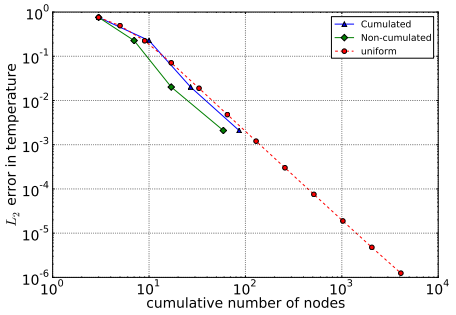

Figure 5.38: L_2 error analysis at rotation $\theta = 4°$ of outer cylinder.

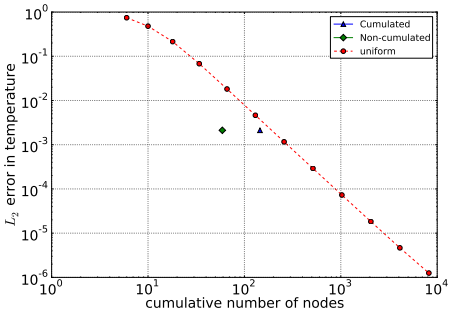

Figure 5.39: L_2 error analysis at rotation $\theta = 5°$ of outer cylinder.

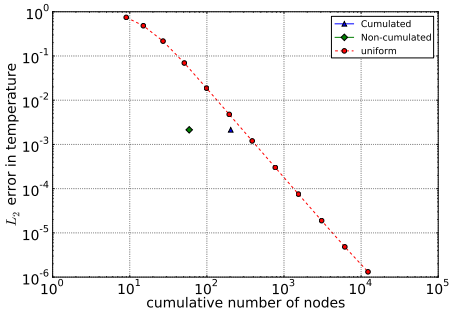

Figure 5.40: L_2 error analysis at rotation $\theta = 6°$ of outer cylinder.

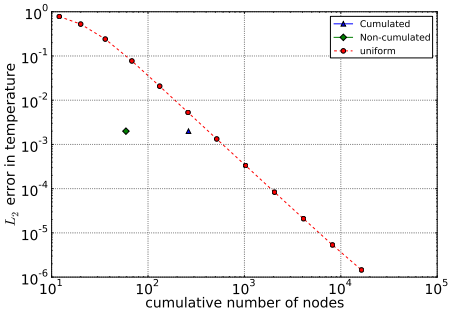

Figure 5.41: L_2 error analysis at rotation $\theta = 9°$ of outer cylinder.

Figures 5.38, 5.39, 5.40, and 5.41 show the L_2 error of the adapted mesh. One can observe that mesh adaption has taken place only at rotation of 4 degrees, all other time steps use the same mesh. The adaptive meshing still appears more economical than a uniform mesh.

5.5 Conclusion

In this chapter, various 1D test cases were studied. Simplicity of unidimensional problems allows to perform a deeper analysis of the algorithm. First, a purely thermal steady state problem with an analytical solution was considered. In this problem, a sharp temperature gradient allowed to have a very visible mesh adaption. The presence of analytical solution allowed exact error analysis and superiority of the mesh adaption over uniform meshes was established. Parametric analysis of algorithmic parameters was performed.

As seen, the parameter Tol_r controls the required accuracy of the solution. Therefore, if very accurate solution is needed, smaller value of Tol_r parameter should be selected so that the adapted mesh is very fine and captures the solution field accurately. However, accurate solution and fine meshes are associated with high computational cost. So, if computational cost is of concern, a higher Tol_r should be chosen. Therefore, chosen value of Tol_r parameter is a trade-off between accuracy and the computational cost. Parameter Tol_d depends on the parameter Tol_r and it should be chosen equal to or less than Tol_r parameter. On the other hand, parameter Tol_0 controls the convergence

to the adapted mesh. This parameter needs to be chosen such that the algorithm stops as soon as it is converged to the optimal mesh no earlier, no later. However, tracking of this exact value is often difficult, therefore, one can choose to be on the conservative side and a few more iterations can be allowed after convergence rather than terminating before convergence. In practice, this does not add significant computational cost because as seen earlier, the cost estimate used in this work is the most pessimistic one.

Second, a strongly coupled thermo-elasticity problem was analyzed. This problem was analyzed in [3] which allowed to obtain a reference solution. Again, cost-effectiveness of the algorithm over uniform meshing was established. Third, an intermediate test cases with weak coupling was presented. In every test case presented, the mesh adaption algorithm was shown to be cost effective with respect to uniform meshing technique.

Having evaluated the algorithm on simpler 1D problems, it is now time to consider more complex problems with geometric intricacies. Therefore in the next chapter, 2D test cases are presented.

Cas test bidimensionnel

Les problèmes nécessite des techniques d'adaptation plus sophistiquées que les problèmes 1D, et permettent de définir des géométries plus complexes. Comme expliqué dans le quatrième chapitre, deux techniques seront étudiées. La première est la technique de bisection à bord unique (SEB) et la seconde est la technique du chemin de propagation de bord le plus long de Rivara (LEPP).

Tout d'abord, un problème thermique stationnaire admettant une solution analytique est étudié, et la performance de l'algorithme d'adaptation est analysée sur ce problème. L'existence d'une solution analytique permet ici aussi de démontrer la meilleure efficence de l'approche proposée par rapport à un raffinage uniforme du domaine de calcul. Deuxièmement, un cas de test thermique transitoire est présenté. Le but de ce cas test est d'analyser l'adaptation des mailles en cas de problèmes transitoires et de montrer le raffinement et le déraffinement du maillage lorsque les domaines d'intérêt bougent au cours de temps. Troisièmement, un problème fortement couplé en thermo-élasticité est étudié afin de comparer l'adaptation des mailles en utilisant les techniques SEB et LEPP. On constate que, en termes de potentiel énergétique, SEB converge vers une solution exacte plus rapide que LEPP. Ceci est conforme à nos attentes car, en ce qui concerne LEPP, il existe une contrainte sur le rapport d'aspect de l'élément, alors que la technique SEB est seulement guidée par des critères d'adaptation. Quatrièmement, un cas test considérant une bande de cisaillement adiabatique est présenté, ce qui a permis de démontrer l'efficacité de l'algorithme dans des problèmes complexes avec de grandes déformations. Enfin, un cas test industriel de soudage par friction linéaire est présenté.

Chapter 6

Bidimensional test cases

6.1 Introduction

The previous chapter examined the mesh adaptation algorithm on 1D test cases. While it allowed a deep analysis of the adaptation criteria, the mesh adaptation technique was quite simple. Problems in 2D (and 3D) are the major problem one needs to tackle with geometric complexities. This requires more sophisticated adaptation techniques than 1D problems. As explained in the fourth chapter, two techniques will be studied. First is the single edge bisection (SEB) technique and second is Rivara's longest edge propagation path (LEPP) technique.

The second section introduces a steady state thermal test case with an analytical solution. Cost analysis is performed for this test case as it has an analytical solution. In order to demonstrate effective refinement and coarsening in case of transient problems, in third section a transient thermal test case is studied. This test case is set up such that the domains on interest change their spatial location with time and mesh refinement and coarsening is visible. In order to compare the SEB and LEPP techniques, a strongly coupled test case with linear thermo-elasticity is presented. In case of strongly coupled problems, a very important phenomenon is that of shear bands. This is a very complex phenomenon and is presented in next test case with an axisymmetric geometry. Finally, in order to present a test case similar to an industrial process, a representative test case of linear friction welding is

presented.

6.2 Steady state thermal

The first test case is a steady state thermal test case that admits a known analytical solution. Therefore, one can easily compare the numerical error in case of uniform meshing technique and mesh adaption technique.

Consider a rectangular plate of width W and height H subjected to the following boundary conditions as shown in figure 6.1:

$$\begin{aligned} T &= T_1 \qquad \text{at } x = 0 \text{ and } x = W \ \forall y \in]0, H[,\ y = 0 \ \forall x \in]0, W[\\ T &= T_2 \qquad \text{at } y = H \ \forall x \in]0, W[\end{aligned} \tag{6.1}$$

Here, the boundary conditions impose a jump in temperature from T_1 to T_2 at the two top corners of the plate. Because of this jump, the energy like potential (3.28) should indicate drastic improvement in the solution through refinement of patches near these two corners. Therefore, the expected adapted mesh obtained by the mesh adaption algorithm explained earlier in chapter 3 should be very fine near these corners due to this singularity. This simulation of mesh adaption was carried out using a starting mesh of four 6-Node triangular elements as shown in figure 6.1. The final adapted mesh and the solution field is shown in figure 6.2. As expected, the adapted mesh obtained is very fine near the corners with temperature discontinuity. This simulation was carried out using SEB technique.

Note that here the obtained mesh is symmetric and well structured. This is because of the symmetry of the geometry and loading of this problem and the usage of quadratic elements. But, in general this is not true. One often obtains anisotropic adapted meshes with elongated elements when a SEB technique is used. The algorithm can be combined with other patching strategies to produce meshes with desired geometric characteristics as it has been done when using LEPP technique.

The analytical solution for this test case can be found in [32, Chapter 3]. The solution reads:

$$\frac{T - T_1}{T_2 - T_1} = \frac{2}{\pi} \sum_{n=1}^{\infty} \sin\left(\frac{n\pi x}{W}\right) \frac{\sinh(n\pi y/W)}{\sinh(n\pi H/W)} \tag{6.2}$$

The efficiency of the algorithm is analyzed by comparing the error in the numerical solution with respect to the analytical solution (6.2), as a function of the number of nodes of the mesh.

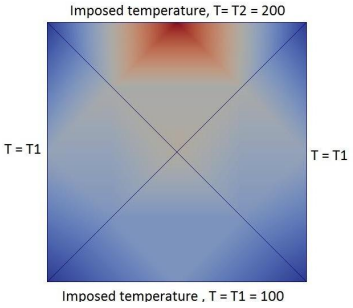

Figure 6.1: Solution field on initial mesh along with the boundary conditions.

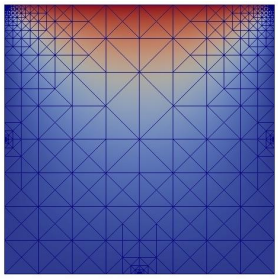

Figure 6.2: Numerical solution on adapted mesh.

Three cases are considered as explained in previous chapter. First for uniform meshes used as a reference, second with number of nodes and third for cumulated number of nodes.

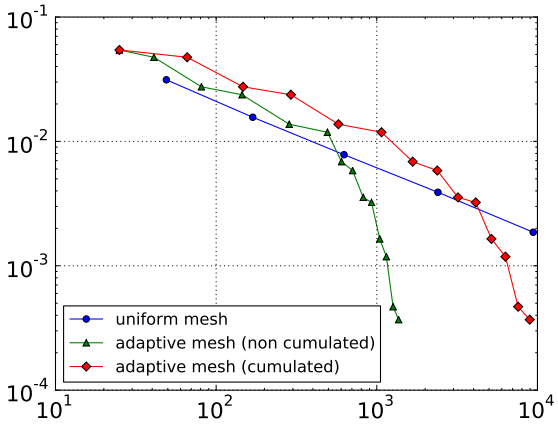

Figure 6.3: Analysis of the algorithm. Number of nodes on X axis and L_2 error in temperature on Y axis.

Figure 6.3 shows this plot for L_2 norm of error in temperature field with respect to the analytical solution (6.2). One can observe that even the curve

using cumulated number of nodes crosses the line for uniform meshes. In other words, beyond this crossing point, more precise solution is obtained with less computational cost using variational mesh adaption.

6.3 Transient purely thermal test case

In order to demonstrate mesh adaption in case of transient problems, a transient thermal test case is presented. Let's consider a rectangular region of size $10m \times 10m$, the boundary temperature of which is prescribed to zero. An external heat source is introduced that follows a circular path in time with center coinciding with that of the rectangle. The width of the heating area at one instant is the arc length of 1 degree and the length is 1m. This can be seen in figure 6.4. Every second, the heat source location moves one degree in anticlockwise direction.

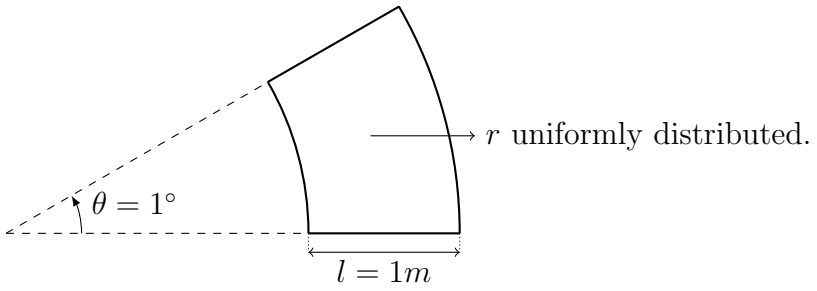

Figure 6.4: Representation of heating area at an instant.

Figures 6.5, 6.6, 6.7, 6.8, 6.9 and 6.10 show the solution fields on the adapted meshes at different time steps. A strong mesh adaption is performed in this test case because the location of strong temperature gradients moves with the prescribed heat source. The mesh coarsening upstream from the heat source appears as efficient as the mesh refinement where the heat source is located. It is therefore evident that this adaption strategy works well and is more cost effective than using a simple uniform mesh.

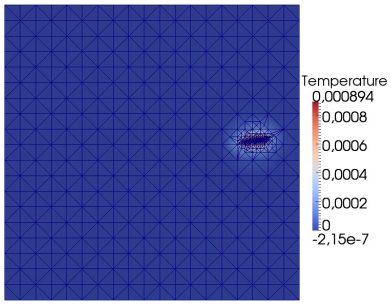

Figure 6.5: Temperature field at time step 1.

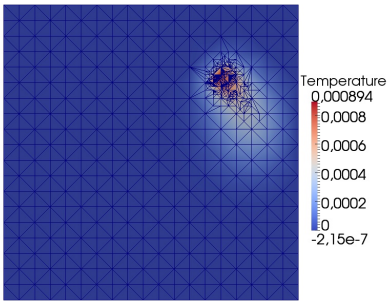

Figure 6.6: Temperature field at time step 8.

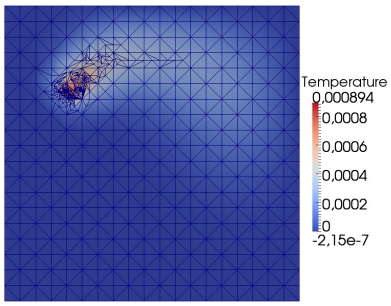

Figure 6.7: Temperature field at time step 24.

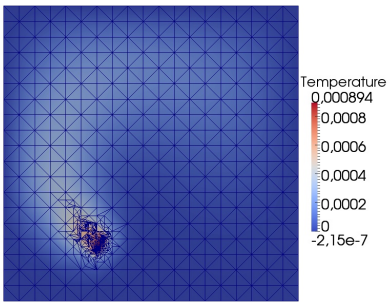

Figure 6.8: Temperature field at time step 40.

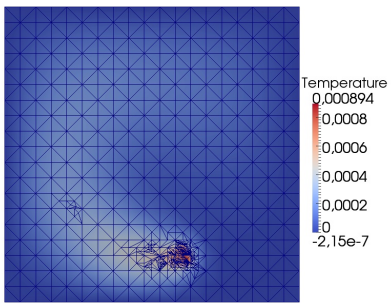

Figure 6.9: Temperature field at time step 48.

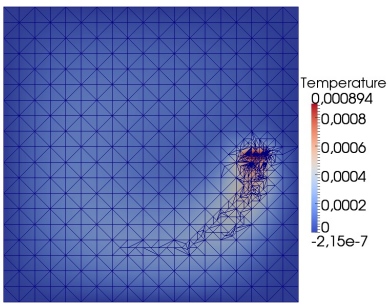

Figure 6.10: Temperature field at time step 60.

6.4 Linear thermo-elasticity

The purpose of this test case is to compare SEB and Rivara's LEPP mesh adaption techniques. Also, the test case demonstrates the application of mesh adaption algorithm on a strongly coupled problem.

Consider a rectangular plate of size $32mm \times 50mm$ with a circular hole of radius $2.5mm$ at its center. The plate is submitted to compression through imposed displacement in its Y direction. Making use of the symmetries, only one quarter of the plate is modelled. Zero heat flux boundary condition is prescribed for the thermal part whereas for the mechanical part, negative displacement is imposed on top which increases at a rate of 0.0001 per second; with symmetry conditions on planes x = 0 and y = 0, and free boundaries on the remaining faces. Figure 6.11 shows the computational domain and the boundary conditions.

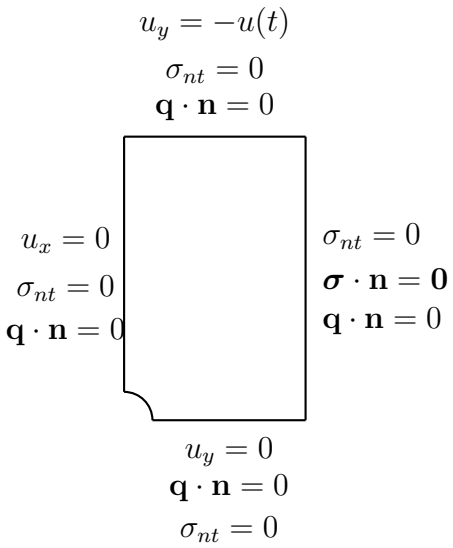

Figure 6.11: Geometry and boundary conditions for thermo-elasticity problem. $\sigma_{nt} = 0$ on all boundaries.

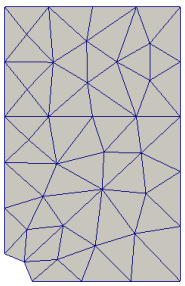

Figure 6.12: Initial thermal and mechanical mesh for thermo-elasticity problem.

Due to the stress concentration near the hole as shown in figure 6.13, the

mechanical mesh adaption should produce a finer mesh around the hole at the first time step. Similarly, due to high temperature gradients near the hole as shown in figure 6.14, the thermal mesh adaption should also produce a finer mesh around the hole. Unlike the transient thermal test of section 6.3, severe mesh coarsening and refinement should not be observed at each time step because the domain of interest does not change with respect to time.

Initial mesh for both thermal and mechanical part is shown in figure 6.12. Figures 6.15 and 6.16 show adapted meshes for mechanical part obtained by using SEB technique and by using LEPP technique respectively. Observe that in both cases, we have a fine mesh near the hole and a coarser mesh far from the hole. Therefore, both these meshes represent a good solution field. However, one can observe that in figure 6.15, the mesh has elongated elements (anisotropic mesh). This difference is even more evident in the temperature field shown in figures 6.17 and 6.18. Observe the four elongated elements in figure 6.17, which shows the solution field on a mesh obtained by SEB technique. This anisotropy is avoided in Rivara's LEPP algorithm as shown in figure 6.18. It is important to note that the mesh adaption is performed only at the first time step and no major changes in the mesh are observed after the first time step. The high computational cost associated with using a uniform fine mesh is avoided by using adaptive algorithm irrespective of the nature of patch used.

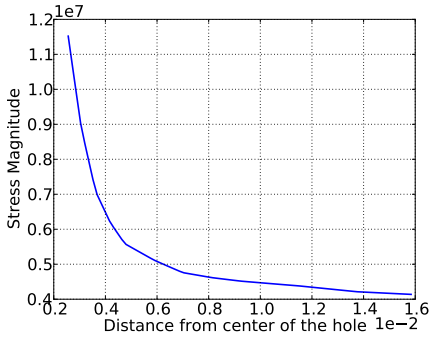

Figure 6.13: Stress magnitude along the radial direction on the x-ligament.

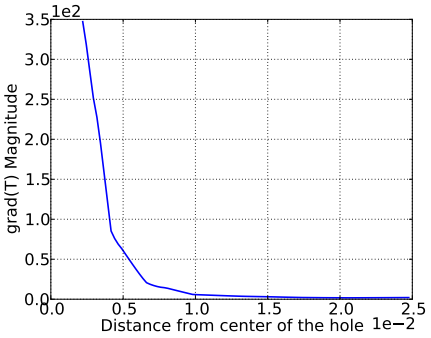

Figure 6.14: Magnitude of gradient of temperature along the radial direction on the x-ligament.

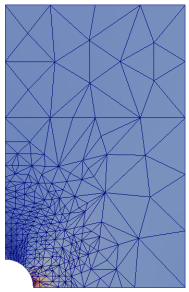

Figure 6.15: Mechanical adapted mesh obtained using single edge bisection technique.

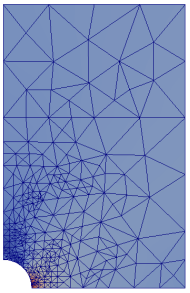

Figure 6.16: Mechanical adapted mesh obtained using Rivara's technique.

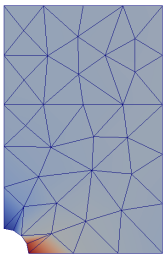

Figure 6.17: Thermal adapted mesh obtained using single edge bisection technique.

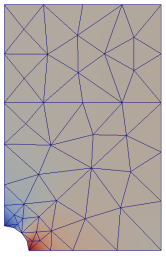

Figure 6.18: Thermal adapted mesh obtained using Rivara's technique.

In order to compare SEB and LEPP techniques, at the first time step, mesh adaption is allowed to continue for more iterations. However, while making these comparisons, parameters for both the cases are chosen such that precision level of required solution is of the similar order. Here we leverage the fact that the mesh adaption is observed only at first time step. In case of Rivara's technique, there is a constraint on element aspect ratio. However, in case of edge bisection technique, the sole criterion is the value of energy potential. Therefore, only the underlying physics drives mesh adaption without any geometrical constraint. Figures 6.19 and 6.20 show the comparison of energy potential values for mechanical and thermal mesh respectively. Recall that the mechanical step of the staggered scheme is associated to a minimum of the functional while the thermal step is associated

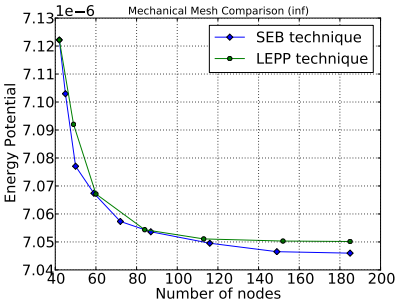

Figure 6.19: Comparison of mesh adaption techniques for mechanical mesh.

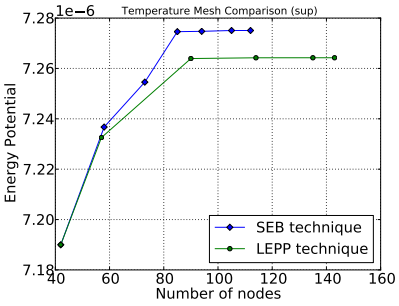

Figure 6.20: Comparison of mesh adaption techniques for thermal mesh.

to a maximum. The results show that SEB gives slightly better results in terms of potential which is in accordance with the previous reasoning.

6.5 Shear bands

A shear band is a narrow region presenting large deformation and high temperature rise which appears due to thermal softening in various ductile materials [68]. The hat shaped specimen [68] is a well known experimental apparatus, used to trigger shear bands and study rate dependent behaviour. This system proves to be an interesting test case to demonstrate mesh adaption in case of complex coupled problems in the framework of finite strains with thermo-elasto-visco-plasticity. Its geometry as well as the considered boundary conditions in a longitudinal cut are shown in figure 6.21. Zero heat flux is imposed on all the boundaries, and the specimen is compressed by means of an imposed displacement on the top. The geometry and imposed displacement on the top (at a rate of $1mm$ per second) causes high shear stress along segment AB, i.e. vector $\mathbf{t}$ in figure 6.21. The dissipation causes temperature to rise along $\mathbf{t}$ and this leads to the softening of the $\alpha-$Titanium alloy considered in this test case which is known to be sensitive to shear banding. The constitutive model used is thermo-visco-elasto-plasticity; one can refer to Stainier er al. [67] for details material properties of $\alpha-$Titanium alloy. Softening causes intensification of plastic strains and the shear band appears.

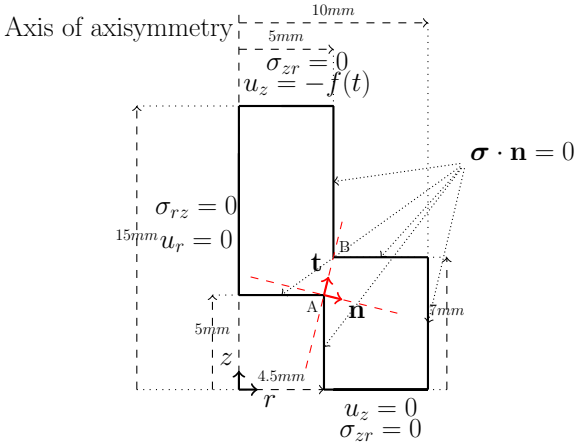

Figure 6.21: Geometry and mechanical boundary conditions of shear band specimen.

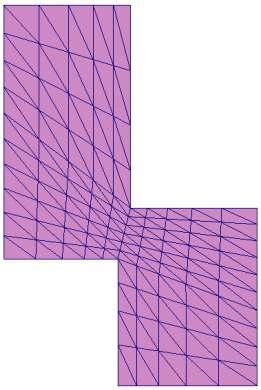

Figure 6.22: Initial mesh for thermal and mechanical parts.

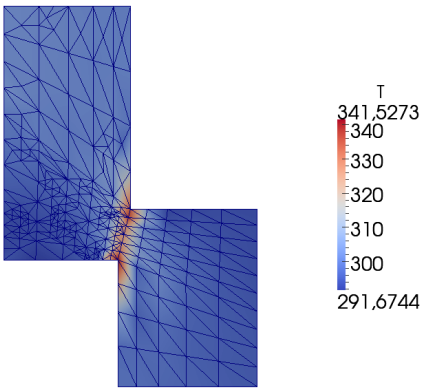

Figure 6.23: Final adapted thermal mesh with temperature field.

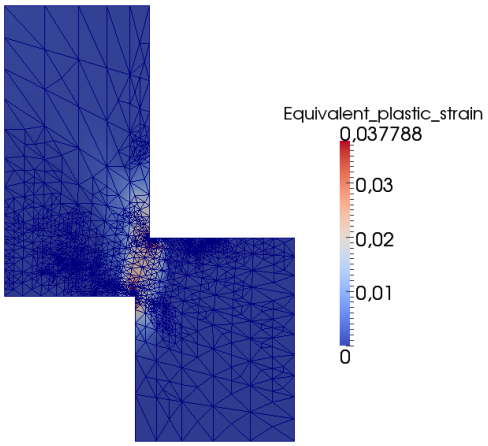

Figure 6.24: Final adapted mechanical mesh with equivalent plastic strain.

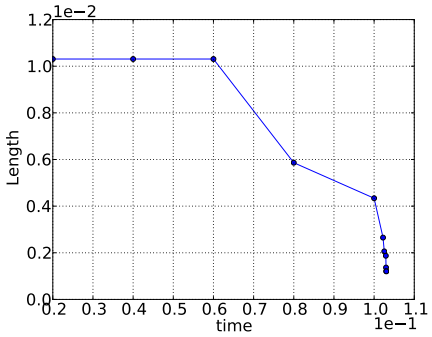

Figure 6.25: Evolution in time of length of segment l for $k = 0.3$ in equation (6.3).

The initial mesh for mechanical and thermal part is the same and is shown in figure 6.22. Rivara's LEPP mesh adaption technique is used in the presented results. The final adapted thermal mesh at the final time step is shown along with temperature distribution in figure 6.23. Mesh adaption can be seen in areas where sharp temperature gradients need to be captured. The final adapted mechanical mesh at final time step along with equivalent plastic strain is shown in figure 6.24. In case of mechanical part, the mesh adaption is driven by stress field and the concentration of high strain rate caused by high temperature concentration.

In order to analyze the evolution of the temperature concentration over time, the length of a segment l along direction $\mathbf{n}$ defined in figure 6.21 is plotted. The segment l is defined as:

$$l = \{x \mid T(x) > kT_{max}\}, 0 < k < 1. \tag{6.3}$$

It corresponds to a certain width of a domain within which sharp temperature rise occurs due to the appearance of a shear band with time. At the beginning, uniform temperature causes segment l to cover the whole domain. As the shear band starts appearing, temperature concentration in the band region starts increasing, this causes the chracteristic length of segment l to reduce drastically and it covers the domain close to that of the actual shear band when it propagates upto an arbitrary factor k. Evolution of this length l in time is shown is figure 6.25. The length reduces representing the increase of

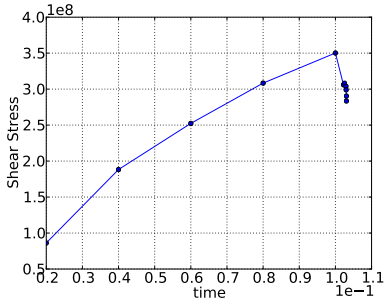

Figure 6.26: Evolution of $\langle \sigma_{nt} \rangle_{AB}$ with time.

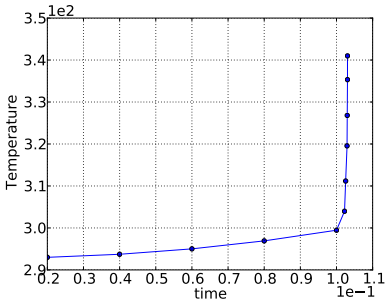

Figure 6.27: Evolution of maximum temperature T_{max} with time.

temperature concentration in time. In order to study the evolution of the shear stress in the band region, we consider the vector $\mathbf{t}$ along the segment AB and the vector $\mathbf{n}$, orthogonal to segment AB as shown in figure 6.21. The evolution of the average shear stress σ_{nt} along segment AB is shown in figure 6.26. The shear stress increases till time 0.10 seconds when material softening due to increased temperature starts, leading to reduction in shear stress. This temperature rise is evident in figure 6.27. Here, maximum temperature is plotted with time. A kink in temperature increase can be clearly observed at time 0.10 seconds.

In the work of Su et al. [68], authors use an analytical solution developed by Leroy et al. [40] for a 1-D shear band problem. The temperature distribution is given by:

$$T(y) = T_{max} - (T_{max} - T_{ref}) \frac{\log\left(\cosh\left(\frac{y}{h}\right)\right)}{\log\left(\cosh\left(\frac{H}{h}\right)\right)} \tag{6.4}$$

and the velocity is given by:

$$V(y) = V_0 \frac{\tanh\left(\frac{y}{h}\right)}{\tanh\left(\frac{H}{h}\right)} \tag{6.5}$$

However, this solution is valid for 1-D problem and Dirichlet boundary conditions in temperature are applied. Therefore, a regression[1] is used in order to find the parameter h appearing in equations (6.4) and (6.5) and it is assumed that all the displacements lead to plastic strains so that the

[1]Regression is a process of finding values of parameters that represent best fit with minimum L_2 error.

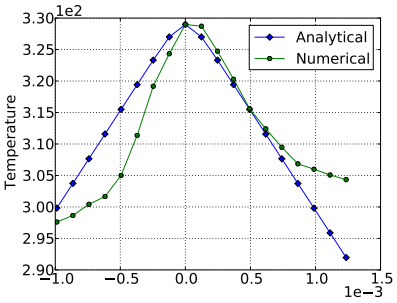

Figure 6.28: Numerical and analytical temperature profile along **n** at time 0.103037.

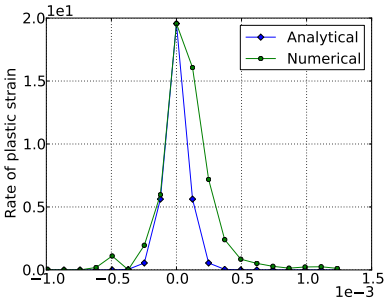

Figure 6.29: Numerical and analytical rate of plastic strain along **n** at time 0.103037.

analytical expression of the plastic strain rate can be obtained by taking the gradient of V (6.5). The plots in figures 6.28 and 6.29 show the numerical and analytical solutions of temperature and plastic strain rate along **n** neglecting the domains close to boundaries. It can be seen that analytical and numerical profiles are close, the differences are due to the different boundary conditions. This test case demonstrates how precise solutions of complex strongly coupled problems can be obtained using the proposed mesh adaption strategy.

6.6 Linear Friction Welding (LFW)

Linear friction welding is an industrial process that involves very strong thermo-mechanical coupling. Two parts to be welded are rubbed against each other; the friction causes temperature to rise which causes material to soften on a small skin depth and parts get welded by diffusion bonding. Therefore, this is an interesting test case to demonstrate the mesh adaption technique for industrial-like processes. Numerical simulation of linear friction welding has been studied among others by Debeugny *et* al. [20], whereas M. Foca *et* al. [23] use a mesh free approch for simulating the process. Li et al. [41] use complete remeshing to advance their simulations. However, this costs loss in precision due to significant numerical diffusion. Figure 6.30 shows the geometry and boundary conditions for test case used by Li *et* al. [41].

In order to avoid stresses due to discontinuity in boundary conditions

and to focus on stresses generated by linear friction welding, the sole bottom part with free lateral boundary conditions is considered. Second, half of this bottom part is meshed due to symmetry, so that $u_x = 0$, $\sigma_{xy} = 0$ and $\mathbf{q} \cdot \mathbf{n} = 0$ are applied on segment AD. This modelling assumes the horizontally blocked top part of figure 6.30 to be rigid, hence the loading is prescribed by means of a displacement u_y imposed segment DC. Segment BC is free, i.e. there is zero traction and zero heat flux. On segment AB, contact is applied for mechanical part, and in order to represent heat generation due to friction, heat flux is applied. The modelled geometry and boundary conditions are shown in figure 6.31. The applied heat flux consists of the friction shear stress $\boldsymbol{\tau}$ times the tangential velocity of oscillations $\mathbf{v}$, here assuming that all the heat generated in friction is assumed to contribute to the input heat flux $\bar{q}$:

$$\bar{q} = \boldsymbol{\tau} \cdot \mathbf{v} = 4\tau\alpha f \tag{6.6}$$

where α is the magnitude of oscillations, f is the frequency of oscillations and τ is the magnitude of friction stress given by:

$$\tau = \mu\sigma_N \tag{6.7}$$

where μ is the coefficient of friction and σ_N is the magnitude of normal pressure applied. Johnson-Cook model for thermo-elasto-visco-plasticity is used for computations.

The initial mesh used for thermal part is coarser than that of the mechanical part, they are shown in figures 6.32 and 6.33 respectively. Single edge bisection technique is used for mesh adaption in this problem. In the beginning of loading, high strains occur close to boundary that cause mechanical mesh refinement in that region as shown in figure 6.34. After a few time steps, when the stress field is well developed, the mesh is adapted according to the stress field as shown in figure 6.35. Figure 6.36 shows the stress field at the final calculated time step.

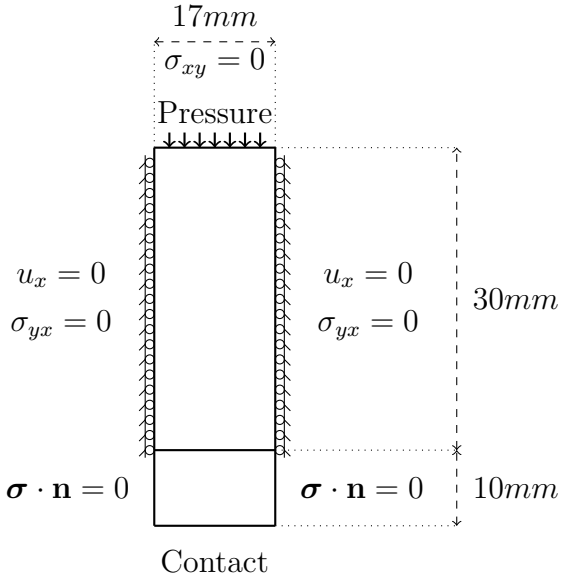

Figure 6.30: Geometry and boundary conditions of the linear friction welding problem in [41].

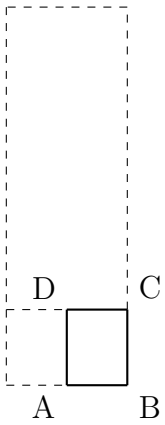

Figure 6.31: Simplified modeling of the problem. Boundary conditions of symmetry on AD, contact and heat flux on AB and imposed displacement on DC are applied. Boundary BC is free.

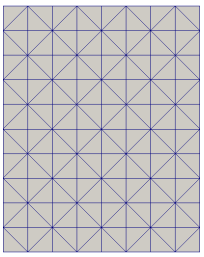

Figure 6.32: Initial mesh for thermal part for linear friction welding test case.

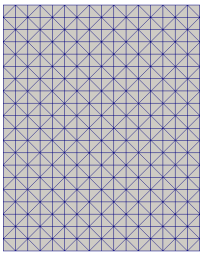

Figure 6.33: Initial mesh for mechanical part for linear friction welding test case.

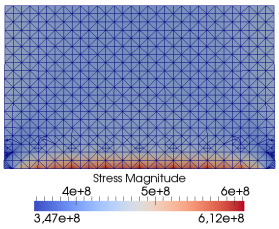

Figure 6.34: Stress field and mechanical mesh (along with reflection) at preliminary stages.

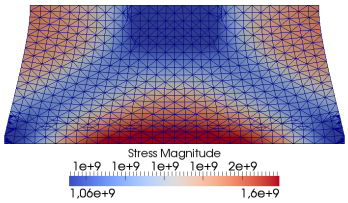

Figure 6.35: Mechanical mesh (along with reflection) after developed stress field.

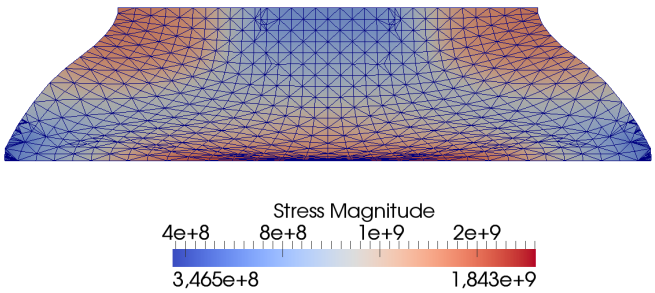

Figure 6.36: Stress field at last calculated time step along.

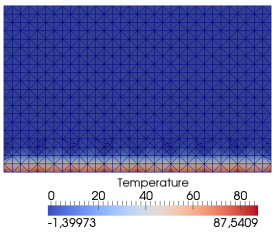

Figure 6.37: Temperature field and thermal mesh (along with reflection) at preliminary stages.

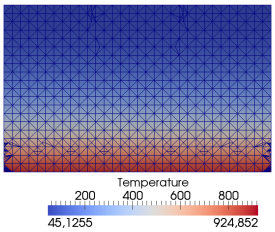

Figure 6.38: Thermal mesh (along with reflection) at final time step.

The adapted thermal mesh captures a smooth temperature field, which is clearly shown with the adapted mesh at the beginning in figure 6.37. Near the contact surface, the maximum temperature is reached and far from contact surface temperature is almost uniform. This causes finer mesh in between these two zones in order to capture the gradient of temperature field. The adapted thermal mesh along with the associated temperature field at final calculated time step is shown in figure 6.38. Because the temperature gradient is smooth, mesh is relatively coarser compared to figure 6.37. Fine mesh near contact boundaries is seen because of distortions seen in figure 6.36.

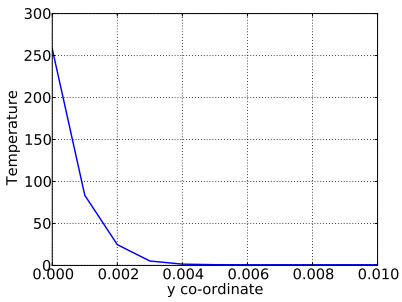

Figure 6.39: Temperature profile on a line along y direction passing through mid-points of segments AB and DC in figure 6.31.

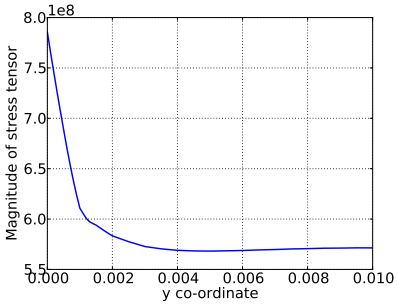

Figure 6.40: Magnitude of stress tensor on a line along y direction passing through mid-points of segments AB and DC in figure 6.31.

From the adapted meshes in figures 6.34,6.35,6.37 and 6.38 one can also

observe refinement along x axis at some distance from bottom. This is because the material is very soft in the skin depth which is being welded and there is an interface between the soft part and the hard part. The adaptation of mesh in the above mentioned region captures this interface. This can be seen when a plot of temperature field and magnitude of stress tensor is made along y direction. These plots are shown in figures 6.39 and 6.40 respectively. One can observe the curvature of the field from $y = 0.01$ to $y = 0.02$. Comparing this with the adapted meshes, the reason behind mesh adaptation can be identified. As seen from results, the proposed mesh adaption strategy can be useful in test cases involving strong thermo-mechanical coupling along with large deformations.

6.7 Conclusion

This chapter presented several test cases in two dimensions. First, a steady state thermal problem with an analytical solution was analyzed for performance. The availaibility of an analytical solution allowed to demonstrate the cost effectiveness over uniform mesh. Second, a transient thermal test case was presented. The purpose of this test case was to analyze mesh adaption in case of transient problems and to show the dynamic mesh refinement and coarsening when domains of interest change their spatial location drastically. Third, a strongly coupled problem in thermo-elasticity was studied. A comparison of mesh adaption using SEB and LEPP techniques was carried out. Fourth, a shear band test case was presented which allowed to demonstrate the effectiveness of the proposed algorithm in complex problems with large strains. Finally, an industrial like test case of friction welding was presented.

General conclusion and perspectives

General conclusion

In this work, a mesh adaptation strategy for strongly coupled problems was proposed. In the second chapter, thermo-mechanical problems were introduced starting the balance equations. The monolithic approach for coupled problems consists in simultaneously solving all field equations of concerned physical phenomena. This leads to big systems to be solved and needs same mesh for all considered physical phenomena. Due to this, in order to capture different scales and domains of interest of different phenomena, one needs to use a very fine mesh everywhere which leads to an even bigger system. Such huge systems are generally too costly for commercial simulations. On the other hand, staggered approaches consist in sequential resolution of field equations in which one physical phenomenon is considered at a time. This strategy divides one big system into smaller systems that are cheaper to solve. This also allows using different meshes for different physical phenomena and one can adapt them separately to capture different scales and domains of interest for each physical phenomenon. For thermo-mechanical problems, two staggered techniques were presented: one using isothermal setting and another using adiabatic setting. In isothermal setting, mechanical part is solved assuming isothermal conditions. Whereas in adiabatic setting, mechanical part is solved assuming adiabatic thermal conditions. The adiabatic setting gives the required stability as shown in [3].

The proposed mesh adaptation approach is based on the variational framework introduced in third chapter. Using a variational approach, thermo-

mechanical problems can be restated as a saddle point problem of an energy like functional. Generally, the functional is convex with respect to displacement field and concave with respect to temperature field. Therefore, the thermo-mechanical problem can be restated in terms of an energy like potential I as shown in chapter 3:

$$\{\mathbf{u}, T\} = \arg \inf_{\mathbf{u}} \sup_{T} I(\mathbf{u}, T) \tag{6.8}$$

In case of staggered approaches, mechanical and thermal parts are sequentially solved:

$$\begin{aligned} \mathbf{u} &= \arg \inf_{\mathbf{u}} I(\mathbf{u}, T) \\ T &= \arg \sup_{T} I(\mathbf{u}, T) \end{aligned} \tag{6.9}$$

An indicator for mesh adaptation is derived from the above representation of thermo-mechanical problem. Significant improvement in the value of energy like potential upon refinement indicates significant error. This allows to define mesh adaptation as an optimization problem as shown in chapter 4:

$$\begin{aligned} \inf_{\mathbf{u}\in\mathcal{V}_h} \left\{ I_h(\mathbf{u}_n, \theta_{n-1}) + \mu_g^u N_u \right\} &\equiv \inf_{\mathbf{u}\in\mathcal{V}_h} \mathcal{I}_u(\mathbf{u}_n, \theta_{n-1}, N_u) \\ \sup_{\theta\in\mathcal{W}_h} \left\{ I_h(\mathbf{u}_n, \theta_n) - \mu_g^T N_T \right\} &\equiv \sup_{\theta\in\mathcal{W}_h} \mathcal{I}_T(\mathbf{u}_n, \theta_n, N_T) \end{aligned} \tag{6.10}$$

That is, the problem is to find a mesh that represents the solution field accurately with a computational cost derived from parameters μ_g^u and μ_g^T. This definition of mesh adaptation problem makes the approach free from error estimates based on field reconstructions. The additive property of the variational functional allows to use the local patch by patch approach to mesh adaptation. Refinement process consists in solving a small (computationally very cheap) problem on local patch to decide if that patch should be refined in

the global mesh. Coarsening is also a similar patch by patch process. Doing this for all patches gives a new adapted mesh. This is an iterative process and the convergence criteria is related to the relative improvement in the value of energy like potential between two successive iterations. Internal variables are assumed to be constant over piece of Voronoï cells as explained in fourth chapter. This avoids excessive numerical diffusion caused by avoiding the complex remapping procedures.

Two mesh adaptation techniques were studied. First, the single edge bisection (SEB) technique in which a patch consists of a ring of elements around an edge. The patch is refined by adding a new node on that edge and splitting the adjacent elements into two. Second, Rivara's longest edge propagation path (LEPP) technique. In this, a patch is constructed in such a way that longer edges are bisected prior to shorter ones in immidiate viscinity. Therefore, a patch consists of a series of edges of increasing length and ring of elements around them; edges are bisected starting from the longest edge every time dividing adjacent elements in two. This means a bigger LEPP patch than a SEB patch if the edge under consideration is not the longest edge for all adjacent elements. In case of SEB technique, one often obtains highly anisotropic meshes. However, this anisotropy is related to the underlying physics as sole mesh adaption criterion drives mesh refinement and coarsening without constraining the element aspect ratio. Whereas, LEPP technique constrains the element aspect ratio that allows to obtain meshes with smallest angle grater than 30°. This avoids highly anisotropic meshes at additional computational cost. The superiority of SEB technique in terms of energy like potential value was established using a linear thermo-elasticity test case in the sixth chapter.

In order to analyze the algorithm, 1D test cases were introduced in fifth chapter and 2D test cases were introduced in sixth chapter. The algorithm was applied to steady state thermal problem with an analytical solution in 1D and in 2D. In both cases, cost effectiveness and superiority of the mesh adaptation strategy over using a uniform mesh was established. A detailed parametric analysis of all algorithmic parameters was carried out. Indeed, the parameters Tol_0, Tol_r and Tol_d are not independent, but keeping other two

parameters constant, the sole effect of each parameter was studied. The Tol_r parameter should be chosen from a trade-off between required accuracy and computational cost; parameter Tol_0 should be chosen such that the algorithm stops as soon as it is converged; lastly, Tol_d parameter should be chosen less than Tol_r parameter for ensuring stability. The transient thermal problem in 2D demonstrated effective refinement and coarsening of the mesh in a case with rapid change of domain of interest. Thermo-elasticity problem in 1D introduced as a first example of strongly coupled problem. Thermo-elasto-plasticity problem in 1D was an intermediate problem with weak coupling. It adapted only one mesh whereas the other mesh was kept constant. The cost effectiveness over uniform mesh was also established for these two test cases in 1D. A strongly coupled problem of shear band was presented and effective mesh adaptation was demonstrated. As an example of industrial like test case, a test case of friction welding was presented. All these test cases demonstrate the adaptability of the algorithm to different problems.

Perspectives

Adaptation criteria

First, the proposed adaptation criteria remains valid as long as the variational functional is convex (or concave). Some extra development is necessary to take into account non-convex functionals. This would mean to use a technique similar to simulated annealing that will allow to escape the local minimum. Problems of material instabilities and buckling can be considered as potential applications of this development. Second, the improved algorithm of fifth chapter that introduces another parameter can be extended to problems in 2D. Therefore if local improvement upon refinement is highly significant, then patch can be considered for double refienement, so that an element would be divided into four elements instead of two as shown in figure 6.41. Indeed, if the patch is to be divided as shown, the patch would need subdivision of elements out of the patch. This will reduce the number of interations thereby

reducing the number of full solutions and allow to gain more computational cost.

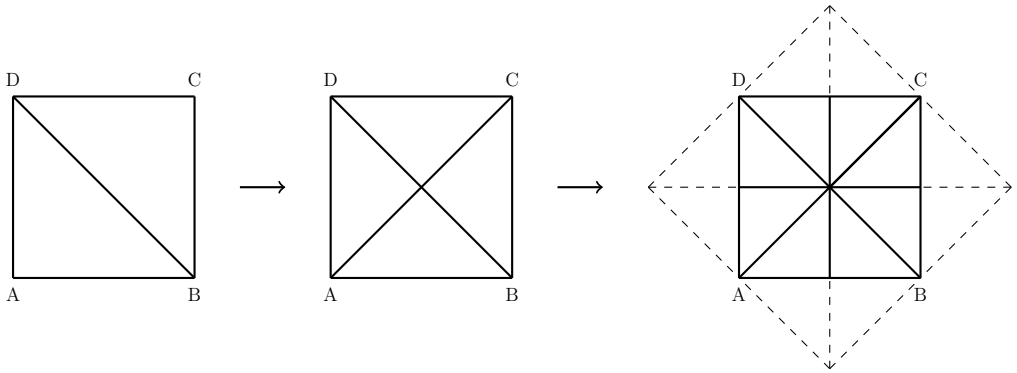

Figure 6.41: If the initial patch is $ABCD$ as shown in the diagram on the left. The refined patch on which local problem will be solved is shown in the middle diagram. If the error indicated is highly significant, even more refined version of patch would be used in the global mesh as shown in the diagram on the right.

Third, a robust parameter selection process needs to be investigated. This would probably mean developing another algorithm that will choose correct parameters for a given problem and required level of accuracy. One can also imagine to generate data by running the algorithm for different test cases using different parameters and use machine learning techniques to predict the correct parameters for the given problem and given level of accuracy.

Adaptation techniques

First, similar to SEB technique, one can also imagine dividing a single triangle in different ways. For example, a triangle can be divided into three by inserting a new node at its centroid as shown in figure 6.42. Then a combination of SEB and this technique can be used.

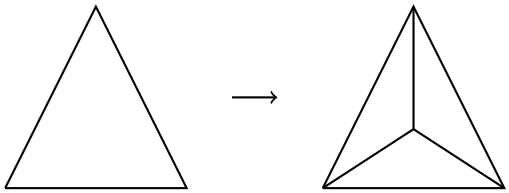

Figure 6.42: Diagram on left shows an original triangle which can be divided into three by inserting a new node at its centroid as shown in diagram on right.

Second, other local refinement techniques in literature like CHARMS [26, 55] can be tested.

Third, the algorithm should be extended to take into account 3D problems. This perspective is more related to adaptation technique as the same adaptation criteria can be used. One can easily extend the SEB technique in 3D. The patch involves the whole ring of tetrahedra around an edge in 3D and refined version divided each tetrahedron into two. This technique is described by Mosler et al. [48] in their work. Rivara's LEPP technique is also available in 3D [60].

Fourth, the strategy can be extended to take into account p-adaptation. This is quite straightforward, one can take one element and change the interpolation order within the element by introducing more nodes along the edges without changing spatial location of original nodes, and then one can use the proposed mesh adaptation criteria. The coarsening would involve reducing the interpolation order. However, this would require use of mixed-order elements on a patch.

Bibliography

[1] Chapter 16: Arbitrary lagrangian-eulerian formulation. `https://www.sharcnet.ca/Software/Ansys/17.0/en-us/help/ans_lsd/Hlp_L_aleform.html`. Accessed: 21-07-2017.

[2] M. Ainsworth and JT. Oden. A posterior error estimation in finite element analysis. *Wiley: New York*, 2000.

[3] F. Armero and J.C. Simo. A new unconditionally stable fractional step method for non-linear coupled thermomechanical problems. *International Journal for Numerical Methods in Engineering*, 35:737–766, 1992.

[4] I. Babuska and B.A. Szabo. On the rate of convergence of finite element method. *International journal of numerical methods in engineering*, 18:323–341, 1982.

[5] K.J. Bathe and H. Zhang. A mesh adaptivity procedure for cfd and fluid-structure interactions. *Computers and Structures*, 87:604–617, 2009.

[6] G. Batra. On a principle of virtual work for thermo-elastic bodies. *Journal of Elasticity*, 21:131–146, 1989.

[7] R.C. Batra and K.I. Ko. An adaptive mesh refinement technique for the analysis of shear bands in plane strain compression of a thermoviscoplastic solid. *Computational mechanics*, 10:369–379, 1992.

[8] M. Ben-Amoz. On a variational theorem in coupled thermoelasticity. *Journal of Applied Mechanics*, 32:943–945, 1965.

[9] M. Biot. Thermoelasticity and irreversible thermodynamics. *Journal of Statistical Physics*, 27:250–253, 1956.

[10] M. Biot. Linear thermodynamics and the mechanics of solids. *Proceedings of the third US National Congress of Applied Mechanics*, pages 1–18, 1958.

[11] H. Borouchaki, P. Laug, A. Cherouat, and K. Saanouni. Adaptive remeshing in large plastic strain with damage. *International journal of numerical methods in engineering*, 63:1–36, 2005.

[12] H. Borouchaki, P. Laug, A. Cherouat, and K. Saanouni. Adaptive remeshing in large plastic strain with damage. *International journal of numerical methods in engineering*, 63:1–36, 2005.

[13] D. Brancherie, P. Villon, and A. Ibrahimbegovic. On a consistent field transfer in non linear inelastic analysis and ultimate load computation. *Computational Mechanics*, 42(2):213–226, 2008.

[14] L. Brassart, L. Stainier, I. Doghri, and L. Delannay. Homogenization of elasto-(visco) plastic composites based on an incremental variational principle. *International Journal of Plasticity*, 36:86–112, 2012.

[15] G.T. Camacho and M. Ortiz. Adaptive lagrangian modeliing of ballistic penetration of metallic targets. *Computer Methods in Applied Mechanics and Engineering*, 142:269–301, 1997.

[16] W. Cao, R.C. Gonzalez, and R.D. Russell. Variational mesh adaptation methods for axisymmetrical problems. *SIAM Journal on Numerical Analysis*, 41:235–257, 2003.

[17] P. Ciarlet. Mathematical elasticity. *Three-dimensional Elasticity, North-Holland*, 1:1482–1496, 1988.

[18] J.P. Combe, P. Ladevéze, and J.P. Pelle. Discretization error estimation for transient dynamic simulation. *Advances in Engineering Software*, 33:553–563, 2002.

[19] J.C.A. Costa and M.K. Alves. Layout optimization with h-adaptivity of structures. *International journal of numerical methods in engineering*, 58:83–102, 2003.

[20] Loïc Debeugny. *Contribution à la modélisation et à la compréhension du procédé de soudage par friction linéaire*. PhD thesis, Ecole Centrale Nantes, 2013.

[21] P. Diez and A. Heurta. A unified approach to remeshing strategies for finite element h-adaptivity. *Computer Methods in Applied Mechanics and Engineering*, 176:215–229, 1999.

[22] T. Erhart, W. Wall, and E. Ramm. Robust adaptive remeshing strategy for large deformation transient impact simulations. *International journal of numerical methods in engineering*, 65:2139–2166, 2006.

[23] Mathieu Foca. *On a Local Maximum Entropy interpolation approach for simulation of coupled thermo-mechanical problems. Application to the Rotary Frictional Welding process*. PhD thesis, Ecole Centrale Nantes, 2015.

[24] T. Grätsch and B. Klaus-Jürgen. A posteriori error estimation techniques in practical finite element analysis. *Computers and Structures*, 83:235–265, 2005.

[25] Anthony Gravouil and Alain Combescure. Multi-time-step explicit-implicit method for non-linear structural dynamics. *International Journal for Numerical Methods in Engineering*, pages 199–225, 2001.

[26] Eitan Grinspun, Petr Krysl, and Peter Schröder. Charms: A simple framework for adaptive simulation. *ACM Trans. Graph.*, 21(3):281–290, July 2002.

[27] M.E. Gurtin. Configurational forces as basic concepts of continuum physics. *Springer, New York*, 2000.

[28] Bernard Halphen and Quoc Son Nguyen. Sur les matériaux standard généralisés. *Journal de Mécanique*, 14:39–63, 1975.

[29] O. Hassan, E.J. Probert, K. Morgan, and J. Peraire. Mesh generation and adaptivity for the solution of compressible viscous high speed flows. *International Journal of Numerical Methods in Engineering*, 38:1123–1148, 1987.

[30] G. Herrmann. On variational principles in thermoelasticity and heat conduction. *Quarterly of Applied Mathematics*, 22:151–155, 1963.

[31] T. Heuzé, H. Amin-El-Sayed, J. B. Leblond, and J.M. Bergheau. Benchmark tests based on the couette viscometer - II: Thermo-elasto-plastic solid behaviour in small and large strains. *Computers and mathematics with applications*, 67:1482–1496, 2014.

[32] J.P. Holman. *Heat Transfer*. McGraw-Hill Companies, 1996.

[33] W. Huang. Variational mesh adaptation: isotropy and equidistribution. *Journal of computational physics*, 174:903–924, 2001.

[34] W. Huang and W. Sun. Variational mesh adaptation ii: error estimates and monitor functions. *Journal of computational physics*, 184:619–648, 2003.

[35] D.W. Kelly, J. Gago, O.C. Zienkiewicz, and I. Babuska. A posteriori error analysis and adaptive processes in the finite element method. *International journal of numerical methods in engineering*, 19:1593–1619, 1983.

[36] P. Ladevéze and N. Möes. A new a posteriori error estimation for nonlinear time-dependant finite element analysis. *Computational Methods for Applied Mechanical Engineering*, 157:45–68, 1997.

[37] P. Ladeveze, J-P. Pelle, and Ph. Rougeot. Error estimation and mesh optimization for classical finite elements. *Engineering Computations*, 8:69–80, 1991.

[38] P. Ladevéze and J.P. Pelle. Mastering calculations in linear and nonlinear mechanics. *Springer, Mechanical Engineering Series*, 2004.

[39] S. Lakshmanan, B.K. Soni, and K. Balasubramaniam. r-adaptation in finite element modelling of elastic solids. *Computers and Structures*, 63:249–257, 1997.

[40] Y.M. Leroy and A. Molinari. Stability of steady states in shear zones. *Journal of the Mechanics and Physics of Solids*, 40:181–212, 1992.

[41] W. Li, T. Ma, and J. Li. Numerical simulation of linear friction welding of titanium alloy: Effects of processing parameters. *Materials and Design*, 31:1497–1507, 2010.

[42] X.D. Li and N.E. Wiberg. A postprocessed error estimate and an adaptive procedure for the semi-discrete finite element in dynamic analysis. *International journal of numerical methods in engineering*, 37:3585–3603, 1994.

[43] R. Lohner. Adaptive remeshing for transient problems. *Computer Methods in Applied Mechanics and Engineering*, 75:195–214, 1989.

[44] R. Lohner, K. Morgan, and O.C. Zienkiewicz. An adaptive finite element procedure for compressible high speed flows. *Computer Methods in Applied Mechanics and Engineering*, 51:441–465, 1985.

[45] T.D. Marusich and M. Ortiz. Modelling and simulation of high speed machining. *International journal of numerical methods in engineering*, 38:3675–3694, 1995.

[46] A. Molinari and M. Ortiz. Global viscoelastic behavior of heterogeneous thermoelastic materials. *International Journal of Solids and Structures*, 23(9):1285–1300, 1987.

[47] J.F. Molinari and M. Ortiz. Three-dimensional adaptive meshing by subdivision and edge-collapsing in finite-deformation dynamic-plasticity problems with application to adiabatic shear banding. *International journal of numerical methods in engineering*, 53:1101–1126, 2002.

[48] J. Mosler and M. Ortiz. Variational h-adaptation in finite deformation elasticity and plasticity. *International Journal of Numerical Methods in Engineering*, 72:505–523, 2007.

[49] J. Mosler and M. Ortiz. An error-estimate-free and remapping-free variational mesh refinement and coarsening method for dissipative solids at finite strains. *International Journal of Numerical Methods in Engineering*, 77:437–450, 2009.

[50] M. Ortiz and J.J. Quigley. Adaptive mesh refinement in strain localization problems. *Computer Method in Applied Mechanics and Engineering*, 90:781–804, 1991.

[51] M. Ortiz and L. Stainier. The variational formulation of viscoplastic constitutive updates. *Computational Methods for Applied Mechanical Engineering*, 171:419–444, 1999.

[52] M. Papadrakakis, G. Babilis, and P. Braouzi. Efficiency of refinement procedures for the p-version of the adaptive finite element method. *Engineering Computations*, 14:98–118, 1997.

[53] M. Parashivoiu, J. Peraire, and A. T. Patera. A posteriori finite element bounds for linear functional outputs of elliptic partial differential equations. *Computer Methods in Applied Mechanics and Engineering*, 150:289–312, 1997.

[54] J. Peraire, M. Vahdati, K. Morgan, and O.C. Zienkiewicz. Adaptive remeshing for compressible flow computations. *Journal of computational physics*, 72:449–466, 1987.

[55] F. Perales, F. Dubois, Y. Monerie, R. Mozul, and F. Babik. Xper : une plateforme pour la simulation numérique distribuée dinteractions multiphysiques entre corps. In *Proceedings of 13ème colloque national en calcul des structures*, CSMA 2017, Giens (Var), France, May 2017.

[56] Pijaudier, G. Cabot, L. Bode, and A. Huerta. Arbitrary eulerian lagrangian finite element analysis of strain localization in transient problems. *International journal of numerical methods in engineering*, 38:4171–4191, 1995.

[57] W. Rachowicz, J.T. Oden, and L. Demkowicz. Toward a universal h-p adaptive finite element strategy, part 3, design of h-p meshes. *Computer Methods in Applied Mechanics and Engineering*, 77:181–212, 1989.

[58] R. Radovitzky and M. Ortiz. Error estimation and adaptive meshing in strongly nonlinear dynamic problems. *Computer Methods in Applied Mechanics and Engineering*, 172:419–444, 1999.

[59] M. Ramadan, L. Fourment, and H. Digonnet. A parallel two mesh method for speeding-up processes with localized deformations: application to cogging. *International Journal of Material Forming*, 2(1):581, Dec 2009.

[60] M. Rivara. Local modification of meshes for adaptive and/or multigrid finite-element methods. *Journal of Computational and Applied Mathematics*, 36:79–89, 1991.

[61] M. Rivara. New longest edge algorithm for the refinement and/or improvement of unstructured triangulations. *International Journal for Numerical Methods in Engineering*, 40:3313–3324, 1997.

[62] M. Rivara and P. Inostroza. Using longest-side bisection techniques for the automatic refinement of delaunay triangulations. *International Journal for Numerical Methods in Engineering*, 40:581–597, 1997.

[63] I. Romero and L.M. Lacoma. A methodology for the formulation of error estimators for time integration in linear solid and structural dynamics. *International journal of numerical methods in engineering*, 66:635–660, 2006.

[64] P. Solin, J. Cerveny, L. Dubcova, and D. Andrs. Monolithic discretization of linear thermoelasticity problems via adaptive multimesh hp-fem. *Journal of Computational and Applied Mathematics*, 234:2350–2357, 2010.

[65] L. Stainier. Consistent incremental approximation of dissipation pseudo-potentials in the variational formulation of thermo-mechanical constitutive updates. *Mechanics Research Communications*, 38(4):315–319, 2011.

[66] L. Stainier. A variational approach to modeling coupled thermo-mechanical nonlinear dissipative behaviors. volume 46 of *Advances in Applied Mechanics*, pages 69–126. Elsevier, 2013.

[67] L. Stainier and M. Ortiz. Study and validation of a variational theory of thermo-mechanical coupling in finite visco-plasticity. *International Journal of Solids and Structures*, 47(5):705 – 715, 2010.

[68] S. Su and L. Stainier. Energy-based variational modeling of adiabatic shear bands structure evolution. *Mechanics of Materials*, 80:219–233, 2015.

[69] P. Thoutireddy and M. Ortiz. A variational r-adaptation and shape-optimization method for finite-deformation elasticity. *International journal of numerical methods in engineering*, 61:1–21, 2004.

[70] D.A. Venditti and D.L. Darmofal. Anisotropic grid adaptation for functional outputs: application to two-dimensional viscous flows. *Journal of Computational Physics*, 187:22–46, 2003.

[71] R. Verfürth. A review of a priori error estimation and adaptive mesh-refinement techniques. *Wiley/Teubner: New York/Stuttgart*, 1996.

[72] C. Vokas and M. Kasper. Adaptation in coupled problems. *The international journal for computation and mathematics in electrical and electronic engineering*, 29:1626–1641, 2010.

[73] Q. Yang, L. Stainier, and M. Ortiz. A variational formulation of the coupled thermo-mechanical boundary-value problem for general dissipative solids. *Journal of the Mechanics and Physics of Solids*, 54:401–424, 2006.

[74] O.C. Zienkiewicz and J.Z. Zhu. A simple error estimator and adaptive procedure for practical engineering analysis. *International journal of numerical methods in engineering*, 24:337–357, 1987.

UNIVERSITE BRETAGNE LOIRE

Centrale Nantes

Thèse de Doctorat

Rohit PETHE

Titre de la thèse : Adaptation variationnelle pour des problèmes fortement couplés en thermo-mécanique

Title of thesis: Variational h-adaptation for strongly coupled problems in thermo-mechanics

Résumé

Une approche d'adaptation en mesh pour des problèmes fortement couplés est proposée, selon un principe variationnel. La technique d'adaptation repose sur une erreur indiquée par un potentiel énergétique et est donc exempte d'estimations d'erreur. Selon la nature du point de chevauchement de ce principe variationnel, une solution de solution décalée apparaît plus naturelle et conduit à une adaptation de maille distincte pour les champs mécaniques et thermiques.
En utilisant différents maillons pour différents phénomènes, des solutions précises pour différents domaines à l'étude sont obtenues. Les variables internes sont considérées comme constantes par rapport aux cellules de Voronoi, de sorte qu'aucune procédure de remappage complexe n'est nécessaire pour transférer des variables internes. Étant donné que l'algorithme est basé sur un ensemble de paramètres de tolérance, des analyses paramétriques et une étude de leur influence respective sur l'adaptation de maille sont réalisées. Cette analyse détaillée est effectuée sur des problèmes unidimensionnels. La méthode proposée se révèle être rentable qu'un maillage uniforme, certaines applications de l'approche proposée pour différents exemples 2D, y compris les bandes de cisaillement et le soudage par friction, sont présentées.

Mots-clés
Adaptions de maillage, approche variationnel, problèmes couplée, thermomécanique, Multiphysique, problèmes non-linaire.

Abstract

A mesh adaption approach for strongly coupled problems is proposed, based on a variational principle.
The adaption technique relies on error indicated by an energy-like potential and is hence free from error estimates.
According to the saddle point nature of this variational principle, a staggered solution approach appears more natural and leads to separate mesh adaption for mechanical and thermal fields.
Using different meshes for different phenomena, precise solutions for various fields under consideration are obtained.
Internal variables are considered constant over Voronoi cells, so no complex remapping procedures are necessary to transfer internal variables.
Since the algorithm is based on a set of tolerance parameters, parametric analyses and a study of their respective influence on the mesh adaption is carried out.
This detailed analysis is performed on uni-dimensional problems.
The proposed method is shown to be cost effective than uniform meshing, some applications of the proposed approach to various 2D examples including shear bands and friction welding are presented.

Key Words
Mesh adaptation, Variational approach, Strongly coupled problems, Thermo-mechanics, Multiphysics, Non linear coupled problems.